Vacuolar acidification relies on the combined activity of endomembrane proton pumps

Dissertation

zur Erlangung der Doktorwürde
der Naturwissenschaftlich-Mathematischen Gesamtfakultät
der Ruprecht - Karls - Universität Heidelberg

vorgelegt von
Anne Kriegel
aus Dresden

Heidelberg
2015

INAUGURAL - DISSERTATION

zur Erlangung der Doktorwürde
der Naturwissenschaftlich-Mathematischen Gesamtfakultät
der Ruprecht - Karls - Universität Heidelberg

vorgelegt von
Dipl. Agr. Biologin Anne Kriegel
aus Dresden

Tag der mündlichen Prüfung: _____

Vacuolar acidification relies on the combined activity of endomembrane proton pumps

Gutachter: Prof. Dr. Karin Schumacher
Prof. Dr. Jan Lohmann

Table of contents

Summary

The vacuole is not only the largest organelle of mature plant cells, it is also vital for the plants life. Due to their sessile lifestyle plants accumulate essential ions and metabolites inside their vacuole in times of excess but they can also serve as a reservoir under starvation conditions. Moreover, harmful compounds can be sequestered inside vacuoles in order to detoxify plant cells. Vacuoles provide structural support for the plant and are required for growth since osmotically driven water uptake generates turgor pressure that leads to cell expansion. To enable all transport processes, two proton pumps exist at the vacuolar membrane (tonoplast), the vacuolar H^+-ATPase (V-ATPase) and H^+-pyrophosphatase (V-PPase) that catalyse energy-dependent proton translocation to build up a proton gradient that is the driving force for secondary active transport. In contrast to the V-PPase, the V-ATPase is a multisubunit enzyme complex that consists of a cytosolic V_1-subcomplex where ATP hydrolysis takes place and a membrane-bound V_o-subcomplex that is responsible for H^+ translocation. Depending on the VHA-a subunit isoform that is incorporated into the complex, the proton pump is localized at the TGN/EE (VHA-a1) or at the tonoplast (VHA-a2, VHA-a3). Vacuoles of the tonoplast V-ATPase double mutant *vha-a2 vha-a3* are known to have an increased pH, however they remain acidic to a certain extent. Thus, in the first chapter we aimed to elucidate how the remaining H^+ gradient is established. First, we overexpressed the V-PPase in *vha-a2 vha-a3*, however no rescue of the mutant phenotype was observed. To gain insights into the role of the V-PPase for vacuolar acidification we created triple mutants lacking the tonoplast V-ATPase and the V-PPase and found that those plants are viable and have a neutral pH in rosette leaves. Since root vacuoles of the triple mutant were still acidified, we suggest that TGN/EE localized V-ATPase complexes and additional transport processes are involved in vacuolar pH regulation. With the second chapter of this thesis we clarify contradictory results concerning V-PPase overexpression and mutant lines. We show that the increased biomass of the *35S:AVP1* line is not due to constitutive overexpression, since neither RNA nor protein level and enzyme activity were elevated. Moreover, we found that the mutant growth phenotype of *avp1-1* is caused by a second site T-DNA insertion in *GNOM*.

Zusammenfassung

Die Vakuole ist nicht nur das größte Kompartiment ausgewachsener Pflanzenzellen, sondern auch unerlässlich für das pflanzliche Leben. Da Pflanzen eine sessile Lebensweise führen, ist es für sie von grundlegender Bedeutung, in ihren Vakuolen essentielle Ionen und Metabolite zu akkumulieren, wenn diese im Überschuss vorhanden sind. Unter Nährstoffmangelbedingungen können Pflanzen auf die Vakuole als Vorratsspeicher zurückgreifen. Zudem können zur Entgiftung von Pflanzenzellen auch schädliche Substanzen in die Vakuole eingelagert werden. Sie spielen eine wichtige Rolle für den Aufbau der Pflanze und deren Wachstum, da osmotisch getriebene Wasseraufnahme den sogenannten Turgor erzeugt, der zur Zellstreckung führt. Um diese sekundär aktiven Transportvorgänge zu energetisieren, gibt es zwei Protonenpumpem an der vakuolären Membran (Tonoplast): die vakuoläre H^+-ATPase (V-ATPase) und die H^+-Pyrophosphatase (V-PPase). Zusammen katalysieren sie den energieabhängigen Protonentransport mit dem Ziel, einen Protonengradienten zu erzeugen, der den sekundär aktiven Transport antreibt. Im Unterschied zur V-PPase ist die V-ATPase ein Enzymkomplex, der aus mehreren Untereinheiten zusammengesetzt ist. Dieser besteht aus einem zytosolischen V_1-Komplex, der für die ATP Hydrolyse verantwortlich ist, und einem membrangebundenem V_o-Komplex, der H^+ transportiert. Die Isoform der VHA-a Untereinheit entscheidet über die Lokalisierung des gesamten Enzymkomplexes; enthält dieser die VHA-a1 Untereinheit, so ist der Komplex am TGN/EE lokalisiert, oder beinhaltet er VHA-a2 oder VHA-a3, dann befindet er sich am Tonoplasten. Es ist bereits bekannt, dass die Vakuolen der am Tonoplasten lokalisierten V-ATPase Doppelmutante *vha-a2 vha-a3* einen erhöhten pH-Wert haben, jedoch verbleibt eine gewisse Restansäuerung. Demnach war die zentrale Frage des ersten Kapitels, wie der verbliebene H^+ Gradient aufrechterhalten wird. Zu Beginn der Untersuchungen wurde die V-PPase in der *vha-a2 vha-a3* Mutante überexprimiert, allerdings führte dies nicht zu einer Verbesserung des mutanten Phänotyps der Doppelmutante. Um mehr über die Rolle der V-PPase bei der vakuolären Ansäuerung zu erfahren, wurden Trippelmutanten generiert, denen die V-ATPase und die V-PPase fehlt. Diese Trippelmutanten sind lebensfähig und verfügen über einen neutralen pH-Wert in den Rosettenblättern. Da die Vakuolen in den Wurzeln der Trippelmutante jedoch noch angesäuert sind, gehen wir davon aus, dass der vakuoläre pH-Wert durch V-

ATPasen am TGN/EE und durch weitere Transportprozesse reguliert wird. Das zweite Kapitel dieser Arbeit befasst sich mit der Aufklärung widersprüchlicher publizierter Ergebnisse zu V-PPase Überexpressionslinien und knock-out Mutanten. Wir zeigen, dass der gesteigerten Biomasse der *35S:AVP1* Linien keine konstitutive Überexpression zugrunde liegt, da weder RNA noch Proteingehalt und Enzymaktivität erhöht sind. Desweitern haben wir herausgefunden, dass der mutante Wachstumsphänotyp von *avp1-1* durch eine zweite T-DNA Insertion in *GNOM* verursacht wird.

General Introduction

Plant vacuoles - essential for plant survival

Among plant endomembrane compartments the vacuole occupies a very prominent position. It’s tremendous size of up to 90% of the cellular volume evokes the question whether this organelle is as important as it appears. Indeed, a mutant defective in vacuole development resulted in lethality at the torpedo stage of embryogenesis (Rojo et al., 2001). Undeservedly, the name of this essential organelle is derived from "vacuum" since Felix Dujardin, in 1872, thought he observed an empty space (Viotti, 2014). In fact, vacuolar constituents (cell sap) which are separated from the cytosol by the vacuolar membrane (tonoplast) fulfil diverse functions and cell sap composition greatly varies depending on the cell type (Marty, 1999). One of the most important features of plant vacuoles is the ability to promote cell growth by generating turgor pressure through the accumulation of water. Turgor pressure is the driving force for cell elongation and the maintenance of mechanical stability of plants and describes the difference of osmotic pressure between the inside and outside of a cell (Geitmann and Ortega, 2009). When plants face osmotic stress, turgor pressure inside the cell cannot be sustained which directly affects cell growth (Zhang et al., 2014). Besides establishing and maintaining turgor, vacuoles are important for the temporary storage of a multitude of compounds to maintain cytosolic homeostasis. This is also of great relevance for stress conditions like nutrient limitation. The vacuolar cell sap usually contains a variety of primary metabolites such as amino acids, carbohydrates, organic acids and inorganic ions such as nitrate, potassium, chloride and sodium (Neuhaus and Martinoia, 2001). However, plant vacuoles of different plants and organs play distinct roles. Carbohydrates are usually stored for a short time in leaf mesophyll vacuoles, in contrast vacuoles of sugar cane or tuber can store sugars for a long time (Martinoia et al., 2012). There are many compounds of the secondary metabolism which are almost exclusively found in the vacuole and serve for plant defence and detoxification of the cytosol (Neuhaus and Martinoia, 2001). Vacuoles in leaf cells of specialized hyperaccumulater plants store toxic heavy metals which are used to defend plants against pathogens and herbivores (Martinoia et al., 2012). Secondary compounds in the vacuole also include pigments that give flowers their characteristic colour (Becker, 2007). In addition, a large number of

hydrolytic and oxidizing enzymes have been found in vacuoles and it has therefore been suggested that the plant vacuole corresponds to lysosomes of animal cells. Interestingly, the composition of hydrolytic enzymes is very similar to lysosomes (Wink, 1993). Due to this important feature vacuoles are described as lytic compartments. In addition to lytic vacuoles (LV's) a second type of vacuoles, termed protein storage vacuoles (PSV's), exists in plants (Paris et al., 1996). PSV's are characterized by a higher pH and lower hydrolytic activities than LV's and are present in vegetative tissue as well as storage tissue's such as cotyledons, seed endosperm, and tubers (Xiang et al., 2013). PSV's in seeds are important for the storage of proteins and many essential nutrients that are used for anabolism during seedling growth. The fact that certain biochemical processes occurring simultaneously have different pH optima explains the existence of various compartments within one cell. Another key feature of vacuoles is the regulation of pH homeostasis which is a prerequisite for many vacuolar functions. The vacuole is acidified to varying degrees by the action of three classes of proton pumps, namely the P-type and V-type H^+-adenosintriphosphatases (P-ATPase and V-ATPase) as well as the H^+-pyrophosphatase (V-PPase). They generate an electrochemical gradient of protons which is used to energize secondary active transport of metabolites against a concentration gradient. Monovalent anions can accumulate by the action of channels which depend on the membrane potential. Ion channels and pumps together create the membrane potential which at the tonoplast is assumed to be -30 to -40 mV (Martinoia et al., 2012). Importantly, the coupling ratio (amount of protons transported per ATP hydrolyzed) of V-ATPases is larger than the 1:1 ratio of plasma membrane ATPases, indicating that they can generate large pH gradients (Rienmüller et al., 2012).

Proton pumps energize a variety of cellular processes

The V-ATPase - complex and essential

The V-ATPase is a highly conserved, multisubunit enzyme complex that shares a common ancestor with the F-type ATP synthase (F-ATPase) and archaebacterial A-ATPases and is found at endomembranes of all eukaryotes (Nishi and Forgac, 2002). Therefore, it is not surprising that the tonoplast V-ATPase of plants is highly abundant, representing 6.5 to 35% of the tonoplast-localized protein (Ratajczak,

2000). V-ATPases consist of two subcomplexes; a membrane peripheral complex (V_1) and a membrane integral complex (V_o) that are together built by 13 subunits encoded by a total of 27 VHA-genes (Sze et al., 2002). The V_1-subcomplex is responsible for ATP hydrolysis and is composed of VHA-A, VHA-B, VHA-C, VHA-D, VHA-E, VHA-F, VHA-G and VHA-H while the V_o-subcomplex translocates protons across the membrane and is formed by VHA-a, VHA-c, VHA-c'', VHA-d and VHA-e (Schumacher, 2014). Comparison of the peripheral V_1 domain of the V-ATPase with the peripheral F_1 domain of the chloroplastic and mitochondrial F-ATPase reveal striking similarities in their subunit pattern (Ratajczak, 2000). In fact, the membrane integral V_o subcomplex of the V-ATPase was named after the oligomycin-binding F_o subcomplex of F-ATPases. Due to the importance of this complex enzyme in many cellular processes such as receptor-mediated endocytosis, protein degradation, and protein sorting, V-ATPase activity has to be tightly controlled. Therefore, diverse regulatory mechanisms such as phosphorylation of V-ATPase subunits (Hong-Hermesdorf et al., 2006), oxidation and reduction of certain cysteine residues (Dschida and Bowman, 1995) or stimulation of the V-ATPase by cytoplasmic Cl^- (Ward and Sze, 1992) exist. Furthermore, it has been shown that cytoplasmic ATP/ADP ratios regulate V-ATPase activity during light/dark transition (Dietz, 1998). In addition, the presence of asolectin or different molecular species of phosphatidylcholine (PC) resulted in maximal activation of the V-ATPase, indicating that the lipid environment of the enzyme plays a role in its regulation (Yamanishi and Kasamo, 1993).

To study the V-ATPase function in more detail, pharmacological treatments and mutant analysis can be applied. Efficient inhibitors of the V-ATPase are Concanamycin A (ConcA) and Bafilomycin A (BafA), which are membrane-permeable macrolide antibiotics that bind to the subunits a and c and thereby can block proton translocation into the lumen of various compartments (Huss et al., 2002; Bowman et al., 2004; Wang et al., 2005). The application of ConcA compromises secretory and endocytic trafficking of cargo molecules and strongly affects Golgi and TGN morphology (Dettmer et al., 2006). In addition to antibiotics, nitrate has also been shown to inhibit the V-ATPase in an irreversible manner (Dschida and Bowman, 1995).

Interestingly, the VHA-a subunit exists as three different isoforms in Arabidopsis which determine the subcellular localization of individual V-ATPase complexes. V-ATPase complexes containing the subunit VHA-a1 are localized to the trans-Golgi network/early endosome (TGN/EE), whereas holoenzymes including VHA-a2 or VHA-a3 isoforms are destined for the tonoplast (Dettmer et al., 2006). In the double mutant lacking both tonoplast-localized VHA-a isoforms, the vacuolar lumen is alkalized to a pH of 6.4 compared to wild type vacuoles that have a pH of 5.8 (Krebs et al., 2010). The increase in vacuolar pH led to strong growth defects and impaired ion storage with reduced levels of nitrate and calcium and increased sensitivity to the micronutrient zinc, which can become toxic at high cytosolic concentrations. However, salt tolerance is mainly dependent on a functioning TGN/EE localized V-ATPase since RNAi lines against *VHA-a1* are more salt-sensitive, while *vha-a2 vha-a3* plants are not (Krebs et al., 2010). Moreover, the *det3* mutant that has a reduced mRNA level of VHA-C resulting in only 40% of the wild type V-ATPase activity shows strongly reduced cell expansion and a reduced response to brassinosteroids (Schumacher et al., 1999). The V-ATPase subunit isoform VHA-E1 encoded by the Arabidopsis *TUFF* gene is essential during embryo development, since *vha-E1* mutants are impaired in Golgi organization and are defective in cell wall deposition and cell division resulting in embryo lethality (Strompen et al., 2005). In addition, a mutant line defective in VHA-A which is a single copy gene and part of the catalytic V_1 complex of the V-ATPase led to complete male and partial female gametophyte lethality (Dettmer et al., 2005). The aforementioned examples demonstrate that a properly functioning V-ATPase is the basis of many cellular processes and is essential for plant development.

The V-PPase

In contrast to the V-ATPase, the V-PPase uses the energy of a phosphoanhydride bond of the simple, low-cost substrate pyrophosphate (PP_i) (Maeshima, 2000). This compound is generated during many metabolic processes, such as the polymerisation of DNA and RNA, the synthesis of proteins, cellulose and sucrose as well as the formation of phosphoenolpyruvate (PEP) from pyruvate (Martinoia et al., 2006; Maeshima, 2000). Therefore, it has been proposed that the V-PPase is the dominating proton pump in vacuoles of young, growing tissues which can provide

large amounts of PP_i (Maeshima, 2000). Indeed, this assumption has been experimentally confirmed by Shoji Segami and colleagues demonstrating that the V-PPase mainly accumulates in root tips, growing hypocotyls, young cotyledons and petals (Segami et al., 2014). In contrast to the complex structure of the V-ATPase, the V-PPase consists of a single polypeptide that results in a molecular mass of 80 kDa and is functioning as a homodimer in order to fulfil its functions. V-PPases are present in membranes of higher plants, algae, photosynthetic bacteria, protozoa and archaebacteria but have not been found in the plasma membrane or endomembranes of yeast or mammals (Drozdowicz and Rea, 2001). The existence of two types of V-PPases, type I and type II, has been reported for several organisms (Drozdowicz and Rea, 2001). The Type I V-PPase is activated by the presence of cytosolic K^+ and is moderately sensitive to Ca^{2+}, while type II V-PPases are insensitive to K^+ but strongly Ca^{2+}-sensitive. Three genes encode Arabidopsis V-PPases; the type I V-PPase is represented by one single gene, VHP1 (also known as AVP1), while two genes exist for the second type V-PPases, VHP2;1 and VHP2;2 (Drozdowicz and Rea, 2001; Segami et al., 2010). Both types of V-PPases localize to distinct membranes and their expression levels are very different. The type I V-PPase is specifically found at the vacuolar membrane but can be missorted to the plasma membrane when excessively expressed (Segami et al., 2014). Type II enzymes localize to the Golgi apparatus and TGN/EE but their total amount is very low with <0.2 % of type I V-PPases (Segami et al., 2010). Due to their Golgi localization and extremely low expression levels, type II V-PPases may be negligible and are therefore left aside in this thesis.

The elimination of PP_i from the cytosol has been shown to play an important role during early seedling development, since accumulation of excessive PP_i produced during biosynthetic reactions can serve as a metabolic inhibitor (Ferjani et al., 2011). Expression of the yeast cytosolic inorganic PPase (IPP1) rescued cell proliferation defects and so called compensation phenotypes, defined through increased cell expansion triggered by the reduced number of cells in leaf primordia of V-PPase mutants (*fugu5,* Ferjani et al., 2011). This shows that the V-PPase is important for cytosolic PP_i removal besides acting as a proton pump. Importantly, the knock-out of the tonoplast V-PPase resulted in a moderate vacuolar alkalinisation of about 0.25 pH units which is nearly the half of the level of alkalinisation observed in the tonoplast

V-ATPase double mutant (Ferjani et al., 2011; Krebs et al., 2010). In fact, a controversy about the true V-PPase mutant phenotype emerged, since in addition to three V-PPase point mutation lines (*fugu5-1* to *fugu5-3*), also a V-PPase T-DNA insertion line (*vhp1-1*) that all lack V-PPase activity completely, show cellular phenotypes but are perfectly viable (Ferjani et al., 2011). This is in contrast to the T-DNA insertion mutant *avp1-1*, that has severely altered root and shoot development and mostly developed no floral organs (Li et al., 2005).

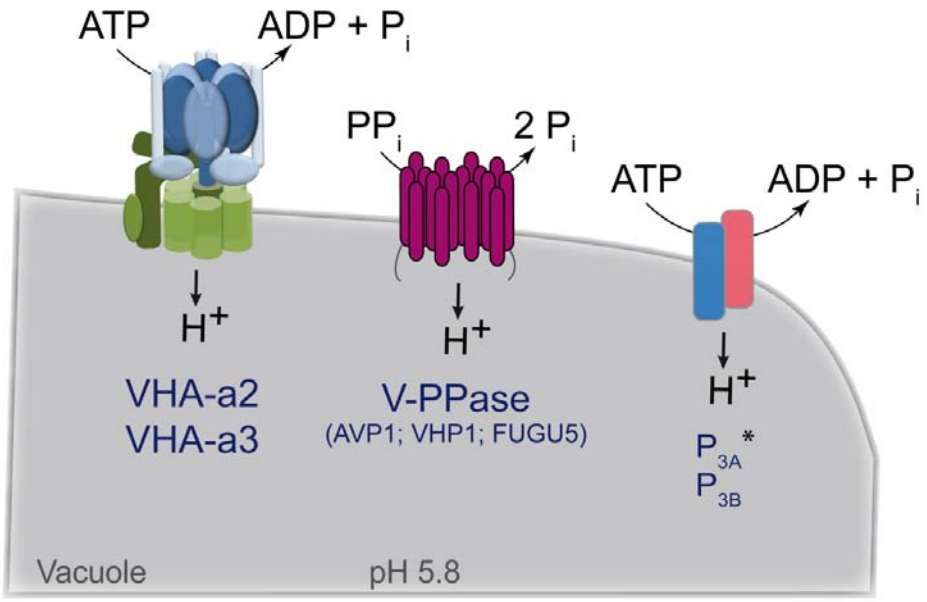

Figure 1. Proton pumps present at the tonoplast.

The vacuolar membrane contains up to three proton pumps, namely V-ATPases (containing subunit VHA-a2 or VHA-a3), V-PPases and in some species/cell types (indicated by *) P_3-type-ATPases. Vacuolar proton pumps together acidify the vacuolar lumen, energize the membrane and are required for vacuolar ion homeostasis.

Overexpression of the tonoplast V-PPase (*35S:AVP1-1*, *35S:AVP1-2*) resulted in an overall increased plant growth with a bigger leaf area, higher leaf number and increased root growth (Li et al., 2005). Li and colleagues stated that altering V-PPase expression affects the activity of the plasma membrane H^+-ATPase, resulting in changes of the apoplastic pH that ultimately controls auxin transport, among other things. In fact, overexpression of the V-PPase has been used as a universal strategy to generate plants that are resistant towards various types of environmental stresses. Thus, overexpression of the Arabidopsis V-PPase in cotton resulted in an elevated drought- and salt-tolerance under hydroponic and soil growth conditions (Pasapula et al., 2011). Moreover, tomato plants with an enhanced V-PPase level had an

increased root biomass which led to more drought resistance (Park et al., 2005). Further examples comprise plant species such as rice that are more cold tolerant and tobacco being more drought tolerant resulting from increased shoot size and more closed stomata (Zhang et al., 2011; Arif et al., 2013). Interestingly, enhanced V-PPase expression has also been described to be responsible for enhanced phosphorus utilization in rice, tomato and maize (Yang et al., 2007; Pei et al., 2012).

P-type H^+-ATPases and their importance beyond the plasma membrane

The third class of proton pumps existing in plant cellular membranes are P-type H^+-ATPases that are responsible for establishing and maintaining the electrochemical gradient at the plasma membrane, which is used by secondary transporters to move ions and organic compounds. Besides being important for nutrient uptake from the soil and distribution of minerals within the plant, P-type H^+-ATPases play a role in salinity tolerance, stomata opening, intracellular pH regulation and cell elongation (Sondergaard et al., 2004; Morsomme and Boutry, 2000). P-type pumps form an aspartyl phosphate intermediate during their catalytic cycle and are therefore abbreviated with the 'P-type name' and can be inhibited by vanadate. P-type ATPases do not only translocate protons, but also K^+/Na^+, Ca^{2+} and heavy metals. Arabidopsis contains 11 members of the P-type H^+-ATPase family (*AHA1-11*) (Gaxiola et al., 2007). The highest expression levels are shown by *AHA1* and *AHA2,* with more *AHA1* transcript found in shoots whereas *AHA2* is higher in roots. Among the numerous AHA isoforms expressed in various different tissues and organs one H^+-ATPase isoform (AHA10), which is expressed only in endothelial cells of the seed coat, is of particular interest. Seeds of *aha10* mutants have pale seed coats due to strongly reduced levels of the vacuolar proanthocyanidin (PA) content, which, apart from other flavonoids, plays an important role in UV protection or tolerance against desiccation (Baxter et al., 2005). Moreover, the vacuolar morphology is impaired in *aha10* seeds, pointing to an exceptional case were a plasma membrane proton-pump plays a role in endosomal acidification. Interestingly, Arabidopsis AHA10 has been shown to be a homolog of *Petunia hybrida* PH5 which is a member of the P_{3A}-subfamily of P-type H^+-ATPases and, unlike other P-type H^+-ATPases, is localized at the tonoplast (Verweij et al., 2008; Eisenach et al., 2014). Mutants lacking *PH5* show reduced vacuolar acidification in petal epidermis cells which led to altered flower

coloration. Importantly, constitutive expression of *PH5* in the mutant background rescued the *ph5* phenotype and petal pH but was not able to re-establish the vacuolar pH of other pH mutants such as those of the transcription factor mutants *ph3*, *ph4* and *ph6* (Verweij et al., 2008). However, recently it has been demonstrated that PH5 and PH1, a P_{3B}-ATPase, interact to enhance PH5 H^+ transport activity and thus hyperacidify vacuoles of petunia petals (Faraco et al., 2014). According to these latest findings, P-type H^+-ATPases have to be considered to be involved in acidification of endosomal compartments in concert with the V-PPase and V-ATPase.

Intracellular pH homeostasis

The action of V-ATPase, V-PPase and P-type ATPase proton pumps comprise the major regulatory mechanism of cellular pH regulation and thus constitute the 'biophysical pH-stat' (Felle, 2001). In addition, a metabolic-based mechanism of pH regulation defined as the 'biochemical pH-stat' relies on pH-dependent carboxylation and decarboxylation of malate and related organic acids to generate or consume protons (Davies, 1986). Indeed, it has been shown that the tonoplast malate transporter *A*ttDT is crucial for cytosolic pH homeostasis (Hurth, 2005) since malate-degrading malic enzyme is activated upon acidification while PEP-carboxylase in inhibited (Davies, 1986). Moreover, cytosolic buffer systems such as bicarbonate, phosphate or the histidine's imidazol group play a role in alleviating rapid pH changes (Niñoles et al., 2013). Apart from these long known basic contributors of cellular pH regulation, ion/H^+ exchangers also play an important role in pH regulation serving either as shunt conductances or H^+-leaks (Schumacher, 2014). They directly couple the transport of an ion in exchange with H^+ and are therefore dependent on the proton motive force established and maintained by the V-ATPase and the V-PPase. Hence, a double mutant lacking the two tonoplast-localized K^+/H^+ exchangers NHX1 and NHX2 had more acidic vacuoles in above-ground organs and contained only 30% of the wild type K^+ concentration, resulting in reduced growth and defects in cell expansion and flower development (Bassil et al., 2011). Besides their importance in regulating vacuolar pH and K^+ concentrations in Arabidopsis, a NHX1-like gene from Japanese morning glory (*Ipomoea nil*) has been shown to be important for the characteristic petal color change during flower opening from purple to blue, a process that is dependent on pH (Yamaguchi et al., 2001). Furthermore, cation/H^+ exchanger

(CHX) genes have been implicated in cellular pH regulation and have been suggested to comprise K^+,Na^+/H^+ transport modes due to their substantial similarities to e.g. KHA1 from *Saccharomyces cerevisiae* (Pittman, 2012). Interestingly, *CHX17* which is only expressed in roots, was strongly induced by K^+ starvation and external acidic pH (Cellier et al., 2004). Moreover, CHX20, which is involved in K^+ homeostasis and is localized to endomembrane compartments in guard cells, has been proposed to play a role in addition to the V-ATPase in sustaining growth at high pH levels when other $K^+(Na^+)/H^+$ exchangers are absent (Padmanaban et al., 2007). Yet another type of ion/H^+ exchangers is involved in cellular pH homeostasis. Anion/H^+ exchangers are essential for maintaining charge balance within acidic compartments. It has been demonstrated that plants lacking CLCd, a chloride transporter co-localizing with VHA-a1 of the V-ATPase are hypersensitive towards ConcA and show impaired root growth at acidic pH (von der Fecht-Bartenbach et al., 2007). This could indicate that CLCd and the V-ATPase work together at the TGN. Finally, also Ca^{2+}/H^+ exchangers have been implicated in V-ATPase regulation since the double mutant *cax1cax3* which is impaired in vacuolar calcium accumulation, displayed a 47% decrease in V-ATPase activity (Cheng et al., 2005). Similarily, *cax1* as well as *cax2* mutants show reduced V-ATPase activity (Cheng, 2003; Pittman et al., 2004) and the authors thus suggested that there might be an indirect feedback mechanism resulting from changes in H^+ transport across the tonoplast. Thus, the herein selected examples demonstrate that in addition to proton pumps and organic acids also ion/H^+ exchangers must be considered in the regulation of the cellular pH homeostasis.

Aim

Previous observations demonstrated that vacuoles of the tonoplast V-ATPase double mutant *vha-a2 vha-a3* are still acidic. The aim of this study was to elucidate how the remaining H^+ gradient is established. To this end, the contribution of the V-PPase to vacuolar acidification was examined. This analysis included the characterization of transgenic lines overexpressing the V-PPase in the *vha-a2 vha-a3* double mutant background, the investigation of mutant plants lacking the V-PPase (*vhp1-1, fugu5-1*) and mutants lacking both vacuolar proton pumps, the V-PPase and the V-ATPase (*fugu5-1 vha-a2 vha-a3*). Moreover, P-type H^+-ATPases and the role of TGN/EE localized V-ATPase complexes for vacuolar acidification were investigated. In the second chapter, different V-PPase overexpression and mutant lines have been re-evaluated in order to clarify controversial phenotypes that have been reported previously.

I. Contribution of the V-PPase and the TGN/EE localized V-ATPase to vacuolar acidification

I.1 Abstract

In plant cells, the vacuolar H^+-pyrophosphatase (V-PPase) and the vacuolar H^+-ATPase (V-ATPase) have long been described to be responsible for acidification of the lytic vacuole. Both pumps are thought to act together in establishing the transmembrane proton gradient which drives solute transport across the tonoplast. It was previously shown that in a mutant lacking the tonoplast-specific V-ATPase (*vha-a2 vha-a3*) the vacuolar pH is elevated (pH 6.4), but remains significantly more acidic than the cytosol (pH 7.4; Krebs et al., 2010). However, to what extent the V-PPase is responsible for vacuolar acidification remained to be elucidated. Surprisingly, lack of the V-PPase only slightly affects vacuolar pH and it has been shown that the main function of the V-PPase is the hydrolysis of cytosolic PP_i, rather than vacuolar acidification (Ferjani et al., 2011). In agreement with these findings, plants overexpressing the V-PPase in the tonoplast V-ATPase mutant background failed to restore the wild type phenotype. We will describe the phenotype of a triple mutant lacking both the tonoplast V-ATPase and the V-PPase and further suggest a tissue specific role of V-PPase function. Ultimately, we present data that demonstrate that both pharmacological inhibition of the TGN/EE localized V-ATPase (VHA-a1) and genetic reduction of VHA-a1 alters vacuolar pH. We thus propose that the acidity of plant vacuoles is not only achieved by vacuolar proton pumps but additional transport processes must be involved.

I.2 Introduction

Plant vacuoles are multifunctional cellular compartments that are essential for plant development. They occupy tremendous space in mature cells which is the reason for the cytosol appearing as a thin layer between the plasma membrane and the vacuolar membrane (tonoplast). Vacuoles are lytic organelles containing a range of hydrolytic enzymes responsible for protein breakdown (Wink, 1993). Therefore, the vacuole represents a major site of amino acid recycling which is important for plant development and adaptations towards a changing environment (Müntz, 2007). Moreover, it serves as a reservoir for metabolites, nutrients, sugars and amino acids, but can be also used to detoxify the cytosol (Neuhaus and Martinoia, 2001). The vacuole can further function in the storage of defence and signal compounds in order to improve the fitness of plants in case of herbivore attack, as well as serve in attracting potential pollinators through the accumulation of pigments (Becker, 2007). The accumulation of osmolytes leads to water uptake into the vacuolar lumen which generates turgor essential for cell expansion and thus plant growth. Importantly, turgor pressure generated in the vacuole, also provides mechanical stability for plants. To fulfil all these vacuolar functions, immense transport processes across the tonoplast are necessary. Since accumulation of most compounds found in the vacuole is against their concentration gradient, transport is dependent on energization accomplished through the activity of two proton pumps, the vacuolar H^+-ATPase (V-ATPase) and the vacuolar H^+-pyrophosphatase (V-PPase) (Maeshima, 2001; Gaxiola et al., 2007). The combined activity of the two proton pumps establishes the proton gradient and the membrane potential that is used for vacuolar transport and creates an acidic pH that is the basis for its lytic function. V-ATPases are highly conserved, multisubunit proton pumps that consist of two subcomplexes, the peripheral V_1 complex that hydrolyses ATP and the membrane-integral V_o complex responsible for proton translocation from the cytosol into the lumen of endomembrane compartments (Schumacher and Krebs, 2010). In contrast, the V-PPase is a much simpler enzyme formed by a homodimer of a single polypeptide that uses hydrolysis of pyrophosphate (PP_i) to translocate protons across membranes (Maeshima, 2000; Gaxiola et al., 2007). Arabidopsis contains three genes for the V-PPase that can be subdivided into one gene for the K^+-activated type I V-PPase (VHP1;1 or AVP1) and two genes for K^+-insensitive type II V-PPases

(VHP2;1 = AVP2 and VHP2;2) (Drozdowicz and Rea, 2001; Segami et al., 2010). Type I V-PPases have been shown to exclusively localize to the tonoplast but excessive expression can lead to mislocalization to the plasma membrane (Segami et al., 2014). In contrast, type II V-PPase are localized to the Golgi apparatus and their total amount is <0.2% compared to the type I enzyme (Segami et al., 2010). Under standard growth conditions the V-ATPase seems to contribute to a higher extent to vacuolar acidification than the V-PPase. The vacuolar pH of a mutant lacking both tonoplast-localized VHA-a isoforms (*vha-a2 vha-a3*) was shown to be elevated to 6.4 compared to a pH of 5.8 in the wild type (Krebs et al., 2010). The reduced proton gradient led to defects in nutrient storage capacity and resulted in strong growth reduction. The lack of the V-PPase in turn led to a weaker pH increase in the vacuole (0.25 units) and it was suggested that the main V-PPase function under nonstress conditions is to remove cytosolic PP_i since the latter can otherwise inhibit metabolism (Ferjani et al., 2011). In fact, PP_i is released as a by-product of many biosynthetic reactions for macromolecules such as protein, RNA and cellulose (Maeshima, 2000). Loss of the V-PPase and hence cytosolic PP_i accumulation resulted in nearly complete inhibition of cell division in cotyledons, which was compensated by an increased cell size explaining the elongated cotyledon shape (Ferjani et al., 2011). It has been proposed that under environmental stress conditions the importance of the V-PPase rises, thus a shift of the energy currency used by glycolytic enzymes from ATP to PP_i can occur in order to enable plasticity in metabolism (Huang et al., 2008). This is of particular importance under O_2-limiting conditions, where respiration is restricted thus resulting in an energy crises. Moreover, comparative proteome analysis revealed that the protein abundance of the V-PPase and V-ATPase subunits increase upon cold exposure (Schulze et al., 2012).

In addition to its presence at the tonoplast, V-ATPase complexes characterized by the membrane-integral VHA-a1 subunit localize to the trans-Golgi network/early endosome (TGN/EE) (Dettmer et al., 2006). These TGN/EE V-ATPases have been shown to be essential for the plants life, since a T-DNA insertion allele of *VHA-A* caused gametophytic and the lack of *VHA-E1* (*tuff*) embryo lethality (Dettmer et al., 2005; Strompen et al., 2005). The reduction of V-ATPase activity of about 60% (*det3*

mutant) led to strongly reduced cell expansion and dwarfed plant growth (Schumacher et al., 1999).

The role of the tonoplast V-ATPase for vacuolar acidification and metabolite storage has been studied in detail. Due to the fact that the vacuolar pH of *vha-a2 vha-a3* double mutants is still acidic when compared to the cytosolic pH (6.4 versus 7.4), we aimed to elucidate how the remaining H^+ gradient is generated. To that end, we analyzed the role of the V-PPase by overexpressing the enzyme in the *vha-a2 vha-a3* background. Since overexpression failed to restore wild type phenotypes, we went further and created triple mutant plants lacking both the V-ATPase and the V-PPase. Surprisingly, these plants are viable but show severe dwarfism and reproductive defects. However, root vacuoles of the triple mutant showed residual acidification. Interestingly, inhibition of VHA-a1 containing V-ATPase complexes at the TGN/EE by ConcA in addition to the lack of *VHA-a2* and *VHA-a3* resulted in vacuoles with neutral pH. However, silencing of VHA-a1 did not lead to vacuolar alkalinization as observed with ConcA treatment. Knowing that ConcA also blocks vacuolar transport, we suggest that vacuolar acidification is a combined process not only of vacuolar proton pumps but additional factors must be involved.

I.3 Results

Overexpression of the V-PPase does not complement the tonoplast V-ATPase mutant *vha-a2 vha-a3*

The tonoplast V-ATPase double mutant *vha-a2 vha-a3* has a strongly reduced rosette size as previously described (Krebs et al., 2010). To investigate whether the overexpression of the tonoplast V-PPase (*AVP1*) can compensate the lack of *VHA-a2* and *VHA-a3*, we expressed *AVP1* under the *ubiquitin-10* (*UBQ*) promoter (Norris et al., 1993; Grefen et al., 2010) in the wild type and the *vha-a2 vha-a3* mutant background. Homozygous lines were established and the *AVP1* RNA and protein amounts were determined (Fig. 1A and Fig. S1)

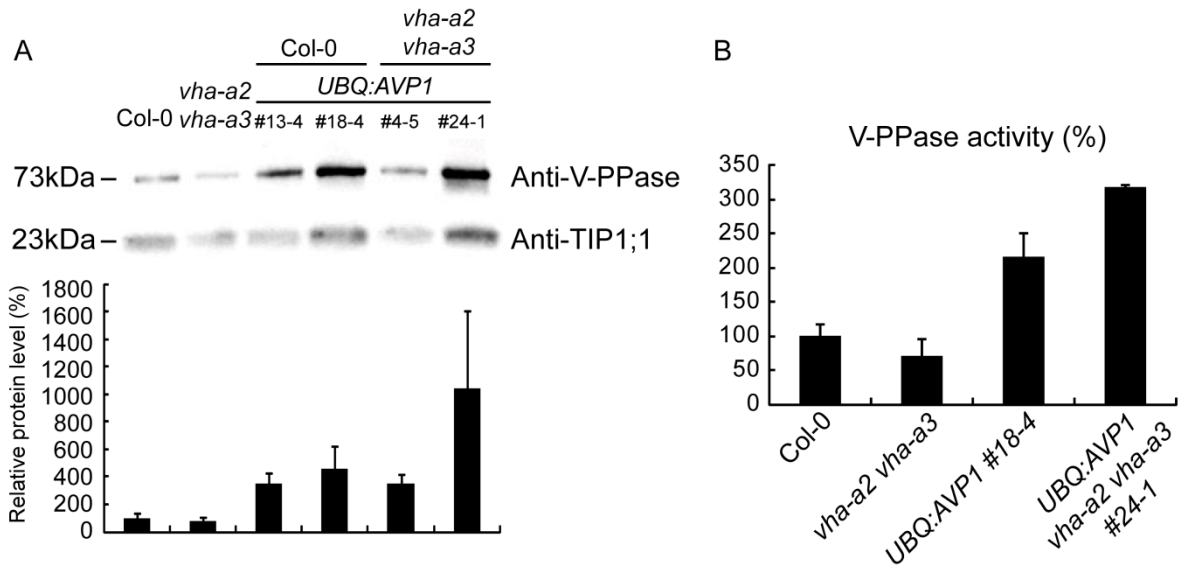

Figure 1. *UBQ:AVP1* lines overexpress vacuolar V-PPase.

(A) Arabidopsis wild type and *vha-a2 vha-a3* mutant plants expressing *AVP1* under the *UBQ* promoter have higher AVP1 protein level. Microsomal membrane proteins of 3-week-old plants were extracted, separated by SDS-PAGE and subsequently immunoblotted with anti-V-PPase antibody. Equal protein loading is indicated by TIP1;1 detection. A quantification of AVP1 protein levels is shown below. Error bars indicate SE of n = 3 technical replicates.
(B) AVP1 overexpressors show increased V-PPase activity. K^+-stimulated PPase activity was determined using microsomal membranes extracted from 3-week-old plants. Wild type activity was set to 100%. Error bars represent SE of n = 3 biological replicates.

Indeed, RNA and protein level of lines expressing *UBQ:AVP1* in the wild type and in the *vha-a2 vha-a3* mutant background were strongly increased compared to plants without the overexpression construct. Quantification of the immunosignals revealed a

3.5- to 4.5-fold increase in the two *UBQ:AVP1* lines, whereas protein amounts in *vha-a2 vha-a3* plants overexpressing *AVP1* ranged from 4-fold in #4-5 to 10-fold in #24-1 (Fig. 1A, bottom). For further analysis, the line with the higher protein level for each genetic background was chosen. To evaluate whether the increased protein amount also resulted in elevated V-PPase activity, KCl-stimulated PP_i hydrolysis was measured in microsomal membranes prepared from 3-week-old plants. Importantly, both V-PPase overexpression lines have an elevated V-PPase activity (Fig. 1B).

The establishment of lines with increased levels of V-PPase protein and enzyme activity enabled us to analyse whether this affects plant growth of *vha-a2 vha-a3*.

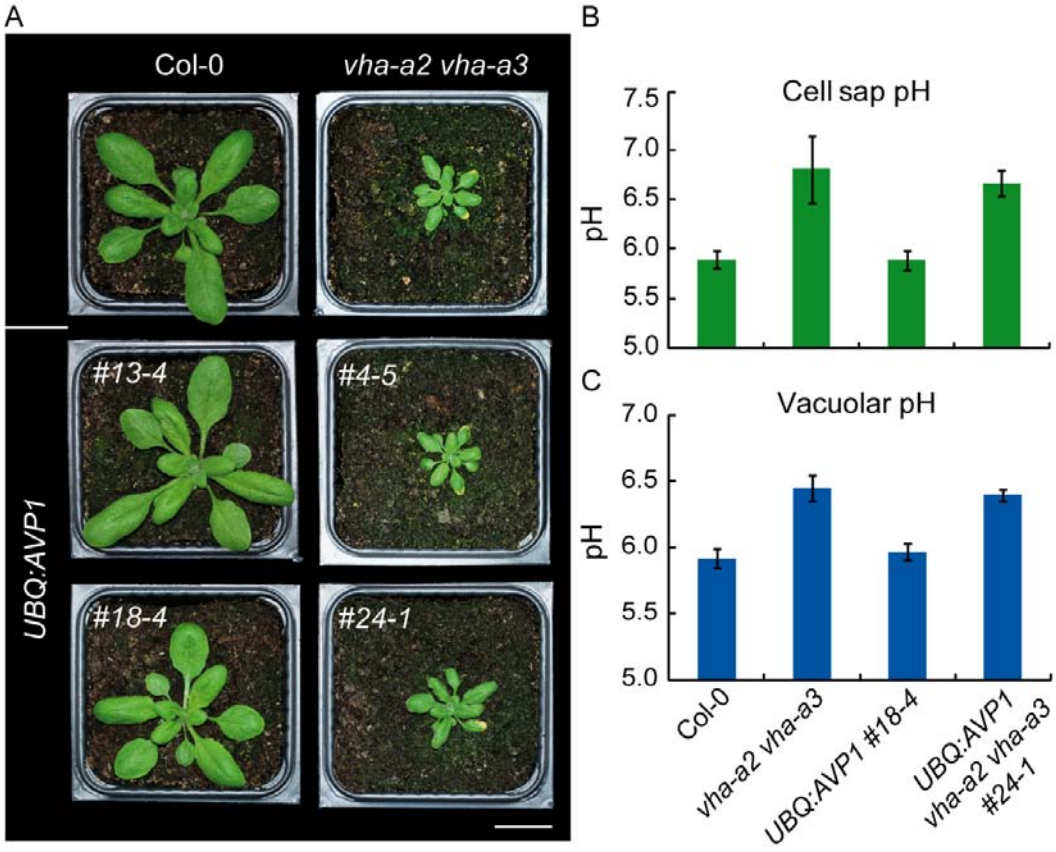

Figure 2. Overexpression of AVP1 does not complement *vha-a2 vha-a3.*

(A) *UBQ:AVP1* cannot restore wild type growth in *vha-a2 vha-a3*. Plants were grown for 3 weeks under LD conditions at 22°C. Bar = 1.75 cm.
(B) Overexpression of AVP1 has no effect on cell sap pH. Plants for cell sap pH measurements were grown for 3 weeks under LD conditions at 22°C. Error bars show SD of n = 3 biological replicates.
(C) Vacuolar pH in root epidermal cells is not changed upon AVP1 overexpression. Vacuolar pH was measured in roots of 6-day-old plants. Error bars represent SD of n = 3 biological replicates.

Surprisingly, the increased enzyme activity did not improve growth of the *vha-a2 vha-a3* mutant (Fig 2A). To analyse whether higher V-PPase activity affects acidification of the vacuolar lumen, the vacuolar pH was measured in cells of rosette leaves and in epidermal root cells. The cell sap pH represents the vacuolar pH (Krebs et al., 2010) since in mature cells the vacuolar lumen occupies up to 90 % of the cell volume. Measurement of the cell sap pH in 3-week-old plants revealed no difference between control plants and those overexpressing AVP1 (Fig. 2B). Wild type and *UBQ:AVP1* had a pH of 5.9 whereas the *vha-a2 vha-a3* mutant overexpressing AVP1 had a pH of around 6.6. Root vacuolar pH was measured in 5-day-old seedlings using the ratiometric pH sensitive dye BCECF-AM (Swanson and Jones, 1996; Krebs et al., 2010). Ratiometric images of the stained roots obtained through confocal laser scanning microscopy (CLSM) were converted to pH values by using an *in situ* calibration curve (see material and methods). Similar to the cell sap pH, also the root vacuolar pH did not differ between *UBQ:AVP1* and control lines (Fig. 2C). Taken together, overexpression of AVP1 does not rescue the retarded growth of *vha-a2 vha-a3*, which indicates that the V-PPase as a proton pump is not able to replace the function of the tonoplast V-ATPase.

Lack of V-PPase has minor effect on vacuolar acidification

Since we aimed to create mutants lacking the V-PPase in addition to the V-ATPase, we first examined the growth behaviour of two published V-PPase mutants under our conditions. For that we used the T-DNA insertion line, *vhp1-1*, and the *fugu5-1* mutant carrying a point mutation (A709T) in the last cytoplasmic loop that confers loss of function (Ferjani et al., 2011). Phenotypic growth analyses revealed that only *vhp1-1* has a reduced rosette size after growth for 3 weeks under LD conditions, whereas *fugu5-1* did not show any difference to the wild type (Fig. 3A). In accordance with previous work, no V-PPase protein was detected in *vhp1-1* while *fugu5-1* contained reduced levels of V-PPase protein (Fig. 3B; Ferjani et al., 2011). However, no KCl-stimulated PP_i hydrolysis activity was measured in both V-PPase mutants indicating that although *fugu5-1* has a reduced protein amount, both V-PPase mutants completely lack PP_i hydrolysis activity (Fig. 3C). The difference in rosette size and protein amount among the two V-PPase mutants suggests that the presence of the non-functional V-PPase protein affects growth positively.

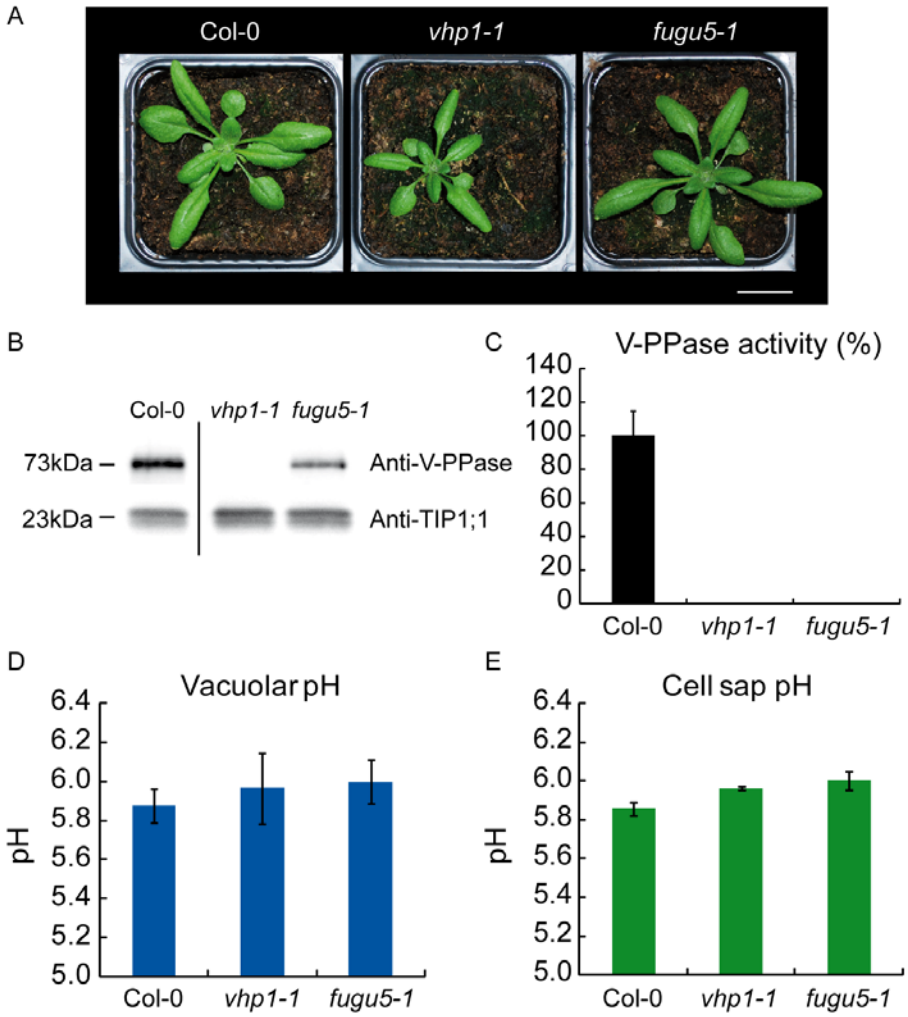

Figure 3. Lack of V-PPase results in growth reduction and less acidified vacuoles.

(A) V-PPase T-DNA line *vhp1-1* shows growth reduction. Plants were grown for 3 weeks under LD conditions at 22°C. Bar = 1.75 cm.
(B) *fugu5-1* but not *vhp1-1* show residual V-PPase protein level. Microsomal membranes were extracted from 3-week-old plants, separated by SDS-PAGE and subsequently immunoblotted with anti-V-PPase antibody. Equal protein loading is indicated by TIP1;1 detection.
(C) Both vacuolar H^+-PPase mutants lack PPase activity. K^+-stimulated PPase activity was determined on microsomal membranes extracted from 3-week-old plants. Wild type activity was set to 100%. Error bar represents SE of n = 3 technical replicates.
(D) Loss of V-PPase activity does not alter root vacuolar acidification. Vacuolar pH was measured in roots of 6-day-old plants. Error bars represent SD of n = 3 biological replicates.
(E) Loss of V-PPase activity results in slightly reduced acidification of the cell sap. Plants were grown for 3 weeks under LD conditions at 22°C. Error bars show SD of n = 2 biological replicates.

Furthermore, we examined to what extent the lack of the V-PPase affects acidification of the vacuole in roots and shoots. Determination of the root vacuolar pH revealed no change in V-PPase mutants, while cell sap pH measurements resulted in

slightly reduced acidification (Fig. 3D and 3E). The results obtained from analysing *vhp1-1* and *fugu5-1* are in accordance with previously published data (Ferjani et al., 2011) and show that *fugu5-1*, which has residual V-PPase protein, grows as well as wild type plants under our conditions while the growth of *vhp1-1* was reduced. The fact that, under nonstress conditions, the vacuolar acidification is not altered in V-PPase mutants suggests that either the tonoplast V-ATPase compensates for the lack of PPase activity or that the V-PPase plays only a minor role for vacuolar pH.

Plants lacking the tonoplast V-ATPase and V-PPase are viable but have severe developmental defects

To find out whether the V-PPase is important for vacuolar acidification, we crossed the *vha-a2 vha-a3* double mutant either with *vhp1-1* or *fugu5-1* in order to create vacuolar proton pump triple mutants. In fact, one has to consider two possible scenarios for the growth of triple mutant plants. If the V-PPase is not important as a proton pump, we would expect no growth difference between *vha-a2 vha-a3* and triple mutants. On the contrary, growth of the vacuolar proton pump triple mutant could be more reduced compared to *vha-a2 vha-a3* if compensation by the V-ATPase would have masked the lacking V-PPase in the single mutants. In fact, we were able to isolate homozygous triple mutants from the segregating F2 progeny and both *vhp1-1 vha-a2 vha-a3* and *fugu5-1 vha-a2 vha-a3* survived when grown on soil. However, the growth of both triple mutants was strongly impaired. This was clearly visible already in 8-day-old seedlings grown on agar plates. Seedlings of both triple mutants showed abnormal cotyledon phenotypes (Fig. S2). Since the growth of *vhp1-1 vha-a2 vha-a3* plants was even more impaired than that of *fugu5-1 vha-a2 vha-a3,* we decided to continue our analysis with the latter triple mutant. Comparing the phenotype of *fugu5-1 vha-a2 vha-a3* to the tonoplast V-ATPase double mutant revealed that the rosette size of the proton pump triple mutant was strongly reduced (Fig. 4A), indicating that the V-PPase is indeed important. Interestingly, homozygous triple mutants could only be isolated when they were initially germinated and grown in vitro on MS plates for a few days before they were transplanted to soil for further cultivation. Proton pump triple mutant plants developed to flowering plants but their growth was strongly delayed, even more than that of *vha-a2 vha-a3*. Since *fugu5-1 vha-a2 vha-a3* mutant plants hardly produced any seeds, we examined whether

flower development and fertility might be impaired. Therefore, we analyzed dissected flowers of the wild type, triple mutants segregating for *vha-a2* (*fugu5-1, vha-a2/+, vha-a3*) and the homozygous triple mutant. We observed that stamen filaments were shortened in the homozygous triple mutant, while they reached the pistil in the wild type flower (Fig. 4B). In addition, wild type anthers were dehiscent, whereas triple mutant anthers were not. Therefore, flowers of *fugu5-1 vha-a2 vha-a3* showed compromised fertilization.

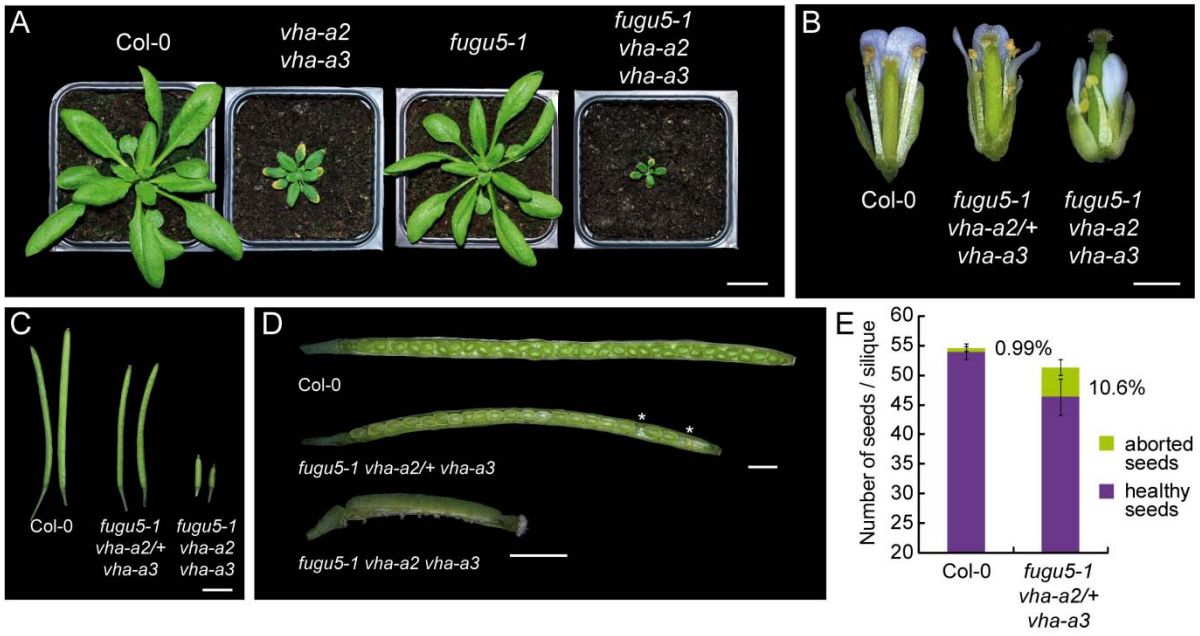

Figure 4. Phenotype of vacuolar proton pump triple mutant and its reproductive defects.

(A) *fugu5-1 vha-a2 vha-a3* growth is even more inhibited than *vha-a2 vha-a3*. Wild type and proton pump mutant plants were grown for 26 days under LD conditions at 22°C. Bar = 1.75 cm.
(B) Proton pump triple mutants exhibit defects in flower development. Bright-field micrographs of dissected flowers are shown. Stamen filaments reached the pistil in the wild type and the segregating proton pump triple mutant flower, whereas they are shortened in the *fugu5-1 vha-a2 vha-a3* flower. Bar = 1 mm.
(C) Silique size of *fugu5-1 vha-a2 vha-a3* is strongly reduced. Excised siliques of wild type, *fugu5-1 vha-a2/+ vha-a3* and *fugu5-1 vha-a2 vha-a3* are shown. Bar = 3 mm.
(D) Siliques of vacuolar proton pump triple mutants mainly contain undeveloped ovules. A wild type silique with full seed set, a *fugu5-1 vha-a2/+ vha-a3* silique with reduced seed set and undeveloped ovules (indicated by an asterisk) and a homozygous vacuolar proton pump triple mutant silique only containing aborted ovules are shown. Bars = 1 mm.
(E) Quantification of aborted seeds in wild type and *fugu5-1 vha-a2/+ vha-a3*. The total seed number and the number of healthy and aborted seeds was counted from ≥ 10 siliques.

As a result, the silique size of the heterozygous triple mutant was slightly shorter than the ones of the wild type. However, siliques of the homozygous triple mutant reached only 25% of the size of the wild type siliques (Fig. 4C). Opening of wild type siliques revealed exclusively fully developed ovules whereas 10% aborted ovules were found in *fugu5-1 vha-a2/+ vha-a3* siliques (Fig. 4D and 4E). In homozygous triple mutant siliques, mainly aborted ovules were found. However, in rare cases *fugu5-1 vha-a2 vha-a3* produced seeds. Together, these results show that although the vacuolar proton pump triple mutant is viable, it has stronger developmental defects than *vha-a2 vha-a3*. This suggests that the V-PPase contributes to vacuolar acidification, thus, acting as a proton pump.

Leaf cell sap pH is nearly neutral in *fugu5-1 vha-a2 vha-a3*

In order to verify that in shoots the V-PPase is indeed functioning as a proton pump, we measured the cell sap pH in vacuolar proton pump triple mutants and compared it to *vha-a2 vha-a3*. To this end, wild type, V-ATPase double mutant, V-PPase mutant and proton pump triple mutant plants were grown for 3 weeks on soil under standard growth conditions with 8h dark/16h light cycles. Shoot material was collected and the cell sap pH was measured. As expected, the pH of *fugu5-1 vha-a2 vha-a3* was more alkaline than that of *vha-a2 vha-a3* (Fig. 5A). The pH in leaf cells of the triple mutant reached values of above pH 7 whereas *vha-a2 vha-a3* had a pH of 6.4. This demonstrates that in shoots the V-PPase plays a substantial role in vacuolar acidification.

Ion homeostasis of *vha-a2 vha-a3* and *fugu5-1 vha-a2 vha-a3* is affected to a similar extent

Given that the proton gradient in shoots of the triple mutant is even less pronounced than in *vha-a2 vha-a3*, we expected that ion storage capacity is drastically affected in *fugu5-1 vha-a2 vha-a3*. Thus, we analyzed the metabolite content of the wild type, *vha-a2 vha-a3*, *fugu5-1* and *fugu5-1 vha-a2 vha-a3*. Previously, the ion content in shoots of *vha-a2 vha-a3* has been examined in detail (PhD thesis Melanie Krebs). A decrease in total inorganic ions, in particular calcium and nitrate was measured in the *vha-a2 vha-a3* mutant. To compare ion concentrations in vacuolar proton pump mutants, plants were grown for 3 weeks under long day conditions at 22°C and

rosettes were collected and subsequently analyzed by high pressure liquid chromatography (HPLC). A comprehensive metabolite profile is depicted in figure 5B to 5G. Surprisingly, the ion profile of *fugu5-1 vha-a2 vha-a3* and *vha-a2 vha-a3* are fairly similar with a few exceptions such as sulfate and sodium which are remarkably elevated in the triple mutant. Proton pump triple mutant rosettes contained eight times more sulfate than the wild type and five times more when compared to *vha-a2 vha-a3*. Moreover, the amount of many carbohydrates is strongly increased in *vha-a2 vha-a3* and *fugu5-1 vha-a2 vha-a3*. This is in accordance with previously measured carbohydrate contents in *vha-a2 vha-a3,* where fructose and glucose were found to be elevated (PhD thesis Melanie Krebs). In addition to glucose, fructose and sucrose, also raffinose was strongly elevated in *vha-a2 vha-a3* and *fugu5-1 vha-a2 vha-a3*. Moreover, trehalose levels are also higher in *vha-a2 vha-a3* and the triple mutant. In contrast to our expectations, nitrate concentrations were similarly low in *vha-a2 vha-a3* and in the triple mutant, indicating that triple mutants are not more impaired in their nitrate storage capacity. Calcium concentrations were found to be the same in *vha-a2 vha-a3* and the wild type which is in contrast to previous measurements. Higher ATP concentrations in both mutants could result from reduced ATP hydrolysis due to the lack of the main ATP consumer, the V-ATPase. Further, elevated concentrations of glutathione and its precursor cysteine indicate that the V-ATPase double mutant and the triple mutant suffer from oxidative stress. Additionally, keto acids are present in higher levels in *vha-a2 vha-a3* and the triple mutant. Moreover, we also analyzed the amino acid content of all mutants and the wild type. Generally the content of all amino acids was elevated in *vha-a2 vha-a3* as well as in *fugu5-1 vha-a2 vha-a3* (Fig. 6) However, there was one major difference between the two mutants. Proline was three times higher in the vacuolar proton pump triple mutant. In summary, we can conclude that the substantial increase in cell sap pH in *fugu5-1 vha-a2 vha-a3* does not result in major changes in ion concentrations when compared to *vha-a2 vha-a3*. However, certain differences in metabolites could give insights into the metabolic state of cells since many of the metabolites with elevated levels in *vha-a2 vha-a3* and more drastically in *fugu5-1 vha-a2 vha-a3* can be associated with adaptations to abiotic stress such as drought and salinity.

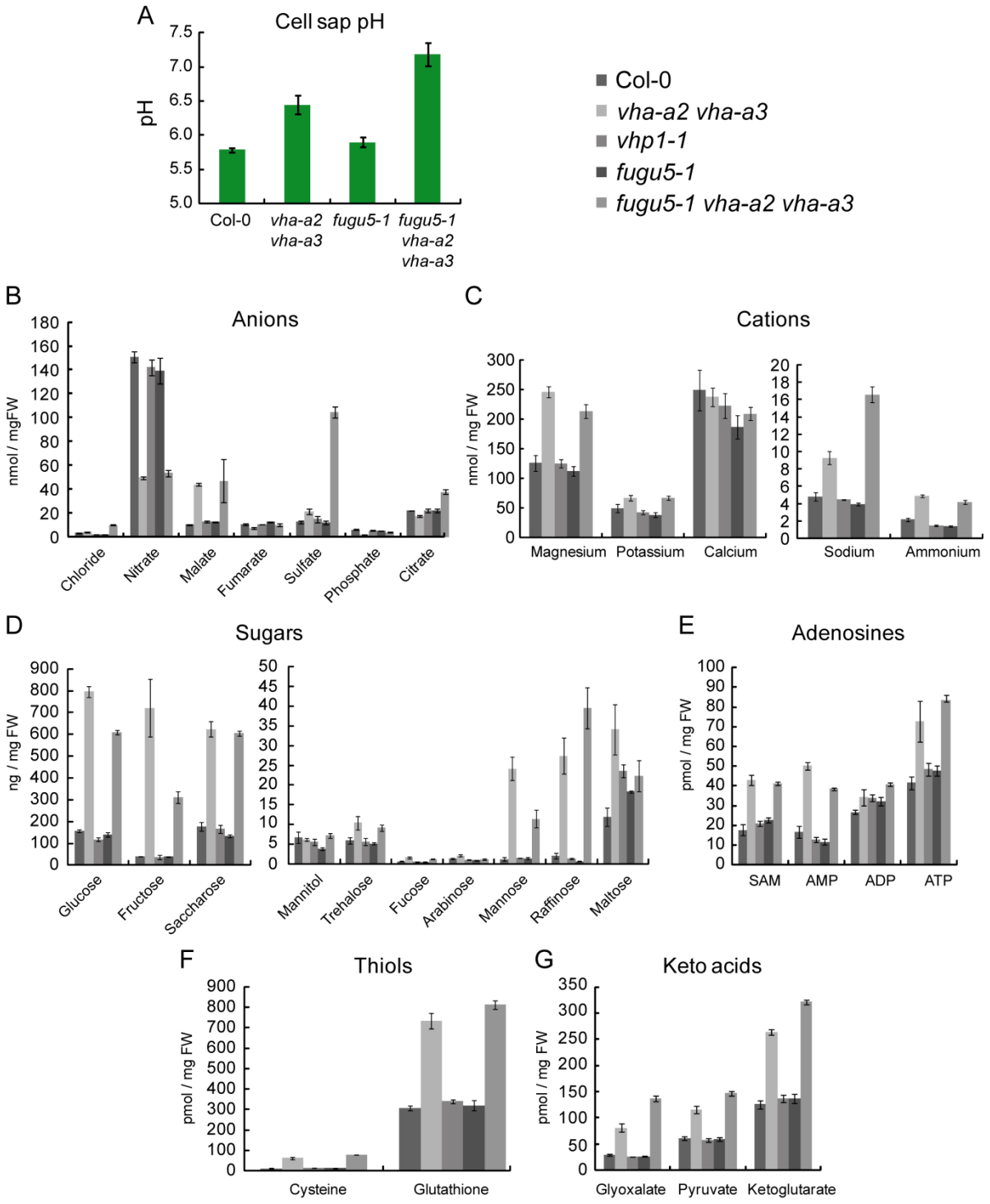

Figure 5. Metabolite profile of vacuolar proton pump mutants.

(A) Cell sap pH of *fugu5-1 vha-a2 vha-a3* is nearly neutral. Plants were grown for 3 weeks under LD conditions at 22°C. Error bars show SD of n = 3 biological replicates.
(B-G) Metabolite analysis on shoot extracts from 3-week-old plants grown on soil under LD conditions at 22°C. Error bars show SE of n = 3 technical replicates.

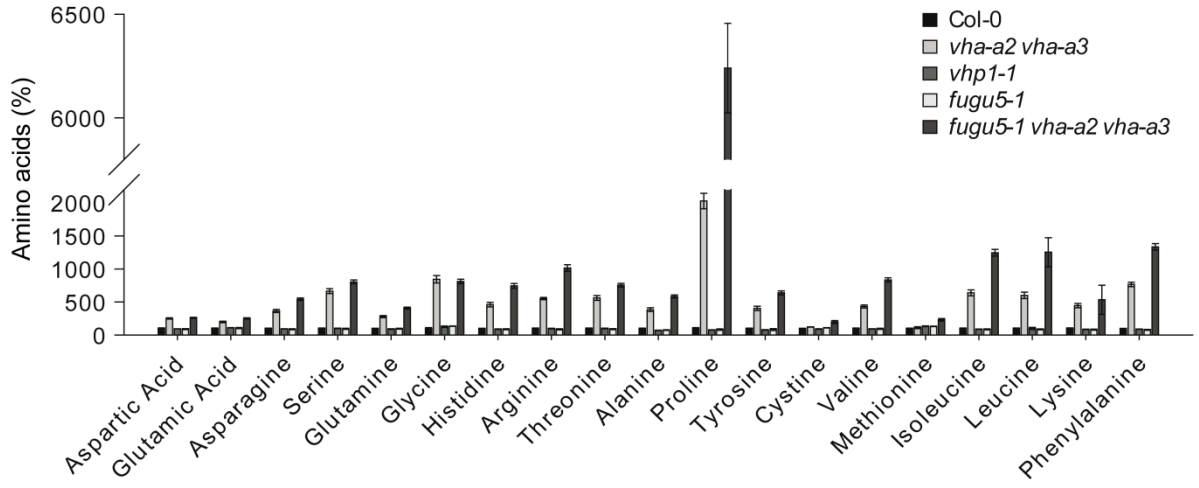

Figure 6. Amino acid content of vacuolar proton pump mutants.

Amino acids were measured in extracts of rosette leaves from 3-week-old plants grown on soil under LD conditions at 22°C. Values are presented as fold change (%) compared to wild type that was set to 100%. Error bars show SE of n = 3 technical replicates.

Cell expansion in *fugu5-1 vha-a2 vha-a3* is independent of vacuolar proton pumps

Next, we analyzed whether plants lacking both vacuolar proton pumps are still able to perform cell expansion. Therefore, we grew etiolated seedlings for 4 days on water agar plates and measured the hypocotyl length, which is widely used as an indicator for cell expansion (Gendreau et al., 1997). Hypocotyls of *fugu5-1 vha-a2 vha-a3* showed 60% reduction in hypocotyl elongation compared to wild type seedlings (Fig. 7A and 7B). Etiolated seedlings of *vha-a2 vha-a3* were reduced by 20% while cell expansion in V-PPase knock out plants was only marginally affected. The fact that the triple mutant is able to perform cell expansion at all indicates that these plants are still able to accumulate osmotically active substances into their vacuoles in order to drive elongation of hypocotyls cells. Nevertheless, the reduced cell expansion suggests severe vacuolar defects in *fugu5-1 vha-a2 vha-a3*.

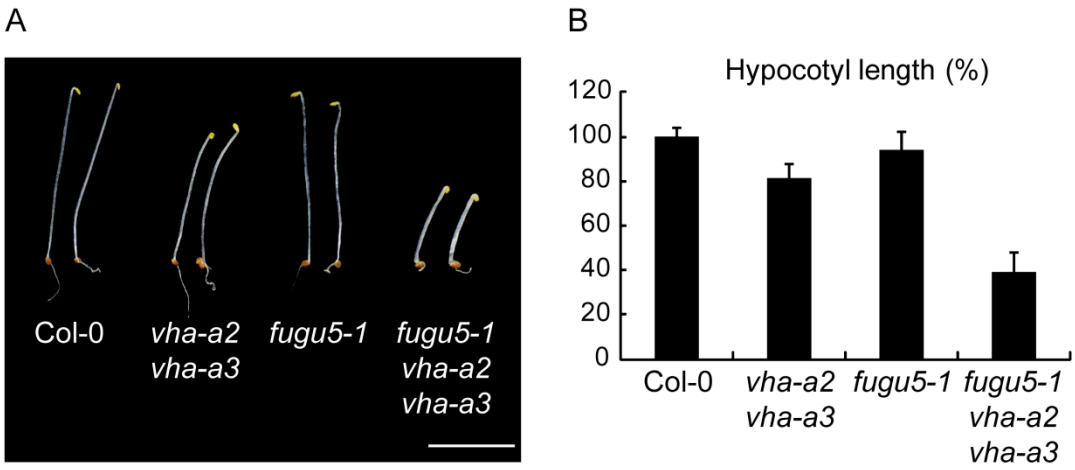

Figure 7. Hypocotyl length of *fugu5-1 vha-a2 vha-a3* is reduced by 60%.

(A) Morphological observation and (B) quantitative measurement of the hypocotyl length of vacuolar proton pump mutants. Etiolated seedlings were grown for 4 days on water agar. Error bars represent SD of n = 3 biological replicates. Bar = 0.5 cm.

Since cell expansion in hypocotyls of the triple mutant is reduced, we next analyzed whether also roots are reduced in their growth. Thus, we conducted root length measurements in the wild type and vacuolar proton pump mutants. Seedlings were grown on vertical agar plates for 10 days and then primary root length was determined. Indeed, root growth of *fugu5-1 vha-a2 vha-a3* was impaired, while the other genotypes examined did not show any difference when compared to wild type roots (Fig. 8). This could indicate that, similar to hypocotyls, also in roots of the triple mutant the absence of the V-PPase leads to changes in vacuolar function restricting cell elongation.

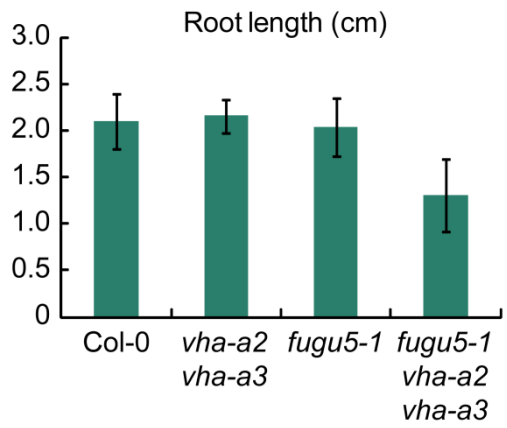

Figure 8. Reduced root length of *fugu5-1 vha-a2 vha-a3.*

Arabidopsis seedlings were grown for 10 days on 0.5 MS plates before root length was measured. Error bars represent SD of n = 15 roots measured per genotype.

Vacuolar morphology is disturbed in vacuolar proton pump mutants

The reduced root length of *fugu5-1 vha-a2 vha-a3* indicated that vacuolar function might be affected since cell growth is dependent on the formation of a large central vacuole. To visualise vacuolar morphology and the plasma membrane of root cells, BCECF, a green fluorescent dye that accumulates in the vacuolar lumen (Swanson and Jones, 1996; Krebs et al., 2010), and FM4-64, a lipophilic styryl dye which initially stains the plasma membrane (Bolte et al., 2004), respectively, were used in combination with the CLSM in three developmental zones of the root. Meristematic cells of wild type roots contain a single tubular vacuolar network surrounding the nucleus as it has been previously described in detail by 3D rendering (Fig. 9A, bottom; Viotti et al., 2013). In the root elongation zone cells start to rapidly expand through the inflation of vacuoles gradually enlarging the cellular volume (Fig. 9A, middle). Finally, in the differentiation zone, cells reach their ultimate size being completely filled by the vacuole (Fig. 9A, top). In comparison to wild type root cells, vacuolar shapes started to become irregular in elongating cells of the *vha-a2 vha-a3* and *fugu5-1* mutant (Fig. 9B and 9C, middle). Intriguingly, the vacuolar morphology was strongly altered in the elongation and transition zone in roots of *fugu5-1 vha-a2 vha-a3* (Fig. 9D, middle and top). Vacuoles appeared as round spheres of different sizes distributed within the cell. Importantly, vacuoles in fully elongated cells of the triple mutant appear to have a completely normal shape (Fig. 9D, top). This suggests that rapid inflation of vacuoles in elongating cells is lacking behind in roots of *fugu5-1 vha-a2 vha-a3* likely due to reduced turgor pressure. In order to check whether alterations in vacuolar morphology coincide with changes of the size of the respective root zones, we measured the length of the meristematic and the elongation zone. In wild type roots, both zones are of similar length, while in *vha-a2 vha-a3* and in the triple mutant, the elongation zone is extended when compared to the meristematic zone (Fig. 9E). In contrast, the elongation zone of the V-PPase mutant is reduced. Together, these results show that, except in the elongation and transition zone, vacuoles of *fugu5-1 vha-a2 vha-a3* develop normally suggesting that a proton gradient can still be established.

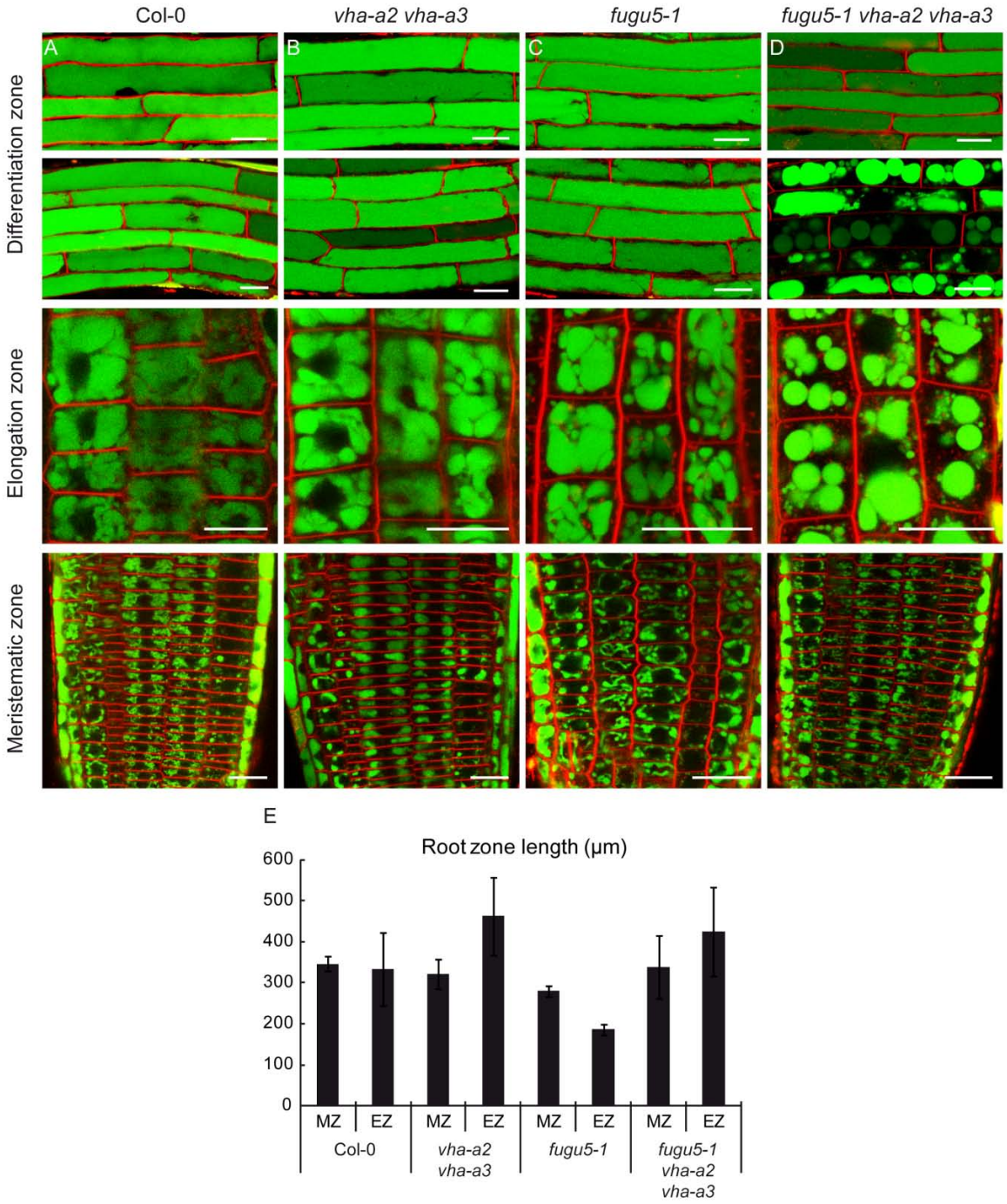

Figure 9. Vacuolar morphology in tonoplast proton pump mutants.

The shape of vacuoles was monitored in the root differentiation zone, elongation zone and meristematic zone of 6-day-old wild type (A), *vha-a2 vha-a3* (B), *fugu5-1* (C) and *fugu5-1 vha-a2 vha-a3* (D) seedlings. Roots were stained with BCECF (green) and FM4-64 (red). Bars = 20 µm.
(E) Root zone length of vacuolar proton pump mutants. The length of the meristematic zone (MZ) and the elongation zone (EZ) was measured in 6-day-old roots. Error bars represent SD of n ≥ 10 roots.
CLSM pictures (A to D) as well as root zone measurements were performed by Falco Krüger.

Root vacuoles of *fugu5-1 vha-a2 vha-a3* are acidified

To test the hypothesis that root vacuoles of the triple mutant are still acidified, we conducted vacuolar pH measurements in the three different root zones. For this, pH calibration was individually performed in each root zone. In fact, vacuoles of the triple mutant were as acidic as those of the *vha-a2 vha-a3* mutant (Fig. 10B to 10D). This is in contrast to cell sap pH measurements, in which the triple mutant showed alkaline pH values compared to *vha-a2 vha-a3* (Fig. 5A). In general we observed that the vacuolar pH of cells of the elongation zone was less acidic compared to cells of the meristematic and differentiation zone.

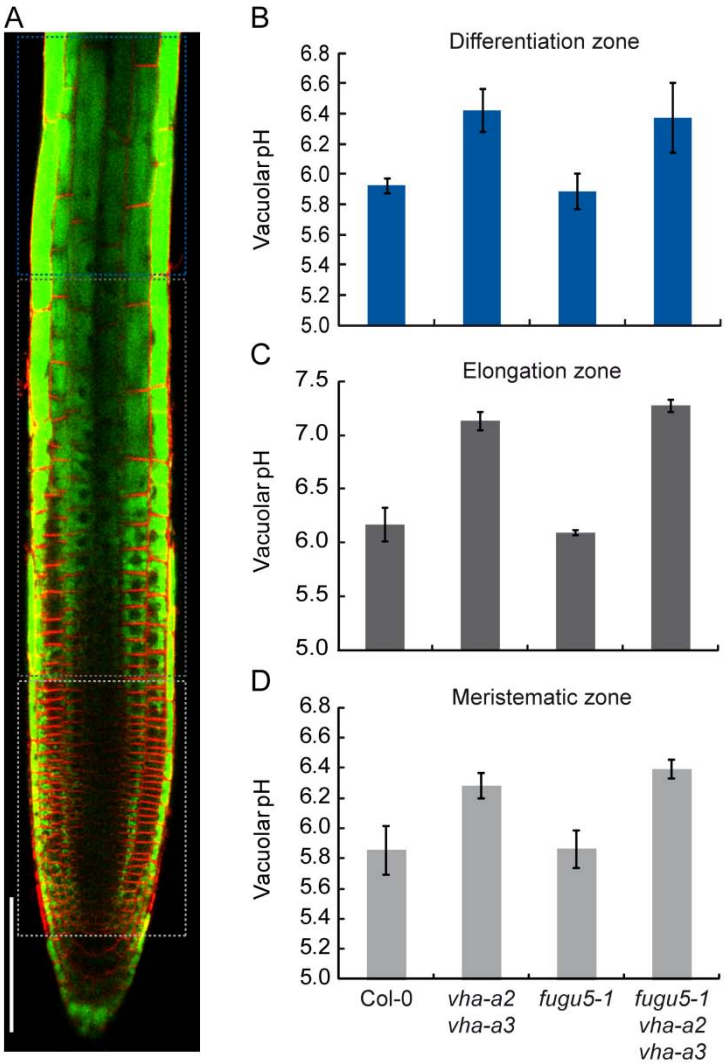

Figure 10. Vacuolar pH is neutralized only in root elongation zone of *fugu5-1 vha-a2 vha-a3*.

(A) Overview of Arabidopsis wild type root. Three root zones for pH measurements are indicated with dashed boxes. Roots were stained with BCECF(green) and FM4-64 (red). Bar = 100 µm. (B-D) Vacuolar pH measurement in three different root zones. pH values were determined in root differentiation zone (B), elongation zone (C) and meristematic zone (D) of 6-day-old wild type and vacuolar proton pump mutant seedlings. Error bars represent SD of n = 3 biological replicates. Image presented in A was provided by Falco Krüger. Data shown in B to D were produced jointly with Stefan Scholl.

Remarkably, the *vha-a2 vha-a3* mutant and the triple mutant reached nearly neutral pH values in the root elongation zone where vacuolar morphology was mainly affected (Fig. 10C). Together, our data suggest that the V-PPase plays different roles for vacuolar acidification in shoots and roots.

ConcA neutralizes vacuolar pH in all vacuolar proton pump mutants

The fact that root cells lacking all vacuolar proton pumps are still able to acidify their vacuoles raises the question of the mechanism responsible for the residual vacuolar acidification. To investigate this, we applied ConcA, a specific V-ATPase inhibitor. ConcA binds to the V-ATPase subunit c of the membrane integral V_O subcomplex and therewith prevents proton translocation from the cytosol into the lumen (Huss et al., 2002). Treatment of 6-day-old Arabidopsis seedlings with 1 µM ConcA for 20 h completely neutralized vacuolar pH not only in the wild type but also in *vha-a2 vha-a3, fugu5-1* and *fugu5-1 vha-a2 vha-a3* (Fig. 11). V-ATPase complexes containing the third isoform VHA-a1 located in the TGN/EE are the only target left for ConcA in the *vha-a2 vha-a3* mutant. We therefore assumed that acidification of the TGN/EE by VHA-a1 containing complexes could be important for vacuolar pH. However, since ConcA not only inhibits the V-ATPase activity but also blocks transport of proteins from the TGN/EE to the vacuole, alkalinization could also be due to the fact that a yet unidentified tonoplast proton pump is prevented from reaching its final destination.

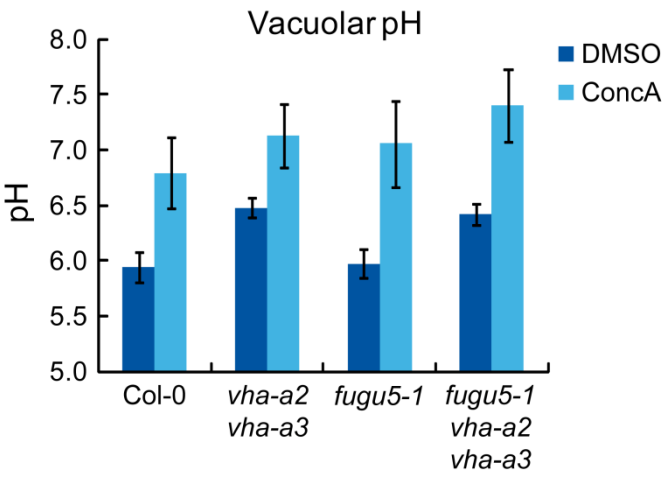

Figure 11. Concanamycin A neutralizes vacuolar pH in all vacuolar proton pump mutants.

Vacuolar pH was measured in roots of 6-day-old plants. Seedlings of Arabidopsis wild type and vacuolar proton pump mutants were incubated for 20 h in 1 µM ConcA or DMSO prior to pH measurements. Error bars represent SD of n = 3 biological replicates.

Do P-type ATPases influence vacuolar acidification?

Previous work speculated that the P-type ATPase AHA10 might be recruited to endosomal or vacuolar compartments to support luminal acidification (Baxter et al., 2005). To assess whether P-type ATPases acidify the vacuolar lumen, we measured vacuolar pH after the application of vanadate, an inhibitor of P-type ATPases. Vanadate inhibits the formation of a phosphorylated intermediate that is characteristic of the enzyme's catalytic cycle and is a common feature of all P-type ATPases (Baxter et al., 2003). Hence, we first tested the inhibitory effect of vanadate to plasma membrane localised P-type ATPases by analysing the level of medium acidification after application of this drug. We incubated 5-day-old Arabidopsis wild type seedlings in assay medium containing 2 mM vanadate and the fluorescent pH indicator fluorescein (Haruta et al., 2010). As shown in figure 12A, we observed that vanadate treatment reduced medium acidification by almost 50%. Knowing that vanadate indeed inhibits P-type ATPases, we went on examining whether this has an influence on the vacuolar pH of the wild type and proton pump mutants. Thus, vacuolar pH measurements were performed on roots previously subjected to 2 mM vanadate. Importantly, the vacuolar pH of the proton pump triple mutant was not affected by vanadate, however we observed an increase of 0.2 - 0.3 pH units in the wild type, the *vha-a2 vha-a3* and the *fugu5-1* mutant (Fig. 12B).

To investigate whether *AHA10* could potentially be activated in vacuolar proton pump mutants, we checked the transcript level of *AHA10* in roots of 6-day-old seedlings. Since *AHA10* is expressed primarily in developing seeds we used RNA extracted from young wild type siliques as a control. Interestingly, *AHA10* expression in proton pump mutants was lower when compared to the wild type (Fig. 12C). However, it is surprising that the expression level of *AHA10* in wild type roots is about 30% of that in wild type siliques pointing to a low, but measureable level of *AHA10* transcript in roots, arguing against a solely seed-specific function. Taken together, these findings demonstrate that the activity of P-type ATPases is not sufficient to explain the remaining vacuolar acidification in *fugu5-1 vha-a2 vha-3* root cells.

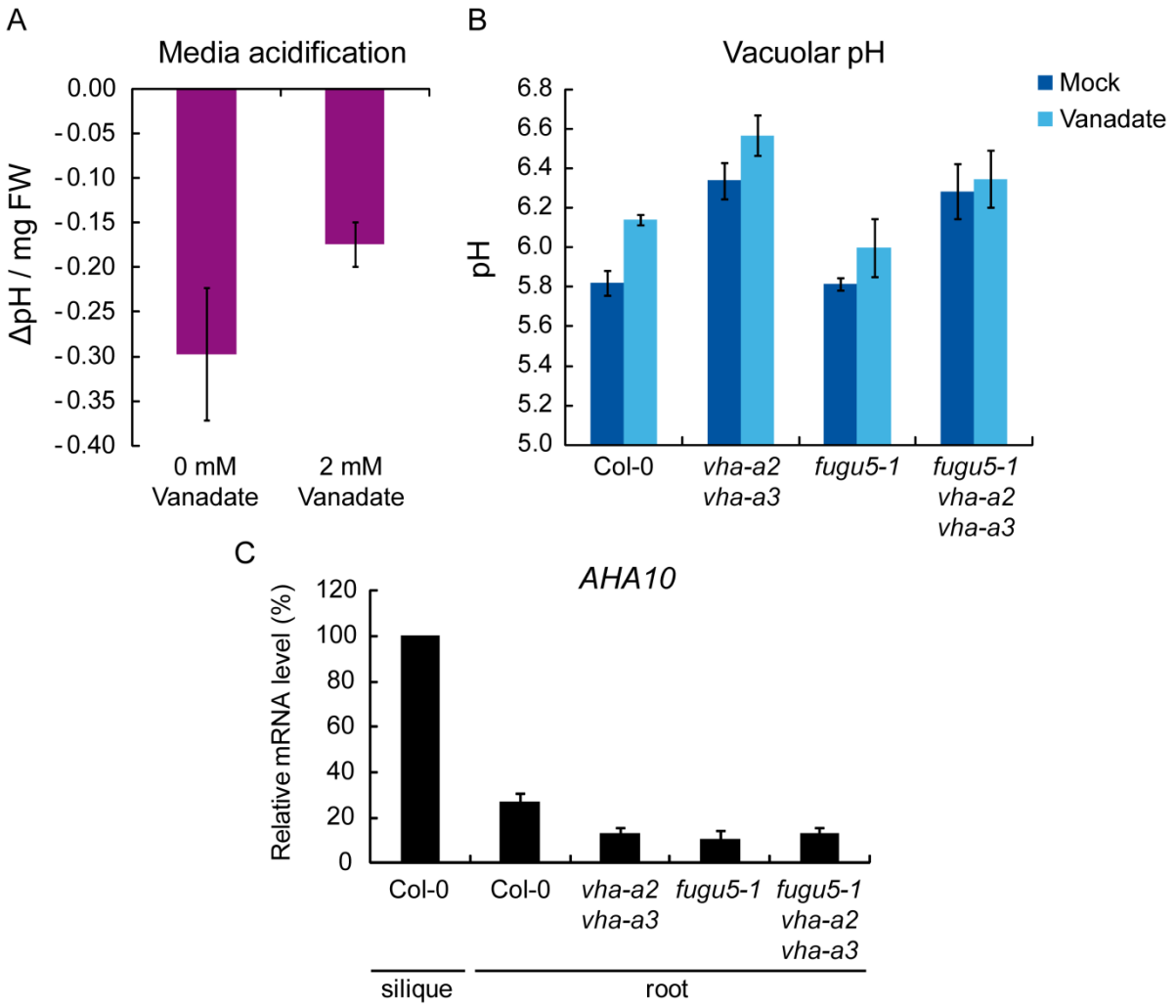

Figure 12. Plasma membrane P-type H^+-ATPase does not account for remaining vacuolar acidification in *fugu5-1 vha-a2 vha-a3*.

(A) Vanadate treatment reduces media acidification. 5-day-old wild type seedlings were incubated for 18 h in plant medium supplemented with or without 2 mM vanadate and then extracellular pH was quantified using fluorescein dye. Error bars represent SD of n = 8 technical replicates.
(B) Slight vacuolar alkalinization after vanadate treatment. Vacuolar pH was measured in roots of 6-day-old seedlings after treatment with or without 2 mM vanadate for 18 h. Error bars represent SD of n = 3 biological replicates.
(C) *AHA10* expression is not induced in vacuolar proton pump mutants. Relative *AHA10* transcript level was measured by qRT-PCR in roots of 6-day-old seedlings of the wild type and vacuolar proton pump mutants. Expression of *AHA10* in siliques served as a control since it was described to be primarily expressed in developing seeds. Error bars show SD of n =2 technical replicats.
Experiments shown in A and B were performed by Simon Delang and *AHA10* mRNA level were determined by M. Görkem Patir Nebioglu.

Generation of *VHA-a1* knockdown lines

Since the inhibition of P-type ATPases did not lead to drastic vacuolar alkalinization in proton pump mutants, we continued our investigations by analyzing the role of the TGN/EE localized V-ATPase that we also suggested to play a role in vacuolar acidification. So far, our hypothesis is based on a pharmacological treatment using ConcA. Therefore, we aimed to genetically confirm the contribution of VHA-a1 containing V-ATPase complexes to vacuolar acidification by using previously established *VHA-a1RNAi* lines that were shown to have reduced V-ATPase activity at the TGN (Brüx et al., 2008). In order to eliminate the possibility of a compensatory upregulation of the tonoplast V-ATPase, we crossed two independent *VHA-a1RNAi* lines with *vha-a2 vha-a3* and generated homozygous triple mutant plants. Due to the fact that the RNAi cassette was expressed under the control of the ethanol-inducible promoter *AlcA,* we first had to establish inducing conditions that resulted in efficient downregulation of *VHA-a1*. Therefore we grew wild type, *vha-a2 vha-a3* and plants expressing *VHA-a1RNAi* in the wild type and the *vha-a2 vha-a3* mutant background under varying ethanol concentrations and subsequently measured vacuolar pH. In general, we observed that not only *VHA-a1RNAi* plants but also wild type seedlings suffered strongly with increasing duration of ethanol treatment by showing reduced growth and pale leaves. However, vacuolar pH measurements revealed surprising results. Regardless of the amount of ethanol, the induction time and the genetic background, vacuoles were always more acidic which was in contrast to our expectations (Fig. S3). This suggests that ethanol stress conditions might induce V-PPase activity. Indeed, it was reported that the transcript and protein level of the rice V-PPase (*OVP3*) can be induced by anoxia indicating that also the Arabidopsis V-PPase might be upregulated under ethanol stress (Liu et al., 2010). Due to the fact that the application of ethanol resulted in strong acidification of the vacuolar lumen, we decided to generate lines expressing an artificial micro RNA specific for *VHA-a1* under the control of the dexamethasone (DEX)-inducible *pOP6/LhG4-GR* system. This transgene expression system consists of the ligand binding domain of a rat glucocorticoid receptor fused to the synthetic transcription factor *LhG4* which is released upon DEX addition, allowing it to enter the nucleus, where *LhG4* binds to the 6x*OP* promoter sequence to induce expression of the amiRNA (Craft et al., 2005). The construct was transformed into wild type, *vha-a2 vha-a3* and VHA-a1-

GFP (Dettmer et al., 2006) expressing plants. A total of 20-30 independent transformants were identified for each genetic background. Due to the previous observation that ethanol-inducible *VHA-a1RNAi* as well as *amiR-vha-a1* plants showed reduced hypocotyl elongation (Brüx et al., 2008), several lines with reduced hypocotyl length were identified by plating T2 families on medium containing dexamethasone. After choosing T2 lines with reduced hypocotyl length, they were further selected on hygromycin containing medium to establish homozygous lines.

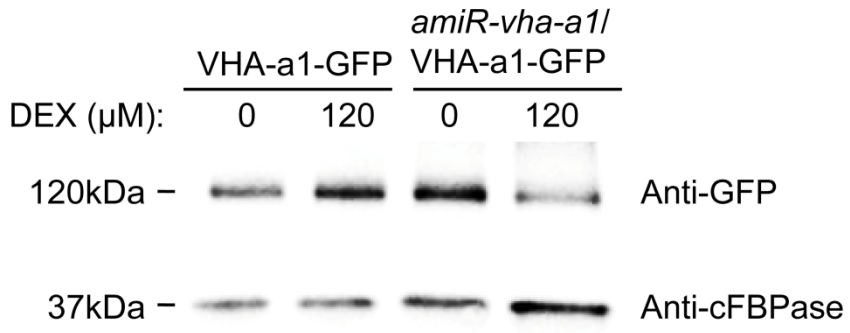

Figure 13. Induction of *amiR-vha-a1* leads to reduced VHA-a1 protein.

amiR-vha-a1 was expressed in the VHA-a1-GFP background in order to examine the VHA-a1 protein level by using a GFP antibody. VHA-a1-GFP served as a control. 10-day-old Arabidopsis seedlings were treated for 4 days with 120 µM dexamethasone and than total proteins were extracted, separated by SDS-PAGE and subsequently immunoblotted with anti-GFP antibody. Equal protein loading is indicated by cFBPase detection. The blot depicted is one representative of 3 independent experiments. Western blot was performed by Mariana Schuster.

In order to check whether the amiRNA against *VHA-a1* is functional, the VHA-a1 protein level was determined after DEX induction. Since to date no VHA-a1 antibody exists, we made use of the amiRNA lines in the VHA-a1-GFP background and detected GFP instead. A homozygous line expressing *amiR-vha-a1* in the VHA-a1-GFP background and the respective control line were grown for 10 days under non-inducing conditions and then subjected to medium containing dexamethasone to continue to grow for more 4 days. The immunoblot clearly demonstrated that the VHA-a1-GFP protein level was reduced after DEX induction (Fig. 13) indicating that the amiRNA is functional and can be used for further experiments.

Knockdown of *VHA-a1* results in TGN/EE aggregation

It has been shown that V-ATPase activity is required for the TGN/EE identity since ConcA treatment induced TGN vesicle aggregations (Viotti et al., 2010). To find out whether reducing VHA-a1 by the amiRNA leads to similar affects, we compared TGN/EE morphology in root cells of DEX-induced *amiR-vha-a1* lines and ConcA-treated plants. For this, we grew VHA-a1-GFP and *amiR-vha-a1* expressing VHA-a1-GFP on medium containing dexamethasone for subsequent analysis at the CLSM.

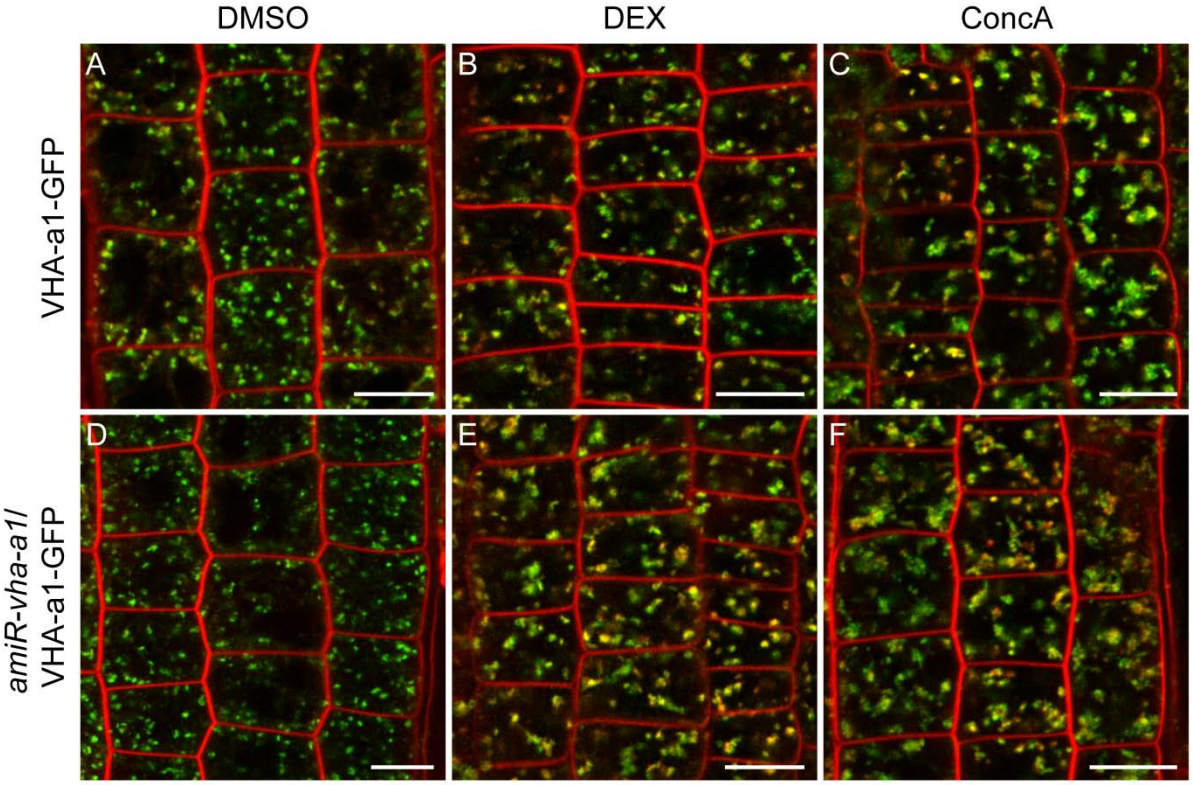

Figure 14. Induction of *amiR-vha-a1* leads to TGN/EE aggregation.

Seedlings of VHA-a1-GFP (first row) and *amiR-vha-a1*/VHA-a1-GFP (second row) were either grown on medium containing 10 µM DMSO ((A) and (D)) or 10 µM DEX ((B) and (E)) for 6 days prior to GFP detection in cells of the root meristem/elongation zone. ConcA treatment was performed for 4 h on 6-day-old roots prior to imaging ((C) and (F)). All root cells were stained with the endocytic tracer FM4-64 for 15 min. Bars = 10 µm. CLSM images were taken by Falco Krüger.

Seedlings for ConcA treatment were cultivated on standard growth medium prior to drug application. In addition, seedlings of both treatments were stained with the endocytic tracer FM4-64. As expected, a mobile, punctuate staining pattern was observed in VHA-a1-GFP and *amiR-vha-a1* expressing VHA-a1-GFP seedlings

treated with DMSO as well as in DEX treated VHA-a1-GFP roots (Fig. 14A, 14B and 14D). As previously described, ConcA treatment resulted in diffuse and enlarged TGN/EE morphology (Fig. 14C and 14F) indicating the establishment of a Golgi/TGN hybrid compartment (Dettmer et al., 2006). DEX-induced knockdown of *VHA-a1* led to a comparable GFP localisation pattern as in ConcA-treated root cells (Fig. 14E). Enlarged GFP fluorescence signals became visible pointing to the formation of TGN vesicle aggregations. Together, these results show that the genetic knockdown of *VHA-a1* has comparable effects on TGN morphology as ConcA inhibitor treatment and confirms that the amiRNA is indeed functional.

Reduced cell expansion and disturbed leaf vein patterning in *amiR-vha-a1* lines

Knowing that *amiR-vha-a1* lines have reduced VHA-a1-GFP protein levels and that they show the expected defects in TGN/EE identity, we analyzed to what extent plant growth is affected after induction. Since previous work already showed that ethanol-inducible knockdown lines of *VHA-a1* have reduced hypocotyl length (Brüx et al., 2008), we next analyzed whether the reduction in hypocotyl growth is comparable to the previously published ethanol-inducible lines. Therefore, we grew *amiR-vha-a1* lines for 4 days on medium supplemented with dexamethasone or DMSO and then measured hypocotyl length. Importantly, DMSO-treated seedlings of all lines showed similar hypocotyl length indicating that the DEX-promoter system is not leaky (Fig. 15A and 15B). The hypocotyl length of *amiR-vha-a1* #2-7 was reduced by around 50% whereas line #16-5 showed a reduction of 40% which in total results in slightly less inhibited cell elongation compared to *VHA-a1RNAi* lines. Moreover, we analyzed the root growth of DEX-induced *VHA-a1* knockdown lines grown for 12 days on vertical agar plates. Similar to the hypocotyl growth experiment, roots of deetiolated seedlings of line #2-7 were even stronger inhibited when compared to line #16-5 (Fig. 15C and 15D). Quantification of root length thus revealed around 75% reduction of line #2-7 whereas roots of #16-5 were shortened by 50%.

To explore the effect of *VHA-a1* downregulation on later developmental growth stages, we cultivated *amiR-vha-a1* plants on soil for 3 weeks and sprayed them twice with dexamethasone at day 13 and 18 after germination. Interestingly, around 3 days after DEX-treatment newly formed leaves exhibited serrations at the leave margins (Fig. 16A).

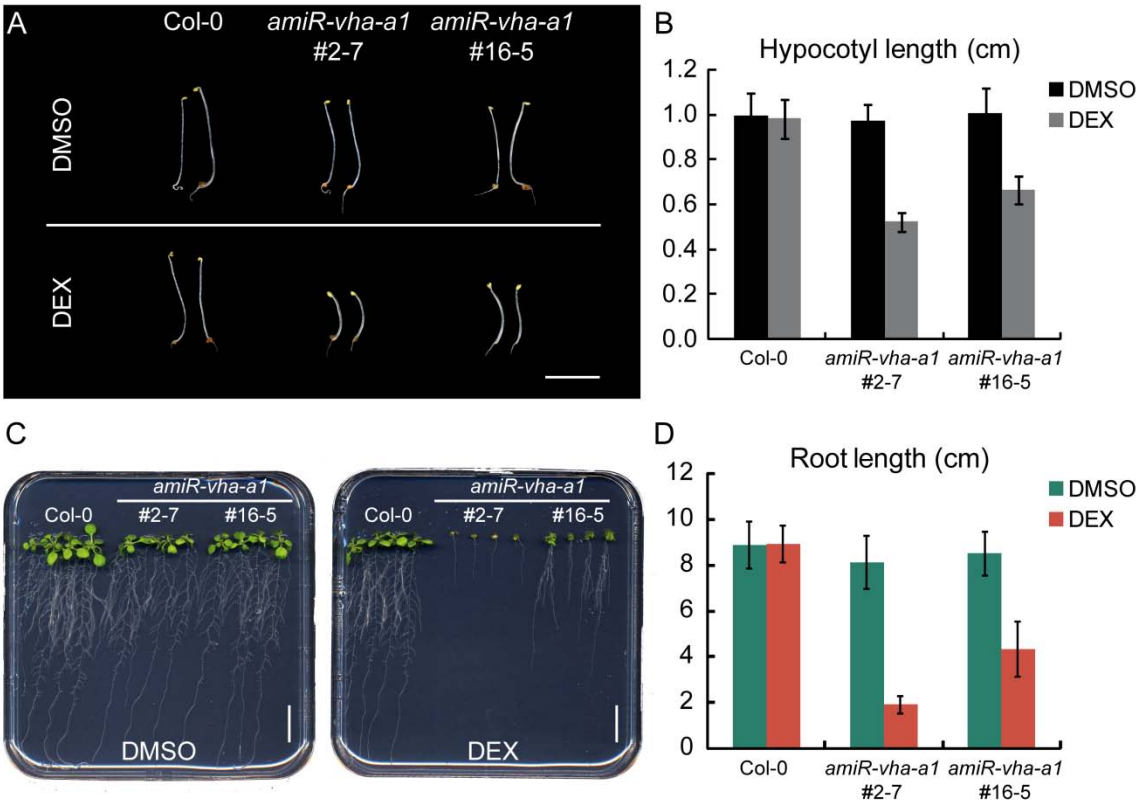

Figure 15. Reduced cell expansion in DEX-induced *amiR-vha-a1* plants.

(A) Morphological observation and (B) quantitative measurement of the hypocotyl length of DEX or DMSO treated wild type and two independent *amiR-vha-a1* lines. Etiolated seedlings were grown for 4 days on water agar containing either 10 µM dexamethasone or an equal amount of DMSO. Error bars represent SD of around 40 seedlings. Bar = 0.5 cm.
(C) Morphological observation and (D) quantitative measurement of the root length of DEX or DMSO treated wild type and *amiR-vha-a1* lines. Seedlings were grown for 12 days on horizontal agar plates supplemented with either 10 µM dexamethasone or an equal amount of DMSO. Error bars represent SD of n = 20 seedlings. Bar = 1.5 cm.

Serrations became more pronounced a few days after induction and moreover leaves started curling. In general, the rosette size of DEX-treated *amiR-vha-a1* plants was strongly reduced while line #2-7 was even smaller than #16-5. A closer look on single leaves clearly showed serrated leaf margins in DEX-induced *VHA-a1* knockdown lines (Fig. 16B). This led us to analyze vein patterning in *amiR-vha-a1* rosette leaves in more detail. Hence, DEX-treated leaves of wild type and *amiR-vha-a1* plants were excised and cleared in order to examine the leaf vein phenotype. In untreated leaves and DEX-treated wild type leaves secondary veins meet distally, whereas in induced *amiR-vha-a1* veins are discontinuous and show open ends inside serrations (Fig. 16C). In general, it appeared that DEX-induced *amiR-vha-a1* leaves had fewer higher order veins. Taken together, reducing VHA-a1 at the TGN inhibits cell expansion

leading to reduced hypocotyl and root growth, while adult *amiR-vha-a1* plants showed leaf serrations due to vein patterning defects.

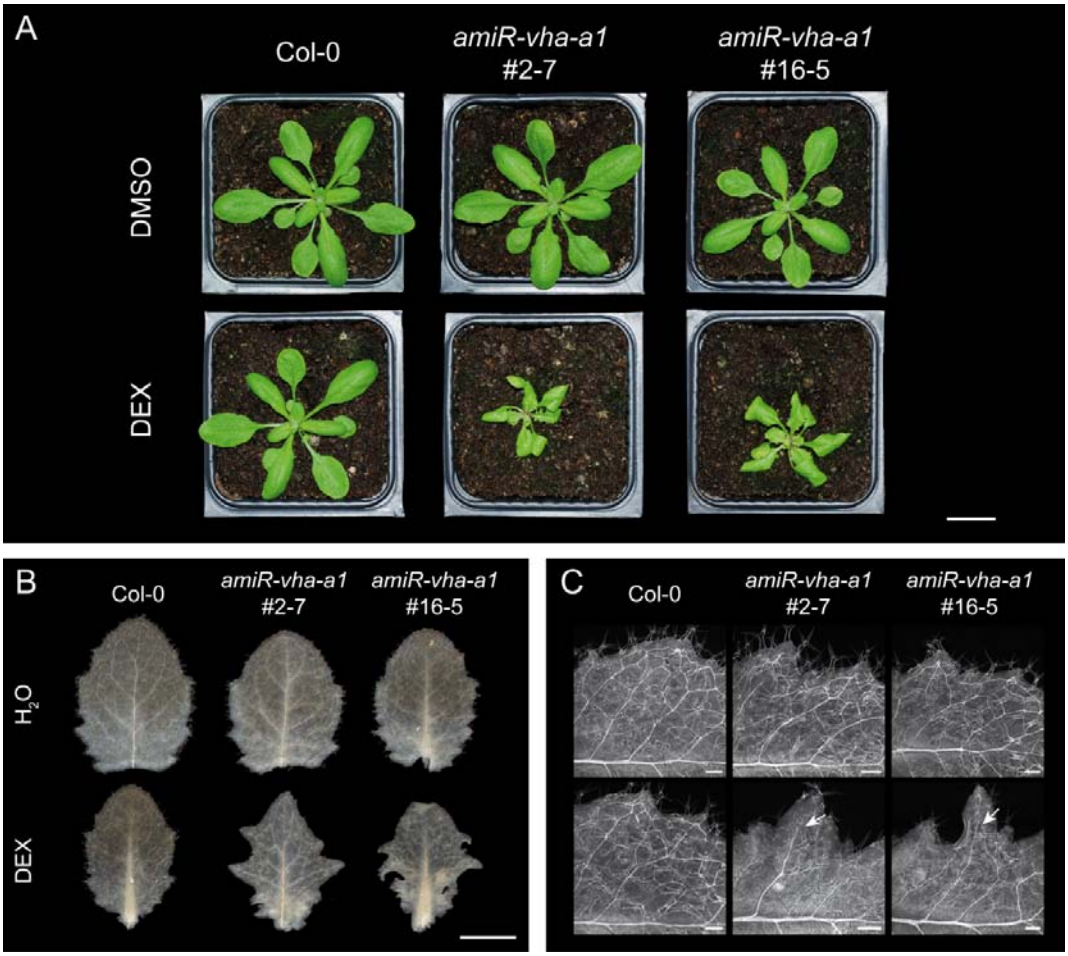

Figure 16. DEX-induced *amiR-vha-a1* plants show serrated leaves and vein patterning defects.

(A) Rosette growth phenotype of DEX-induced *amiR-vha-a1*. Plants were grown for 20 days under LD conditions at 22°C. Wild type, *amiR-vha-a1* #2-7 and *amiR-vha-a1* #16-5 were sprayed with 30 µM DEX or DMSO at 13 DAG and at 18 DAG. Bar = 1.75 cm.
(B) Leaf phenotype and vein pattern (C) of wild type and two *amiR-vha-a1* lines. Plants were grown for 20 days under LD conditions at 22°C. After 13 days of growth, genotypes were sprayed with 30 µM DEX or H_2O. Arrows in C represent secondary veins with open ends. Bars = 2 mm in B; 200 µm in C. Data shown in B and C were produced jointly with Stefan Scholl.

Vacuolar pH and proton pump activities of *amiR-vha-a1* expressing plants

To elucidate whether reduction of VHA-a1 at the TGN affects vacuolar acidification, we measured root vacuolar pH and rosette cell sap pH in *amiR-vha-a1* and wild type seedlings. For root vacuolar pH measurements, seedlings were pre-cultured on standard growth medium for 4 days and then transferred to induction medium

containing 50 µM DEX or DMSO for 2 days. Surprisingly, the induced knockdown of *VHA-a1* resulted in vacuolar acidification by 0.33 pH units in #2-7 and 0.22 pH units in #16-5 compared to non-induced seedlings (Fig. 17A).

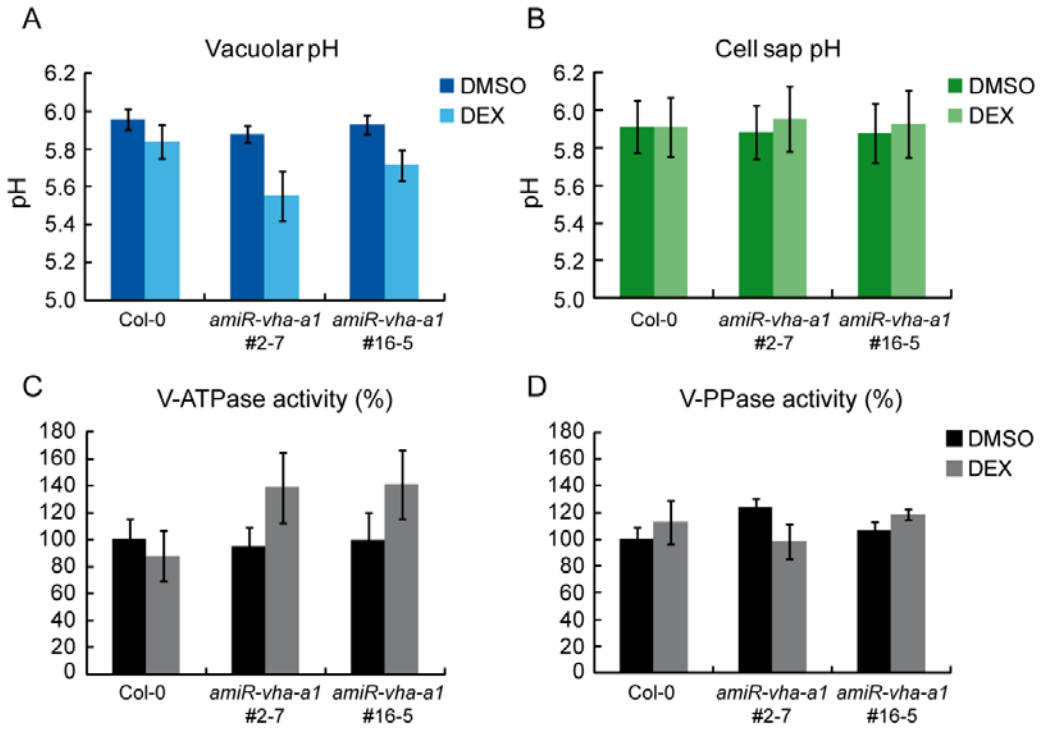

Figure 17. Reduction of TGN/EE V-ATPase induces activity of tonoplast V-ATPase.

(A) Vacuolar acidification after induction of *amiR-vha-a1*. Vacuolar pH was measured in roots of 6-day-old plants. Seedlings were pre-cultured for 4 days on agar plates and then transferred for 2 days to plates containing 50 µM DEX or DMSO. Error bars represent SD of n = 3 biological replicates.
(B) No change in cell sap pH after induction of *amiR-vha-a1*. Plants were grown for 22 days under LD conditions at 22°C. After 12 days wild type and two *amiR-vha-a1* lines were sprayed with 30 µM DEX or DMSO. Error bars show SD of n = 2 biological replicates.
(C) and (D) Induction of *amiR-vha-a1* induces V-ATPase activity. KNO_3-inhibited V-ATPase activity (C) and K^+-stimulated PPase activity (D) was determined on microsomal membranes extracted from 6-day-old plants. Seedlings were pre-cultured for 4 days on agar plates and then transferred for 2 days to plates containing 50 µM DEX or DMSO. The activity of wild type treated with DMSO was set to 100%. Error bars represent SE of n = 3 biological replicates. V-ATPase and V-PPase activity measurements shown in C and D were performed by M. Görkem Patir Nebioglu.

However, the cell sap pH of 3-week-old DEX-treated rosette leaves was unchanged (Fig. 17B). One possibility for the pH shift towards a more acidic vacuolar lumen upon VHA-a1 reduction at the TGN could be an increase of the tonoplast-localized V-ATPase activity. To test this, the V-ATPase activity was measured in plant material cultivated under the same conditions as those used for vacuolar pH measurements.

Intriguingly, V-ATPase activity was elevated by 40% in induced *amiR-vha-a1* lines (Fig. 17C). To check whether the reduced vacuolar pH is specifically caused by increased V-ATPase activity, we further determined V-PPase activity in the same lines. Indeed, V-PPase activity was not elevated after DEX induction (Fig. 17D). In summary, these results demonstrate a crosstalk between the TGN/EE and the vacuole to control pH.

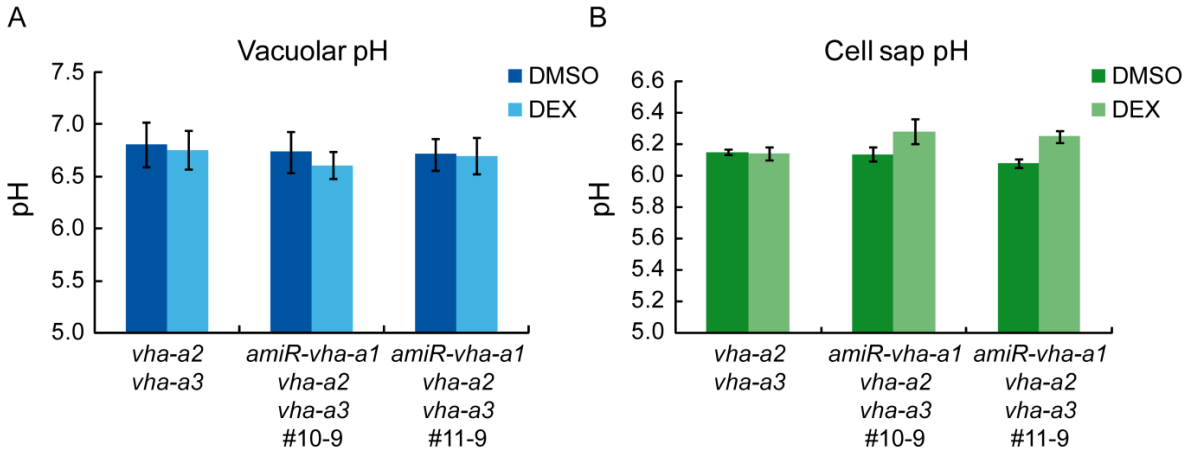

Figure 18. Knockdown of *VHA-a1* in *vha-a2 vha-a3* has no effect on vacuolar pH.

(A) Vacuolar pH in DEX-induced *amiR-vha-a1* expressed in tonoplast V-ATPase double mutant background. Seedlings were grown for 6 days on agar plates containing 30 µM DEX or DMSO. Error bars show SD of n = 15 roots.
(B) Cell sap pH of DEX-induced *amiR-vha-a1* in *vha-a2 vha-a3*. Plants were grown for 22 days under CL conditions at 22°C. After 12 days *vha-a2 vha-a3* and two *amiR-vha-a1 vha-a2 vha-a3* lines were sprayed with 30 µM DEX or DMSO. Error bars show SD of n = 5 technical replicates. Cell sap pH measurements shown in B were performed by M. Görkem Patir Nebioglu.

Due to the increased activity of the tonoplast V-ATPase upon reduction of VHA-a1 at the TGN, we next measured vacuolar pH in mutant plants expressing *amiR-vha-a1* in the *vha-a2 vha-a3* background. As expected, no acidification was observed in the vacuolar lumen of DEX-induced *amiR-vha-a1 vha-a2 vha-a3* plants. However, we also did not measure an increase in vacuolar pH (Fig. 18A). The cell sap pH in turn was slightly less acidic after DEX induction (Fig. 18B). These results reveal that, by using *amiR-vha-a1*, we were so far not able to genetically confirm the vacuolar alkalinization achieved by ConcA treatment.

Supplementary Figures

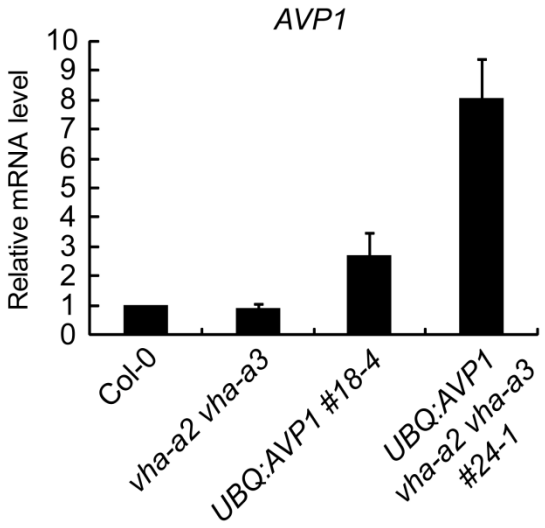

Figure S1. Increased transcript level of the V-PPase in *UBQ:AVP1* lines.

The transcript level of *AVP1* was measured by qRT-PCR in 3-week-old rosette leaves of wild type, *vha-a2 vha-a3, UBQ:AVP1 and UBQ:AVP1 vha-a2 vha-a3* plants grown under LD conditions. Error bars indicate SD of n = 3 biological replicats.

Figure S2. Abnormal cotyledon phenotypes in vacuolar proton pump triple mutants.

Seedlings of the wild type, *fugu5-1 vha-a2 vha-a3* and *vhp1-1 vha-a2 vha-a3* were grown on 0.5 MS medium for 8 days under LD conditions before pictures of individual seedlings were taken. Photographs show examples of seedlings with cup-shaped, fused or single cotyledons.

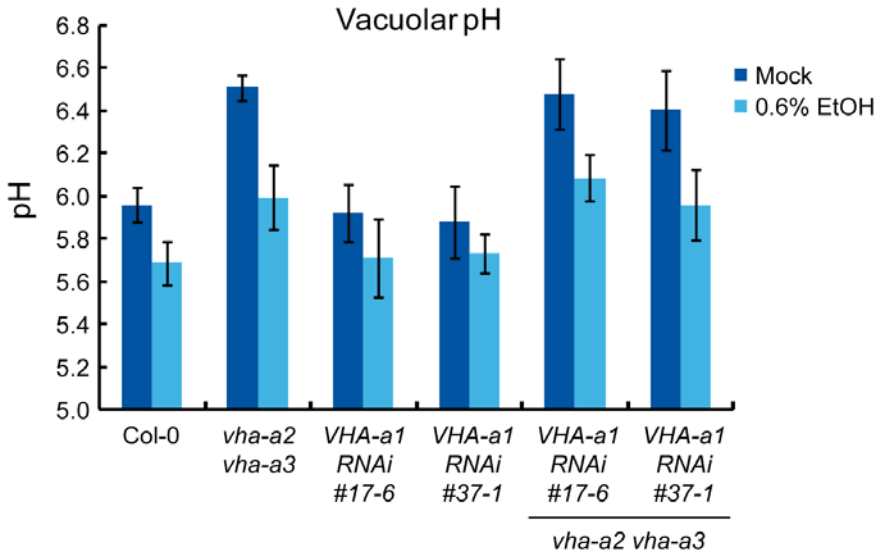

Figure S3. Acidification of the vacuolar lumen after ethanol treatment.

Root vacuolar pH was measured after ethanol treatment of wild type, *vha-a2 vha-a3* and *VHA-a1RNAi* expressed in the wild type and the *vha-a2 vha-a3* background. Seedlings were grown for 10 days in liquid growth medium and then subjected to medium containing 0.6% ethanol for more 2 days. Error bars show SD of n = 8 technical replicats.

I.4 Discussion

The V-PPase cannot replace the V-ATPase at the tonoplast

Based on the fact that the proton concentration in vacuoles of the *vha-a2 vha-a3* mutant (pH 6.4) lacking V-ATPase activity at the tonoplast is still 10-fold higher than in the cytosol (pH 7.4), it was suggested that the activity of the V-PPase could be responsible to a large extent for the remaining proton gradient (Krebs et al., 2010). Moreover, a compensatory response by the V-PPase in the *vha-a2 vha-a3* double mutant could not be determined since neither the *AVP1* transcript, nor PP_i-induced H^+ currents (Krebs et al., 2010) and the V-PPase enzyme activity were elevated. This could indicate that the normal level of V-PPase activity is sufficient to keep the vacuolar pH at the level of *vha-a2 vha-a3*. That the V-PPase indeed is an important player for maintaining vacuolar pH has been demonstrated in shoots of the *fugu5-1 vha-a2 vha-a3* mutant. There, the vacuolar pH was nearly neutral when compared to *vha-a2 vha-a3*. However, the pH in V-PPase single mutants was unchanged. In order to investigate whether increasing the level of the V-PPase can restore the wild type phenotype in *vha-a2 vha-a3,* we ubiquitously expressed *AVP1*. However, an elevated AVP1 protein and activity level in the *vha-a2 vha-a3* background did not re-establish the vacuolar pH to wild type levels in either root or shoot, and did not phenotypically complement the V-ATPase double mutant. One reason could be that not all the increased protein is active. This can be supported by the fact that a 4.5-fold increase of V-PPase protein was observed in *UBQ:AVP1 #18-4* but enzyme activity of this line only doubled. Posttranslational modifications such as phosphorylation, acetylation, methylation and glycosylation are known to affect enzyme activity. It is thus possible that the elevated AVP1 protein lacks certain posttranslational modifications that allow the enzyme to utilize its full potential. Another reason for the lack of complementation might be PP_i substrate limitation. The fact that Arabidopsis contains 5 soluble pyrophosphatases in the cytosol (PPa1 to PPa5; ÖZTÜRK et al., 2014) indicates that the amount of cytosolic PP_i needs to be shared between membrane bound and soluble PPases. In contrast to Arabidopsis, it has been shown that heterologous expression of AVP1 in *S. cerevisiae* indeed can efficiently substitute for the yeast V-ATPase that has been either chemically inhibited through bafilomycin or functionally impaired by mutation of the catalytic subunit (yeast *vma* mutant; Pérez-Castiñeira et

al., 2011). A chimeric AVP1 protein, consisting of the N-terminal V-PPase signal sequence of the protist *Trypanosoma cruzi* (TcVP) fused to *AVP1* (TcAVP1 and TcGFPAVP1) functionally substituted for the lacking V-ATPase more efficiently than the native AVP1 from Arabidopsis which was explained by higher overall expression levels of the chimeric proteins. Thus, the expression of *AVP1* and its chimeric derivatives led to the detection of membrane-associated V-PPase and PP_i-induced H^+ pumping activities and recovered vacuolar acidification in the yeast *vma* mutant. Interestingly, the authors highlight the fact that AVP1 cannot pump protons when the yeast soluble PPase is present in the cytosol likely due to substrate competition. Only when the activity of the soluble PPase was decreased to a negligible level, AVP1 was able to efficiently operate and complement Vma^- phenotypes. To analyze whether also in Arabidopsis substrate limitation affects the function of membrane-bound V-PPases, it would be of interest to measure vacuolar pH in lines expressing the yeast soluble PPase *IPP1* in the wild type background (*AVP1*$_{Pro}$*:IPP1*/WT; Ferjani et al., 2011). In summary, our data show that overexpressing AVP1 is not sufficient for complementing *vha-a2 vha-a3,* which could be explained by the lack of substrate availability and missing protein modifications. In contrast, the plant V-PPase is able to compensate for the lacking yeast V-ATPase.

Abiotic stress triggers the V-PPase

To further elucidate the contribution of the V-PPase for vacuolar acidification, we examined *fugu5-1*/*vhp1-1* loss-of-function mutants. In accordance with previous results, the complete lack of V-PPase activity resulted in only slightly reduced vacuolar acidification suggesting that the V-PPase plays a minor role as a vacuolar proton pump under standard conditions, but is rather important for efficient removal of PP_i from the cytosol (Ferjani et al., 2011). The authors based this on the observation that *fugu5-1* cotyledon and cellular phenotypes could be fully recovered by the expression of yeast *IPP1* under the control of the *AVP1/FUGU5* promoter, hence demonstrating that PP_i removal from the cytosol of *fugu5-1* is necessary and sufficient to restore wild type growth (Ferjani et al., 2011). Although it was shown that neither the V-ATPase activity, nor protein levels of V-ATPase subunits VHA-A and VHA-a were increased in *fugu5-1* mutants (Ferjani et al., 2011), compensation by increased V-ATPase activity can still not be excluded since electrophysiological data

are lacking. Moreover, the fact that removing the tonoplast V-ATPase in addition to the V-PPase led to a neutralized cell sap pH provides evidence for the V-PPase being a proton pump. In addition, it has been suggested that the V-PPase might have to be triggered by certain stimuli to exploit its full potential as a proton pumping enzyme. It was shown that in addition to V-ATPase subunits, the protein abundance of the V-PPase was also increased after cold acclimation (Schulze et al., 2012). To achieve freezing tolerance, solutes such as glucose and fructose are accumulated inside the vacuole at the expense of protons to reduce the freezing point of the vacuolar cell sap (Schulze et al., 2012). Furthermore, hypocotyls of mung bean (*Vigna radiata*) that were incubated at 4°C for up to 72 h showed an increase in V-PPase protein, activity and H^+ pumping (Darley et al., 1995) and rice seedlings that were cold treated showed similar effects (Carystinos et al., 1995). Oxygen deprivation, which is a result of flooding due to reduced diffusion of O_2 in water relative to air, caused a strong increase of the transcript and protein level of the rice V-PPase OVP3 (Liu et al., 2010). Under anoxic conditions the production of ATP drops drastically due to decreased oxidative phosphorylation which results in an energy crisis and a switch from aerobic respiration to anaerobic fermentation. It was therefore suggested that cytosolic PP_i substitutes for ATP as an energy source under anoxia, hence the activity of the V-PPase becomes more relevant in order to maintain proton pumping (Huang et al., 2008). Indeed, results presented herein support the assumption that PP_i-mediated processes are preferred under certain stress conditions. Growth of Arabidopsis seedlings under high ethanol conditions led to a decrease in vacuolar pH in all the mutant lines which could indicate that H^+ pumping mediated by the V-PPase is induced under these stress conditions. A stable concentration of PP_i also seems to be important for adaptation to the lack of O_2. Mustroph and colleagues have shown that sucrose breakdown via the PP_i-dependent pathway is more severely inhibited during hypoxia in potato plants expressing the *E. coli* PPase in the cytosol than in wild type plants indicating that stable levels of PP_i are important to maintain glycolytic metabolism under O_2 deprivation (Mustroph et al., 2005).

Thus, do plants benefit from AVP1 overexpression under abiotic stress? Indeed, *UBQ:AVP1* plants were found to be more resistant to low temperatures compared to wild type plants (M. Görkem Patir Nebioglu, Master thesis). Conversely, V-PPase

mutants *fugu5-1* and *vhp1-1* were more sensitive to cold treatment showing reduced fresh weight and root growth. So far, it is not clear whether PP_i hydrolysis or rather H^+ pumping are responsible for these stress responses. Therefore, it would be interesting to analyse whether cold treatment of *UBQ:AVP1 vha-a2 vha-a3* plants at least partially restores the vacuolar pH to the wild type level. Taken together, our results show that either by eliminating the tonoplast V-ATPase in addition to the V-PPase in Arabidopsis shoots or through induction by certain abiotic stimuli, the function of the V-PPase as a proton pump becomes evident. Additionally, the second role of the V-PPase, PP_i hydrolysis, has to be taken into account when evaluating its importance in adaptation to stress.

The metabolite profile of *fugu5-1 vha-a2 vha-a3* shoots reveals adaptations to drought stress

In accordance with its function as a proton pump, the lack of the V-PPase in addition to the V-ATPase led to a neutralized cell sap pH. Moreover, those plants show severe growth reduction when compared to *vha-a2 vha-a3*. However, although the proton motive force that drives secondary active transport is even more reduced in the triple mutant, the metabolite profile was similar to that of *vha-a2 vha-a3*. The reduced cell sap pH together with the nearly unchanged metabolite profile could indicate that protons were used for ion storage inside the vacuole. It is then questionable where protons end up that accumulate inside the cytosol. Since cytosolic pH has to be kept stable, protons are presumably exported from the cell into the apoplast. This has indeed been suggested for *vha-a2 vha-a3,* where an increased level of external acidification was determined (Melanie Krebs, unpublished). Accordingly, it would be expected that *fugu5-1 vha-a2 vha-a3* has an even higher level of media acidification.

Although the concentration of many metabolites was affected to a similar extent in V-ATPase double mutant and the triple mutant, the few existing metabolic changes were pointing towards one common stress response that was more pronounced in *fugu5-1 vha-a2 vha-a3*. Intriguingly, the amount of all amino acids is elevated in *vha-a2 vha-a3*, however concentrations are much higher in *fugu5-1 vha-a2 vha-a3* with one particular amino acid, proline, being three times higher than in *vha-a2 vha-a3* and more than sixty times increased compared to the wild type. Proline was

described to be among the most widely distributed osmolytes accumulating in various organisms in response to water stress and salinity (Strizhov et al., 1997). It is a ROS scavenger and serves as a molecular chaperone to stabilize protein structure (Krasensky and Jonak, 2012). The ability of proline to directly act as an osmoprotectant in plants was tested in petunia and tobacco overexpressing Δ^1-pyrroline-5-carboxylate synthetase (P5CS), which resulted in elevated proline levels and enhanced salt and drought tolerance (Kishor et al., 1995; Yamada et al., 2005). Arabidopsis plants lacking P5CS1 resulted in the decrease of stress-induced proline synthesis leading to hypersensitivity against salt stress and ROS accumulation (Székely et al., 2008). In addition, it is remarkable that a multitude of sugars are strongly increased in *fugu5-1 vha-a2 vha-a3* as well as in *vha-a2 vha-a3*. Among them, trehalose, a nonreducing disaccharide of glucose, and raffinose, a product of galactose and sucrose, have been implicated in metabolic adaptations against abiotic stress (Krasensky and Jonak, 2012). Trehalose accumulates in desiccation-tolerant plants and at sufficient levels can also function as an osmolyte in addition to stabilizing proteins and membranes. Elevated levels of trehalose improved salt, drought and cold tolerance and decreased oxidative damage in transgenic rice plants overexpressing trehalose biosynthetic genes from *E. coli* (*otsA* and *otsB*). However, constitutive overexpression can result in growth defects and dwarfism under normal growth conditions (Garg et al., 2002; Peleg et al., 2011). Due to overall low levels of trehalose in transgenic plants (below 1 mg/g fresh weight) its relevance as compatible solute is presumably rather low, however the signalling function of trehalose and trehalose-6P could be more important since it was demonstrated that its accumulation correlates with higher soluble carbohydrate levels and increased photosynthetic capacity under stress and nonstress conditions (Garg et al., 2002; Peleg et al., 2011). Raffinose, which was forty times higher in *fugu5-1 vha-a2 vha-a3* than in wild type leaf extracts, has been suggested to scavenge hydroxyl radicals to protect plant cells from oxidative damage. In addition, raffinose accumulated in plants that experience abiotic stress such as drought, salinity and cold (Krasensky and Jonak, 2012; Nishizawa et al., 2008). Overexpression of an Arabidopsis stress-responsive galactinol synthase (*GolS*) caused elevated levels of galactinol and raffinose which led to improved drought tolerance, thus suggesting a role as osmoprotectants (Taji et al., 2002). The fact that many of the metabolites with elevated levels in *vha-a2 vha-a3* and, more drastically, in *fugu5-1 vha-a2 vha-a3* can

be associated with adaptations to abiotic stress such as drought and salinity points to the possibility that the lack of all vacuolar proton pumps leads to reduced vacuolar uptake of solutes that in turn initiates internal stress responses. This can be supported by higher levels of sodium and potassium that are presumably cytosolic due to a reduced proton motive force at the vacuole of proton pump mutants. It is remarkable that the comparison of *nhx1 nhx2* plants, lacking two tonoplast-localized Na^+,K^+/H^+ antiporter, with *fugu5-1 vha-a2 vha-a3* indeed revealed striking similarities with respect to their phenotypes (Bassil et al., 2011). Growth of *nhx1 nhx2* was shown to be strongly compromised originating from reduced cell length and cell width. In addition, hypocotyls were shorter although to a lesser extent than *fugu5-1 vha-a2 vha-a3*. Moreover, *nhx1 nhx2* filaments were shorter and anthers were non-dehiscent which led to the infrequent formation of siliques, which again is similar to defects in *fugu5-1 vha-a2 vha-a3* reproductive organs. Bassil and coworkers suggested that growth reduction of *nhx1* nhx2 plants could be due to an increased cytosolic K^+ concentration, however to date little is known about cellular responses to increased cytosolic K^+. Interestingly, the transcript level of *NHX1* was found to be downregulated in *fugu5-1 vha-a2 vha-a3* (data not shown). In order to confirm the assumption that the triple mutant shows a constitutive stress response, it would be interesting to analyse the expression level of drought-responsive genes in *fugu5-1 vha-a2 vha-a3* and to assess whether levels of abscisic acid (ABA), an integral regulator of abiotic stress signalling, are increased. It was previously shown that the accumulation of stress-induced proteinogenic amino acids, including proline, was induced and dependant on ABA (Kempa et al., 2008; Urano et al., 2009). Taken together, examining the metabolite profile gives insights into cellular adaptations to the reduced proton gradient at the tonoplast.

Cell expansion without vacuolar proton pumps?

Cell expansion is compromised in *fugu5-1 vha-a2 vha-a3*, however it is surprising that these cells are still able to elongate without functioning vacuolar proton pumps. Assuming that the vacuolar proton gradient in hypocotyl cells of *fugu5-1 vha-a2 vha-a3* is decreased, this could lead to reduced accumulation of osmotic ions such as Na^+, K^+ and Cl^- as it was shown for rosette leaves of the triple mutant. Thus, vacuolar storage of alternative solutes presumably becomes important to maintain osmotic

pressure and cell expansion. Possibly, this is mediated by the controlled breakdown and re-synthesis of osmotically inactive polymers such as starch or polyphosphates (Marty, 2001). Indeed, the interconversion of sugar-starch or malate-starch is a known process for osmoregulation. Glucose and fructose can accumulate to keep internal osmotic pressure. The vacuolar buffering capacity is mainly associated with malate, citrate and phosphate and is an important determinant when it comes to vacuolar pH modifications (Mathieu et al., 1989). Interestingly, at pH 6.5 vacuoles that were enriched with inorganic phosphate (P_i) had an increase in their buffering capacity of about 5-fold when compared to vacuoles of normal cells (Mathieu et al., 1989). Together, these metabolic adjustments could cause moderate cell expansion as observed in *fugu5-1 vha-a2 vha-a3*.

Roots have different V-PPase demands as observed in *fugu5-1 vha-a2 vha-a3*

In contrast to rosette leaves, the root vacuolar pH of *fugu5-1 vha-a2 vha-a3* was not altered when compared to *vha-a2 vha-a3*. Importantly, the root elongation/transition zone has to be considered separately since there the vacuolar pH values were in general higher with a maximum of the vacuolar pH in *fugu5-1 vha-a2 vha-a3* (pH 7.28). In line with an increased vacuolar pH, the vacuolar morphology was specifically changed in this root zone. Vacuolar pH changes have been previously demonstrated to go along with altered vacuolar morphology during ABA-induced stomatal closure (Bak et al., 2013). It was demonstrated that guard cell vacuoles of fava bean (*Vicia faba*) became highly convoluted, showing a folded structure during stomatal closure which was accompanied by vacuolar acidification. Accordingly, stomatal closure was delayed in guard cells of plants lacking the tonoplast V-ATPase or V-PPase. Moreover they found that phosphatidylinositol 3,5-bisphosphate [PtdIns(3,5)P_2] is necessary for vacuolar acidification and convolution during ABA-induced stomatal closure. In addition, Oh et al. demonstrated that when mutating SOS1 (Salt Overly Sensitive 1), a Na^+/H^+ antiporter at the plasma membrane, both vacuolar shape and pH changed in the root tip compared to vacuoles of wild type roots (Oh et al., 2010). The fact that mainly vacuoles in the elongation zone are affected by the lack of proton pumps may not be a coincidence since cells are rapidly expanding, thus the need of the proton gradient and the uptake of osmolytes is of particular importance. According to our data, it appears that vacuoles in the

elongation zone of *fugu5-1 vha-a2 vha-a3* are delayed in building up osmotic pressure, however they acquire wild type shape in the differentiation zone. Therefore it is not surprising that determination of the length of individual root zones resulted in a prolonged elongation zone in *fugu5-1 vha-a2 vha-a3* when compared to the wild type. Interestingly, also in *vha-a2 vha-a3* where defects in the vacuolar shape started to develop, the elongation zone was found to be extended, whereas vacuolar morphology of the transition zone was not affected. The fact that vacuoles in the transition zone of *fugu5-1 vha-a2 vha-a3* roots showed disturbed vacuole formation, while *vha-a2 vha-a3* did not, could be the reason for the difference in total root length of the two mutants. The measurement of cell size and cell number in individual root zones would provide evidence to what extent cells are affected by the lack of correct vacuole formation. Oh and co-workers described the root elongation zone as 'particularly vulnerable' since cells of RNAi lines from *Thellungiella salsuginea SOS1* (*thsos1*), a halophytic Arabidopsis-relative, showed specific local injury after growth on high salt concentrations (Oh et al., 2009). Thus, Na^+ exclusion by SOS1 is of special importance in expanding cells, whereas adjacent meristematic root cells seemed to be protected due to the lack of large central vacuoles.
Taken together, our results suggest that the presence of the V-PPase in shoots is indeed important for proper rosette growth while in roots the V-PPase is only transiently required to ensure rapid cell expansion.

Alteration of the TGN/EE V-ATPase pool influences vacuolar pH

As a partial result of our studies that aim to decipher, in addition to the V-ATPase, the main player(s) responsible for establishment of the acidic vacuolar lumen we so far can conclude that in roots the V-PPase plays a minor role under standard conditions, however we found that another pool of proton pumps, the TGN/EE localized V-ATPase, affects vacuolar pH. Application of ConcA, which specifically blocks V-ATPase function and transport of soluble and endocytic cargo to the vacuole (Dettmer et al., 2006; Viotti et al., 2010), led to a completely neutralized vacuolar lumen not only in the wild type but also in all vacuolar proton pump mutants. This severe alkalinization can be attributed to inhibition of VHA-a1 containing V-ATPases at the TGN/EE since these are the only V-ATPase complexes left in *vha-a2 vha-a3* and *fugu5-1 vha-a2 vha-3*. Consequently, we next attempted to confirm the

contribution of VHA-a1 containing complexes to vacuolar pH by genetically reducing VHA-a1. In contrast to our expectations, the induction of *amiR-vha-a1* resulted in even more acidic root vacuoles. Measurement of total V-ATPase activity revealed an increase in both independent lines indicating a compensatory upregulation of the tonoplast V-ATPases that are still present in *amiR-vha-a1*. This was only true for roots of *amiR-vha-a1* since no acidification was observed in adult rosette leaves as revealed by cell sap pH measurements. Moreover, we found that this compensatory response was specifically caused by the tonoplast V-ATPase since the V-PPase activity was unaffected after downregulation of VHA-a1. This was supported by the observation that no vacuolar acidification was observed after induction of *amiR-vha-a1* expressed in the *vha-a2 vha-a3* background. Thus, these results demonstrate that modification of the V-ATPase level at the TGN/EE is recognized by V-ATPases residing at the tonoplast, ultimately leading to alteration of their activity. The question which then arises is how the tonoplast V-ATPase activity is regulated under these conditions. In general, upon environmental changes plants are able to adjust the activity of proteins rapidly in order to maintain optimal functioning of cellular transport processes. This can be achieved by posttranslational modifications that are known to affect enzyme activity, localization and turnover (Mann and Jensen, 2003). One important mechanism of V-ATPase regulation is the reversible disassembly of the V_1 and V_o subcomplexes, which has been described for yeast, insects and mammals (Qi et al., 2007). In yeast, dissociation of V-ATPase complexes occurs rapidly and reversibly in response to glucose depletion and does not require new protein synthesis (Kane, 1995). Thus, it would be interesting to test whether the enhanced tonoplast V-ATPase activity is a result of an increased assembly state of the two complexes, which would allow fast adaptation. In addition, reversible phosphorylation has been described to be important for regulation of vacuolar transport processes (Neuhaus and Trentmann, 2014). A phosphoproteomic approach of tonoplast preparations from barley (*Hordeum vulgare*) mesophyll protoplasts revealed phosphorylation sites in several V-ATPase subunits of the V_1 complex (Endler et al., 2009). It has been shown that SOS2, a Ser/Thr kinase, can interact with peripheral subunits of the V-ATPase to increase ion transport during salt stress and thus promote salt tolerance (Batelli et al., 2007). Tonoplast vesicles isolated from *sos2-2* mutants revealed a reduced H^+ transport activity, whereas *det3* seedlings were shown to be highly salt sensitive, emphasizing that proper functioning of both

proteins is necessary for salt stress responses. Moreover, in etiolated barley coleoptiles, 14-3-3 proteins have been demonstrated to interact with the V-ATPase and enhance its enzyme activity in response to a short blue light treatment (Klychnikov et al., 2007), again suggesting a regulatory role of V-ATPase phosphorylation as 14-3-3 proteins are known to interact with phosphorylated amino acids. Another report shows that the application of gibberellic acid (GA_3) leads to acidification of barley aleurone cells by altering activities but not the protein amount of vacuolar proton pumps, however, the underlying mechanism is unclear (Swanson and Jones, 1996). Accordingly, it is also possible that phosphorylation of certain V-ATPase subunits leads to enhanced activity upon VHA-a1 reduction at the TGN. To test the inverse situation and thereby investigate whether this regulation is bidirectional, it would be interesting to measure the pH of the TGN/EE in the *vha-a2 vha-a3* double mutant.

Vacuolar acidification in *fugu5-1 vha-a2 vha-a3*

In our attempt to uncover proteins responsible for acidification of the vacuole, we found that inhibition of the TGN/EE V-ATPase neutralizes the vacuolar pH as observed through the application of ConcA on *vha-a2 vha-a3* and *fugu5-1 vha-a2 vha-a3* mutant seedlings. However, so far we were not successful in confirming the contribution of VHA-a1 containing V-ATPases to vacuolar acidification by silencing VHA-a1 through the use of VHA-a1-specific artificial microRNAs. Instead, downregulation of VHA-a1 in the wild type background seemed to cause compensatory upregulation of the tonoplast V-ATPase, resulting in even more acidic pH values. Although the removal of VHA-a2 and VHA-a3 in addition to VHA-a1 reduction eliminated vacuolar acidification, an increased alkalinization compared to *vha-a2 vha-a3* was not observed. This can have several reasons. One possibility could be that the amiRNAs do not sufficiently silence VHA-a1. In line with this assumption, the Golgi/TGN morphology in ConcA-treated wild type plants differs from DEX-treated *amiR-vha-a1* seedlings. Golgi/TGN hybrids were more evident in ConcA treated cells when compared to DEX-treated ones. Thus, the strength of VHA-a1 silencing might be insufficient to show obvious effects on vacuolar pH. In fact, we do not know to what extent VHA-a1 is downregulated in *amiR-vha-a1 vha-a2 vha-a3* since we only measured the VHA-a1 protein level in *amiR-vha-a1*/VHA-a1-GFP lines.

Moreover, it is conceivable that the remaining V-ATPase activity at the TGN in *amiR-vha-a1* lines is sufficient for acidification of this compartment. However, even a slight reduction of the VHA-a1 protein might be enough to cause phenotypical growth defects as observed for DEX-induced *amiR-vha*-a1 plants prior to alteration of pH. Proteins from the CLC-family localized to the TGN/EE also have been implicated in TGN/EE pH homeostasis. Mutants lacking *CLCd*, a chloride transporter, showed hypersensitivity towards ConcA (von der Fecht-Bartenbach et al., 2007). However, certainly it is important to confirm whether phenotypes observed in DEX-induced *amiR-vha-a1* plants are indeed caused by silencing of VHA-a1 as opposed to off-target effects (Xu et al., 2006). One possibility to test this, is to introduce a silent mutation into the VHA-a1 microRNA binding site to generate VHA-a1 mRNAs that are microRNA resistant. If phenotypes were indeed caused by VHA-a1 knockdown, introduction of modified VHA-a1 transcripts into *amiR-vha-a1* should disappear. Alternatively, since ConcA treatment inhibits the V-ATPase activity and blocks vacuolar transport it might be that vacuolar alkalinization is not a result of inhibition of the TGN/EE V-ATPase and therewith reduced proton delivery to the tonoplast, but instead proteins essential for the vacuolar pH homeostasis could be prevented from reaching their final destination. This is currently being addressed by Stefan Scholl (PhD student, group of Prof. Schumacher) who investigates how the interference with diverse vacuolar trafficking routes affects vacuolar acidification. A redirection of VHA-a1 containing V-ATPases to the tonoplast has been previously excluded for *vha-a2 vha-a3* and an additional copy of VHA-a1 failed to rescue the double mutant phenotype (Krebs et al., 2010). If this is also the case in *fugu5-1 vha-a2 vha-a3* remains to be investigated. Moreover, we could show that inhibiting P-type ATPases does not influence the vacuolar pH in the *fugu5-1 vha-a2 vha-a3* mutant. All in all, with the *amiR-vha-a1* lines at hand we cannot demonstrate nor exclude the possibility of vacuolar acidification by TGN/EE V-ATPase complexes. Moreover, the V-PPase seems to play a role in vacuolar acidification in certain tissues and under certain growth conditions. More work is needed to elucidate how the remaining proton gradient is maintained, however, it seems likely that it is resulting from the interplay of many vacuolar transport processes.

Conclusion

Results presented herein demonstrate that the previously assumed role of the V-PPase for vacuolar acidification has to be specified to certain tissues and growth conditions. Careful investigations revealed that neither overexpression of the V-PPase in the *vha-a2 vha-a3* mutant background nor V-PPase loss-of-function mutants show alterations in vacuolar acidification compared to control plants. Vacuoles of root cells lacking the V-PPase in addition to the V-ATPase still show moderate vacuolar acidification in contrast to shoots, where vacuoles were nearly neutral indicating tissue dependent V-PPase demands. The reduced proton gradient in triple mutant shoots resulted in a variety of metabolic changes mimicking adaptations towards abiotic stress. Remarkably, ConcA treatment of the wild type and proton pump mutants resulted in a complete neutralization of vacuoles which led us to assume that TGN/EE V-ATPase complexes are involved in vacuolar acidification. Although with the established *amiR-vha-a1* lines it was not possible to confirm their contribution to vacuolar pH, they unveil communication between V-ATPase complexes at the TGN/EE and the vacuole. Thus, it seems that vacuolar pH homeostasis cannot be restricted to tonoplast-localized proton pumps and it will be of future interest to elucidate further mechanisms for vacuolar acidification.

I.5 Material and methods

Plant material and growth conditions

Arabidopsis thaliana, Columbia 0 (Col-0) ecotype was used in all experiments performed during this thesis. The two V-PPase mutant lines *fugu5-1* and *vhp1-1* were previously described (Ferjani et al., 2011). *VHA-a1RNAi* lines and VHA-a1-GFP have been previously established (Brüx et al., 2008; Dettmer et al. 2006). The tonoplast V-ATPase double mutant *vha-a2 vha-a3* has been previously characterized (Krebs et al., 2010). Standard growth medium for plate experiments contained 1/2 MS, 0.5% sucrose, 0.5% phyto agar, 10 mM MES and the pH was set to 5.8 using KOH. Agar and MS basal salt mixture were purchased from Duchefa (Haarlem, Netherlands). For growth on plates, seeds were surface sterilized by shaking them in a solution of 70% Ethanol mixed with 0.05% Triton-X-100 for 20 min followed by 10 min sterilization in 95% Ethanol. Thereafter, seeds were transferred to a sterile filter paper, where they were left to dry before evenly distributing them on plates. Transgenic lines containing the ethanol-inducible promoter system were surface sterilized using a bleach solution consisting of 6% sodium hypochlorite (NaClO) and 1% Triton-X-100 for 5 min and then rinsed in ddH_2O for at least 3 times. For stratification, seeds were kept at 4°C for at least 24 h before transferring plates to light. Plants were grown at 22°C under long day (LD) conditions with 16 h light and 8 h dark. Transgene selection was performed on plates containing standard growth medium supplemented with either 50 µg/µl kanamycin or 50 µg/µl hygromycin B. For hygromycin B selection, after exposure to light plates were covered with one sheet of paper to promote elongation of hypocotyls and therewith easier selection.

Plants used to determine the V-PPase RNA and protein level, for V-PPase activity measurements in *UBQ:AVP1* lines, phenotypings, cell sap pH measurements and metabolite analysis were grown for 3 weeks on soil.

Seedlings for root vacuolar pH measurements, vacuolar morphology and root zone determination, *AHA10* RNA level, enzyme activity measurements in *amiR-vha-a1* lines and TGN morphology experiments were grown for 6 days on plates containing standard growth medium. Medium for root vacuolar pH measurements was lacking the pH buffer MES.

Etiolated seedlings were grown on medium containing 10 mM MES-KOH, pH 5.8 solidified with 1% phyto agar. After seed sterilization and stratification, plates were exposed to light for 4 h, wrapped in two layers of aluminum foil and then kept at 22°C for 4 days.

For root length measurements single seeds were placed on standard growth medium solidified with 0.8% phyto agar and then grown vertically for 10-12 days.

Seedlings for external media acidification were cultivated for 5 days on medium containing 1/2 MS, 0.5% sucrose, 2.5 mM MES-KOH, pH 5.8 solidified with 0.6% phyto agar before they were transferred to a 96-well plate containing 1/2 MS, 0.5% sucrose with the pH set to 6.4.

For determination of the VHA-a1-GFP protein level in *amiR-vha-1*/ VHA-a1-GFP lines seedlings were grown in liquid medium containing 1/2 MS and 0.5% sucrose.

Construct design

Generation of UBQ:AVP1

To generate transgenic plants expressing *AVP1* under the control of the *UBQ10* promoter, the plant binary vector *UBQ:AVP1* was generated. First, a 2331 bp fragment of *AVP1* was amplified from cDNA using AVP1-*Xba*I-Fw and AVP1-*Sal*I-Rv. After subcloning into pJET1.2blunt (Thermo Scientific, www.thermoscientificbio.com) the fragment was released using the introduced *Xba*I and *Sal*I restriction sites and inserted into the backbone of the binary vector pTKan (Krebs et al., 2012) to receive pTKan-AVP1. In addition, a 661 bp fragment of the Arabidopsis *UBQ10* promoter was amplified using UBQ10-*Kpn*I-Fw and UBQ10-*Kpn*I-Rv. After subcloning of *UBQ10* into pJET1.2blunt, the fragment was released via the *Kpn*I site and inserted into pTKan-AVP1 to finally receive *UBQ:AVP1*. The *UBQ:AVP1* construct was cloned by Melanie Krebs.

Generation of dexamethasone inducible amiR-vha-a1

To switch the promoter system from ethanol inducible to dexamethasone (DEX) inducible to drive the artificial microRNA against *VHA-a1* the recently established GreenGate cloning system was applied (Lampropoulos et al., 2013). To create the GreenGate entry module, the *amiR-vha-a1* sequence was PCR-amplified from an

existing plasmid (amiRvha-a1.pBJ36; KS-E679) using VHA-a1ami.B.For and VHA-a1ami.E.Rev primers. The primers contained the restriction site for BsaI, the module specific overhang and a few additional nucleotides (see publication). Thereafter the PCR product and the empty entry module (pGGI000) were digested with BsaI, the digestion was purified and then ligated. After test digestion positive clones were checked by sequencing. To create the two intermediate vectors that will be later on combined on one T-DNA, two GreenGate reactions were performed. Intermediate vector 1 consists of 6 entry modules (pGGM000: UBQ10; N-decoy; LhG4-GR; C-decoy; rbcs; FH adapter) and intermediate vector 2 was created from 5 entry modules (pGGN000: HA adapter; pOP6; amiR-vha-a1; rbcs; hygromycin). The products of these two GreenGate reactions were analyzed by test digestion. In the final step both intermediate constructs were combined on 1 final destination vector (pGGZ003) and checked by test digestion.

Plant transformation

The *UBQ:AVP1* construct was introduced into the *Agrobacterium tumefaciens* strain GV3101:pMP90 and selected on 5 µg/ml rifampicin, 10 µg/ml gentamycin and 100 µg/ml spectinomycin. *Arabidopsis thaliana* ecotype Col-0 and *vha-a2 vha-a3* plants were used for transformation using standard procedures.

The *amiR-vha-a1* construct was introduced into the *Agrobacterium tumefaciens* strain ASE (pSOUP^{+}) and selected on 100 µg/ml spectinomycin, 5 µg/ml tetracycline (for pSOUP), 25 µg/ml chloramphenicol and 50 µg/ml kanamycin. *Arabidopsis thaliana* ecotype Col-0, *vha-a2 vha-a3* and VHA-a1-GFP plants were used for transformation using standard procedures.

Pharmacological treatments and stains

Arabidopsis seedlings were incubated in liquid 1/2 MS medium with 0.5% sucrose, pH 5.8, containing 1 µM ConcA, 1 µM FM4-64, 10 µM BCECF or the equivalent amount of DMSO in control samples for the indicated time at room temperature. Stock solutions were prepared in DMSO.

Dexamethasone was purchased from Sigma, dissolved in DMSO and stored as 20 mM working aliquots at -20°C.

Sodium orthovanadate (Vanadate) was purchased from Sigma and had to be activated prior to use. The following procedure depolymerizes vanadate, converting it into a more potent inhibitor of protein phosphotyrosyl phosphatases. Initially a 10 mM stock solution of vanadate was prepared and the pH was adjusted to 10.0 using either NaOH or HCl. After boiling the solution for about 10 min the solution turned from yellow into colorless. Then, the solution was cooled down to room temperature, the pH was readjusted to 10.0 and the procedure was repeated 3-4 times until it remained colorless and the pH was stable at 10.0. The activated vanadate was stored as aliquots at -20°C. Vanadate used for the extracellular acidification assay was prepared following the same procedure with minor modifications. The vanadate stock solution had a concentration of 200 mM and the pH was adjusted to 6.4.

Root length measurements

Plates with seedlings for root length measurements were opened and scanned upside down. The digitized images were analyzed using the program ImageJ 1.49 (NIH, USA).

Hypocotyl length measurements

The hypocotyl length of etiolated seedlings was determined by placing them between two sheets of acetate before they were scanned. The digitized images were analyzed using the program ImageJ 1.49 (NIH, USA).

Genetic crosses

Flowers that were used as female parents were emasculated by removing the anthers with forceps. These flowers were then pollinated by touching the stigma with anthers from the male parent. For one crossing combination 5-6 flowers were used and their siliques were pooled. Seeds of the F1 progeny were collected.

Extracellular acidification assay

Media acidification was measured according to Haruta et al. with minor modifications (Haruta et al., 2010). Single seedlings were transferred to a 96-well plate containing 200 µl of 1/2 MS, 0.5% sucrose, pH 6.4 supplemented with 30 µg/µl fluorescein dextran (MW = 10.000; Life Technologies) and 2 mM vanadate. After the activation

procedure of vanadate the stock solution is colorless (see above). However after adding 2 mM of vanadate to the liquid MS medium it turned yellow again indicating a pH change. Therefore the pH of the MS medium containing vanadate had to be readjusted to 6.4 following the same procedure described above. When the pH was stable, fluorescein was added to the liquid medium. Before and after an incubation time of 18 h fluorescence emission was detected at 521 nm after excitation at 494 nm and 435 nm using a microplate reader (Tecan Infinite M1000). The media pH was calculated using a calibration curve ranging from pH 3.5 to 6.5.

Observation of leaf vasculature

To study leaf vein patterning in DEX-induced *amiR-vha-a1* plants leaves were cleared according to Li et al. with minor modifications (Li et al., 2013). Leaves of three different sizes were excised and transferred to 70% ethanol for 1 h to remove most of the chlorophyll. Then, leaves were fixed in ethanol/acetic acid (3:1) for 3 h and rehydrated with an ethanol series (70%, 50%, 30% and 10% ethanol) with 30 min at each step. Thereafter leaves were incubated in a clearing solution consisting of chlorate hydrate/acetic acid/water (50:10:5) over night. Leaf section images were taken with a Zeiss Axiovert LSM 510 Meta confocal scanning laser microscope and pictures of entire leaves were captured at the Zeiss stereomicroscope Stemi 2000-CS equipped with an Axio cam HRc.

RNA isolation and cDNA synthesis

For the analysis of *AVP1* transcript levels in *UBQ:AVP1* lines, RNA was isolated using the RNeasy Plant Mini Kit (Qiagen) according to manufacturer's instructions. cDNA was synthesized from 2 µg of total RNA using M-MuLV reverse transcriptase (Thermo) and an oligo dT primer.

Real-time RT PCR

For quantitative analysis of gene expression real-time RT PCR was applied. cDNA samples were diluted 1:50 in nuclease-free water. Real-time PCR reactions were performed using the DNA Engine Opticon System (DNA Engine cycler and Chromo4 detector, BioRad) and ABsolute qPCR SYBR Green Mix (Thermo Scientific). The real-time PCR reaction mixture with a final volume of 20 µl contained 0.5 µM of each

forward and reverse primer, 10 µl SYBR Green Mix, 4 µl cDNA and 4 µl of RNase-free water. The thermal cycling conditions were composed of an initial denaturation step at 95°C for 15 min followed by 40 cycles at 95°C for 15 sec, 59°C for 30 sec and 72°C for 15 sec and ended with a melting curve. For the analysis of each sample three analytical replicas were used. Target genes were normalized to the expression of *Actin2*. Primer sequences for *AVP1*, *AHA10* and *Actin2* amplification are listed in the table below this section.

Genotyping

Genomic DNA was extracted as described previously (Edwards et al., 1991).

To check for the presence of the T-DNA in *vhp1-1*, PCR was performed using a T-DNA left border specific primer (T-DNA LB) and a *VHP1* specific reverse primer (VHP1 Rev). To identify homozygous *vhp1-1* mutants the two gene specific primers were used (VHP1 For and VHP1 Rev).

For identification of the point mutation in *fugu5-1*, PCR was performed using a dCAPs forward primer (fugu5-1 dCAPs For) and the V-PPase specific reverse primer (VHP1 Rev). After gene amplification the PCR product was digested using NlaIII and then seperated on a 3% agarose gel. Two bands with sizes of 119 bp and 94 bp indicated a cutted PCR product and therewith the wild type. Moreover two bands with 145 bp and 94 bp indicated that the PCR product could not be cut leading to the identification of a homozygous knock-out plant. Accordingly, three bands (94 bp, 119 bp, 145 bp) on the agarose gel after digestion implied a heterozygous *fugu5-1* sample.

In order to check for the presence of the T-DNA in *vha-a2*, a T-DNA left border primer (TL1) and a *VHA-a2* reverse primer (S142642.rev) was used. The *VHA-a2* wild type allele was identified using VHA-a2 forward (S142642.for2) and reverse primer.

To identify T-DNA insertions in *vha-a3,* a T-DNA left border primer (TL1) and a *VHA-a3* forward primer (S029786.for) was used. To find the wild type *VHA-a3* allele, gene specific forward and reverse primer (S029786.rev) were applied.

Primer sequences are listed in the table below this section.

Preparation of microsomal membranes

Microsomal membrane proteins were extracted as described before (Schumacher et al., 1999) with minor modifications. Briefly, shoots from wild type and mutant plants were harvested and frozen in liquid nitrogen until further use. For protein extraction, rosette leaves were ground in liquid nitrogen, plant powder was filled into a falcon tube and homogenized in homogenization buffer (2 ml/g fresh weight) containing 350 mM sucrose, 70 mM Tris-HCl (pH 8), 10% (vol/vol) glycerol, 3 mM Na_2EDTA, 0.15% (wt/vol) BSA, 1.5% (vol/vol) PVP-40, 4 mM DTT and 1x complete protease inhibitor cocktail (Roche). The homogenate was filtered through two layers of Miracloth and centrifuged at 15,000 g for 15 min at 4°C. The supernatent was filtered through Miracloth again and then centrifuged at 100,000 g for 45 min at 4°C. The microsomal membrane pellet was resuspended in resuspension buffer containing 350 mM sucrose, 10 mM Tris-MES (pH 7), 2 mM EGTA, 2 mM DTT and 1x complete protease inhibitor cocktail. Protein concentrations were determined as reported previously (Bradford, 1976).

SDS-PAGE and immunoblotting analysis

To analyse the protein level in microsomal membranes extracted from wild type and mutant plants SDS-PAGE and immunoblotting was applied. After electrophoresis, proteins were transferred to a nitrocellulose membrane (Whatman). The following primary antibodies were used: the V-PPase antibody (Cosmo Bio; 1:5000; amino acid sequence of antigen, DLVGKIERNIPEDDPRN; (Kobae et al., 2006)); GFP antibody (1:5000); cFBPase antibody (Agrisera, 1:5000) and anti-γ-Tip (1:3000; against the C-terminal γ-Tip sequence CSRTHEQLPTTDY; (Jauh et al., 1998)). Antigen on the membrane was visualized with horseradish peroxidase-coupled anti-rabbit IgG (Promega) and chemiluminescent substrate (Peqlab). Immunostained bands were analyzed using a cooled CCD camera system (Intas).

Enzyme activity assays

V-PPase and V-ATPase activity were measured colorimetrically as Pi release (Heinonen and Lahti, 1981).

Determination of V-PPase activity

The V-PPase assay medium contained 25 mM Tris-MES (pH 7.5), 2 mM $MgSO_4$ *7 H_2O, 0.1 mM Na_2MoO_4, 0.02% Brij 58, 0.2 mM PPi and 50 mM KCl. The reaction was started by adding 10 µg microsomal membrane proteins to the medium. After 20 min at 28°C the reaction was stopped by the addition of 12 µl of 1 M citric acid. Thereafter the amount of Pi released in the presence or absence of KCl was determined. For that a 30 µl aliquot of the reaction mixture was mixed with 240 µl of acetone-acid-molybdate solution (2.5 mM $(NH_4)_6Mo_7O_{24}$*4 H_2O, 1.25 N H_2SO_4, 50% acetone) and afterwards the Pi release was colorimetrically determined by measuring absorbance at 355 nm in a microplate reader (Tecan Infinite M1000). BSA (10 µg) was used as a control in order to calculate a blank value.

Determination of V-ATPase activity

The V-ATPase assay medium consisted of 25 mM Tris-MES (pH 7), 4 mM $MgSO_4$ *7 H_2O, 50 mM KCl, 1 mM NaN_3, 1 mM Na_2MoO_4, 0.02% Brij 35, 1 mM $NaVO_4$, 50 mM KNO_3 and 3 mM Mg*ATP. To start the reaction 10 µg microsomal membranes were added to the medium. After 30 min at 28°C the reaction was stopped by adding 12 µl of 1 M citric acid. Thereafter the amount of Pi released in the presence or absence of the inhibitor KNO_3 was determined. For that a 60 µl aliquot of the reaction mixture was mixed with 210 µl of acetone-acid-molybdate solution (2.5 mM $(NH_4)_6Mo_7O_{24}$*4 H_2O, 1.25 N H_2SO_4, 50% acetone). Then 30 µl of 1 M citric acid was mixed with the sample and absorbance at 355 nm was measured in a microplate reader. BSA (10 µg) was used as a control in order to calculate a blank value.

pH measurements

Determination of root vacuolar pH

To measure vacuolar pH in the wild type and V-ATPase mutants seedlings were incubated in liquid medium containing 1/2 MS and 0.5% sucrose (pH 5.8) supplemented with 10 µM of the membrane-permeant pH sensitive dye BCECF-AM (Molecular Probes, Invitrogen) and 0.02% Pluronic F-127 (Molecular Probes, Invitrogen). After 1 h of staining in darkness at 22°C with gentle agitation, seedlings were washed twice in liquid MS medium for 5 min. BCECF fluorescence was detected using a Leica SP5II confocal laser scanning microscope equipped with a

HCX PL APO CS 20.0 x 0.70 IMM UV water immersion objective (Leica). BCECF was excited at 458 nm and 488 nm with a VIS-Argon laser and the emission was detected between 510 nm and 550 nm. Images have been taken in fully elongated cells of the root hair zone with one exception when vacuolar pH was additionally measured in the meristematic and the elongation zone. Average fluorescence intensity values of captured images of both excitation wavelengths were obtained using the software ImageJ 1.49 (NIH, USA). Ratios were calculated by dividing values received for 488 nm by values obtained for 458 nm. Ratios were then used to calculate the vacuolar pH on the basis of a calibration curve. To perform in vivo calibration of BCECF, seedlings were incubated in liquid medium containing the dye as described before. Prior to the measurement seedlings were incubated for 20 min in pH equilibration buffers containing 50 mM MES-BTP (pH 5.2 to 6.4) or 50 mM Hepes-BTP (pH 6.8 to 8.0) and 50 mM ammonium acetate. The calibration curve was obtained by plotting ratio values against the pH. To generate calibration curves sigmoidal Boltzman fit was used.

Determination of leaf cell sap pH

For cell sap pH measurements entire rosettes (2 rosettes for Col-0; 4-5 rosettes for *vha-a2 vha-a3*) were excised and crushed for about 1 min in a 1.5 ml eppendorf tube using a sterile pestle. Samples were then centrifuged at RT for 1 min at 20,000 g and the supernatant was transferred to a fresh tube. The pH of the extract was measured using the Five easy Plus microelectrode (Mettler Toledo, Germany). For each genotype at least 3 biological replicats were measured.

Confocal microscopy

Confocal laser scanning microscopy was performed using a Leica TCS SP5II microscope equipped with a Leica HCX PL APO lambda blue 63.0x1.20 UV water immersion objective. GFP and BCECF were excited at 488 nm with a VIS-argon laser and fluorescence emission was detected between 500 and 555 nm. FM4-64 was excited at 561 nm with a VIS-DPSS 561 laser diode and its emission was detected between 615 nm and 676 nm. For image acquisition Leica Application Suite Advanced Fluorescence software was used. Processing of images and root zone measurements was performed using Fiji (based on ImageJ 1.47t).

Imaging

Pictures of rosettes from adult plants were taken using a Nikon D60 digital camera. Images of excised flowers and siliques (intact or opened) were observed at the Zeiss stereomicroscope Stemi 2000-CS equipped with an Axio cam HRc using the AxioVision Rel. 4.7 software. Images were processed using Adobe Photoshop CS4.

Metabolite analysis

Rosettes of wild type and proton pump mutant plants grown on soil were excised, weighed and frozen in liquid nitrogen. Metabolites were extracted from pulverized frozen plant material. Metabolite extraction, separation and detection was performed at the Metabolomics Core Technology Platform (MCTP, COS Heidelberg).

Sugars and adenosines were extracted and determined as described previously (Krussel et al., 2014).

Cations, anions and organic acids were extracted from 40-50 mg powdered leaf material by incubation with 700 µl ultra-pure water for 30 min at 95°C. Cell debris and insoluble material were removed by centrifugation for 10 min at 25,000 g. The resulting supernatant was used for the determination of the cation, anion and organic acid content. These compounds were separated by ion-chromatography. For the measurement of cations 30 µl extract was diluted with 270 µl water prior to the analysis. Cations were separated isocratic with 30 mM methansulfonic acid for 27 min on an IonPac CS16 column (2 mm, ThermoScientific) connected to an ICS-1000 system (Dionex) at a flow rate of 0.36 ml/min and quantified by conductivity detection after anion suppression (CERS-500 2 mm, suppressor current 43 mA). Column temperature was set to 43°C. For the measurement of anions and organic acids 100 µl of the same extract was diluted with 200 µl water. These compounds were separated by an IonPac AS11-HC (2mm, ThermoScientific) column connected to an ICS-3000 system (Dionex) and quantified by conductivity detection after cation suppression (ASRS-300 2mm, suppressor current 95-120 mA). Prior to separation, the column was heated to 30°C and equilibrated with 5 column volumes of solvent A (ultra-pure water) at a flow rate of 0.38 ml/min. Separation of anions and organic acids was achieved by increasing the concentration of solvent B (methanol) and solvent C (100mM NaOH) in buffer A as follows: 8 min 4% C, 11 min 10% C, 18.2

min 20% B / 18.1 % C, 27.5 min 20% B / 21% C, 32 min 24% C, 43 min 30% C, 47 min 40% C, 48 min 90% C for 8 min, and return to 4% C in 9 min. Data acquisition and processing was performed with the Chromeleon 6.6 software (Dionex).

Branched-chain α-ketoacids were extracted from 30-40 mg pulverized plant material in an ultrasonic ice-bath for 10 min after addition of 500 µl cold 1 M perchloric acid. Cell debris and insoluble material were removed by centrifugation for 10 min at 25,000 g. 150 µl of the resulting supernatant were mixed with an equal volume of 25 mM OPD (o-phenylendiamine) solution and derivatized by incubation at 50°C for 30 min. After centrifugation for 10 min, the derivatized ketoacids were separated by reversed phase chromatography on an Acquity HSS T3 column (100 mm x 2.1 mm, 1.7 µm, Waters) connected to an Acquity H-class UPLC system. Prior separation, the column was heated to 40°C and equilibrated with 5 column volumes of solvent A (0.1% formic acid in 10% acetonitrile) at a flow rate of 0.55 ml/min. Separation of ketoacid derivates was achieved by increasing the concentration of solvent B (acetonitrile) in solvent A as follows: 2 min 2% B, 5 min 18% B, 5.2 min 22% B, 9 min 40% B, 9.1 min 80% B and hold for 2 min, and return to 2% B in 2 min. The separated derivates were detected by fluorescence (Acquity FLR detector, Waters, excitation: 350 nm, emission: 410 nm, gain: 500) and quantified using ultrapure standards (Sigma). Data acquisition and processing was performed with the Empower3 software suite (Waters).

Amino acids and thiols were extracted with 500 µl 0.1 M HCl using 40-50 mg fresh weight of grounded plant material. Non-thiol containing amino acids were quantified after specific labeling with the fluorescence dye AccQ-Tag (Waters) according to the manufacturers protocol. The resulting derivatives were separated by reversed phase chromatography on an Acquity BEH C18 column (150 mm x 2.1 mm, 1.7 µm, Waters) connected to an Acquity H-class UPLC system and quantified by fluorescence detection (Acquity FLR detector, Waters). The column was heated to 42°C and equilibrated with 5 column volumes of buffer A (140 mM sodium acetate pH 6.3, 7 mM triethanolamine) at a flow rate of 0.45 ml min^{-1}. Baseline separation of amino acid derivates was achieved by increasing the concentration of acetonitrile (B) in buffer A as follows: 1 min 8% B, 7 min 9% B, 7.3 min 15% B, 12.2 min 18% B, 13.1 min 41% B, 15.1 min 80% B, hold for 2.2 min, and return to 8% B in 1.7 min. Data acquisition and processing was performed with the Empower3 software suite

(Waters). Cys and GSH were determined after labeling with monobromobimane (Calbiochem) as described previously (Wirtz, 2004).

Appendix

Primer sequences

Primer name	Sequence 5'-3'
AVP1-XbaI-Fw	TCCTCTAGAATGGTGGCGCCTGCTTTGTTAACC
AVP1-SalI-Rv	CAGGTCGACTTAGAAGTACTTGAAAAGGATACCACCG
UBQ10-KpnI-Fw	AAGGTACCCGACGAGTCAGTAATAAACGGCG
UBQ10-KpnI-Rv	GATGGTACCCGCACTCGAGCTGTTAATCAG
VHA-a1ami.B.For	AACAGGTCTCAAACATCGAGGTCGACGG
VHA-a1ami.E.Rev	AACAGGTCTCAGCAGAGGATCCCCCCATG
T-DNA LB (VHP1)	AAGAAAATGCCGATACTTCATTGGC
VHP1 For	CCTAGTCTCCTTGGCTCTCTTTG
VHP1 Rev	GTCATCTTCTTCCCTCGGATTGAGT
fugu5-1 dCAPs For	TTCGCAGGCTGGTGTATCAGAGCAT
S142642.for2 (VHA-a2)	CGAATACGAGATCGGAGAC
S142642.rev (VHA-a2)	TGCAACTTGTCGTTATTAGCATTG
S029786.for (VHA-a3)	CTGATGTTACTATTGTACCGAAC
S029786.rev (VHA-a3)	TCGCGATATTCAAATAACAGCT
TL1	GCGTGGACCGCTTGCTGCAACT
AHA10 qPCR for2	CAATGCTGGGAATGCTGCTG
AHA10 qPCR rev2	CACCAGGTACCAAGATAGAAGC
AVP1qRT.For	GGAGACACAATTGGAGACCC
AVP1qRT.Rev	GTGAGTGGCGAAGAAGGGAG
ActinQRT_f	TCTTCCGCTCTTTCTTTCCA
ActinQrt_r	TCACCATACCGGTACCATTG

II. Re-evaluation of lines overexpressing or lacking the V-PPase

II.1 Abstract

In the previous chapter we analyzed the role of the V-PPase for vacuolar acidification in detail. The characterization of this enzyme included the analysis of overexpressing lines and loss-of-function mutants. Due to the fact that in both cases contrasting phenotypes exist, the aim of the second chapter was to provide clarification by comparing the overexpressor lines *35S:AVP1* and *UBQ:AVP1* and the knock-out alleles *avp1-1* versus *vhp1-1/fugu5/avp1-2*. We found that the increased size of *35S:AVP1* transgenic lines is not due to ubiquitous overexpression since neither *AVP1* RNA nor protein levels were elevated, presumably because overexpression was lost due to transgene silencing. We suggest that increased biomass could be due to increased stomatal aperture as observed in two independent *35S*-driven lines. In addition, we provide substantial evidence that the impaired development of *avp1-1* is due to the presence of a second T-DNA insertion in the ARF-GEF GNOM as revealed by whole genome sequencing. This was confirmed by conventional genotyping and allelism tests. The fact that phenotypes of a weak *GNOM* allele are highly similar to *avp1-1* supports our findings.

II.2 Introduction

Chemiosmotic circuits that drive transport across the plasma- and endomembranes of plants are driven by proton gradients created by three classes of proton-pumps, the P- and V-type H^+-translocating ATPases (P-ATPase and V-ATPase) and the H^+-translocating pyrophosphatase (V-PPase). Their activity allows plants to respond to their constantly changing environment and at the same time maintain optimal metabolic conditions (Gaxiola et al., 2007). V-PPases hydrolyse pyrophosphate, a by-product of many biosynthetic pathways, to energize active transport of protons across membranes. Although Arabidopsis has three genes encoding V-PPases, AVP1/VHP1, the only representative of the K^+-dependent type I-class, accounts for more than 99% of the total activity (Segami et al., 2010). Type I V-PPases are found at the tonoplast in most plant cells and have thus originally been considered as alternative vacuolar proton-pumps assisting the ubiquitous V-ATPase particularly in young cells with high PP_i-levels or under ATP-limiting conditions (Maeshima, 2000, 2001). However, loss- and gain-of-function phenotypes described in recent years have indicated a central role for AVP1 in stress tolerance and development. Overexpression of *AVP1* in Arabidopsis, as well as in a considerable number of crop plants such as alfalfa, barley, cotton, rice, tomato and maize, among others, results in improved drought and salt tolerance presumably due to increased vacuolar solute accumulation (Bao et al., 2009; Schilling et al., 2014; Pasapula et al., 2011; Yang et al., 2007; Li et al., 2008). *AVP1* overexpression has also been reported to result in increased cell division at the onset of organ formation and increased auxin transport by indirectly affecting the distribution and abundance of the plasma membrane H^+-ATPase and the PIN1 auxin efflux facilitator (Li et al., 2005). In agreement with a role for AVP1 in facilitating auxin fluxes, a reduction in auxin transport leading to severe defects in root and shoot development was observed in the *avp1-1* T-DNA insertion allele (Li et al., 2005). Homozygous *avp1-1* seedlings showed a variety of shoot abnormalities with most of the cotyledons (~98%) appearing as heart-shaped structures. None of the mutants was able to develop fully and produce seeds due to the lack of floral organs in more than 90% of *avp1-1* plants. However, several additional null alleles of *AVP1*, identified in a screen for compensation mutants with disturbed coordination of cell proliferation and post-mitotic cell expansion, display a much less severe phenotype in establishing heterotrophic growth after germination

(Ferjani et al., 2011). Cotyledons of *fugu5/vhp1* mutants contained fewer but larger cells resulting in an elongated cotyledon phenotype. Apart from that, *fugu5* mutant plants developed normally without showing impaired fertility. The fact that defects observed in the *fugu5/vhp1* mutants could be rescued by expressing a yeast soluble pyrophosphatase suggests that removal of cytosolic PP_i is an additional important function of AVP1 (Ferjani et al., 2011). Most recently another independent V-PPase mutant has been published, *avp1-2*, with a T-DNA inserted in the *AVP1* promoter leading to 30% residual *AVP1* transcript and reduced AVP1 protein (Pizzio et al., 2015). Similar to *fugu5/vhp1* mutants, *avp1-2* did not show severe growth impairment. With this chapter we aim to provide clarity on existing data concerning phenotypes and function of AVP1. We show that the increased biomass and improved stress tolerance observed in *35S:AVP1* lines are not due to constitutive overexpression. Furthermore, we demonstrate that the strong *avp1-1* phenotype is caused by a second site T-DNA insertion in the gene encoding the ARF-GEF GNOM that is known to be essential for the endosomal recycling of the auxin efflux carrier PIN1 to the basal plasma membrane. Taken together, our results explain disparities between the *avp1-1* and *vhp1-1*/*fugu5*/*avp1-2* phenotypes but further studies are necessary to understand the molecular basis of the robust growth phenotypes observed in *AVP1-1* and *AVP1-2* despite transgene silencing.

II.3 Results

35S:AVP1 plants do not overexpress the V-PPase

Throughout our investigations we encountered strong differences among phenotypes of transgenic lines ubiquitously expressing *AVP1* under the *UBQ10* promoter that have been created in our laboratory and published lines expressing *AVP1* under the *35S* promoter (Gaxiola et al., 2001; Li et al., 2005). As demonstrated beforehand in this thesis, *UBQ:AVP1* expression in the wild type background does not cause an increase in biomass despite an elevated V-PPase activity (chapter 1, Fig. 1B and 2A). On the contrary, *35S:AVP1* lines (*AVP1-1* and *AVP1-2*) have an increased number of rosette leaves, greater leaf area and moreover show enhanced root growth when compared to the wild type (Li et al., 2005). Due to this discrepancy we decided to compare growth phenotype, rosette fresh weight, RNA and protein level and enzyme activity side by side among two independent *35S:AVP1* and *UBQ:AVP1* lines (Fig. 1A to 1E). As demonstrated in previous reports, the biomass of the two *35S:AVP1* lines was confirmed to be increased when comparing their rosette growth and fresh weight to the wild type (Fig. 1A and 1B). However, only one of the *UBQ*-driven *AVP1* lines showed an increase in biomass which was less than that of *35S*-driven lines. Strikingly, when comparing the *AVP1* transcript and protein level the *UBQ:AVP1 #18-4* line showed the expected increase while neither of the two was elevated in *35S:AVP1-1* (Fig. 1C and 1D). Instead, the RNA and protein level in *35S:AVP1-1* tend to be even lower than in the wild type. Interestingly, V-PPase activity measurements clearly revealed a decrease in *35S:AVP1* lines compared to the wild type, however enzyme activity was 2-3 times higher in *UBQ:AVP1* plants (Fig. 1E). To find out whether this decrease in PPase activity is reflected on the level of vacuolar acidification, the vacuolar pH was measured in *35S:AVP1-1* and compared to the V-PPase mutant *vhp1-1* (Fig. 1F) that lacks V-PPase activity completely (Ferjani et al., 2011). We found that the vacuolar pH of *35S:AVP1* root epidermal cells was elevated to a similar level as in *vhp1-1* indicating that *35S*-driven lines rather resemble V-PPase mutants than overexpressing lines. Taken together these results showed that the increased size of *35S:AVP1* transgenic lines is not due to ubiquitous overexpression.

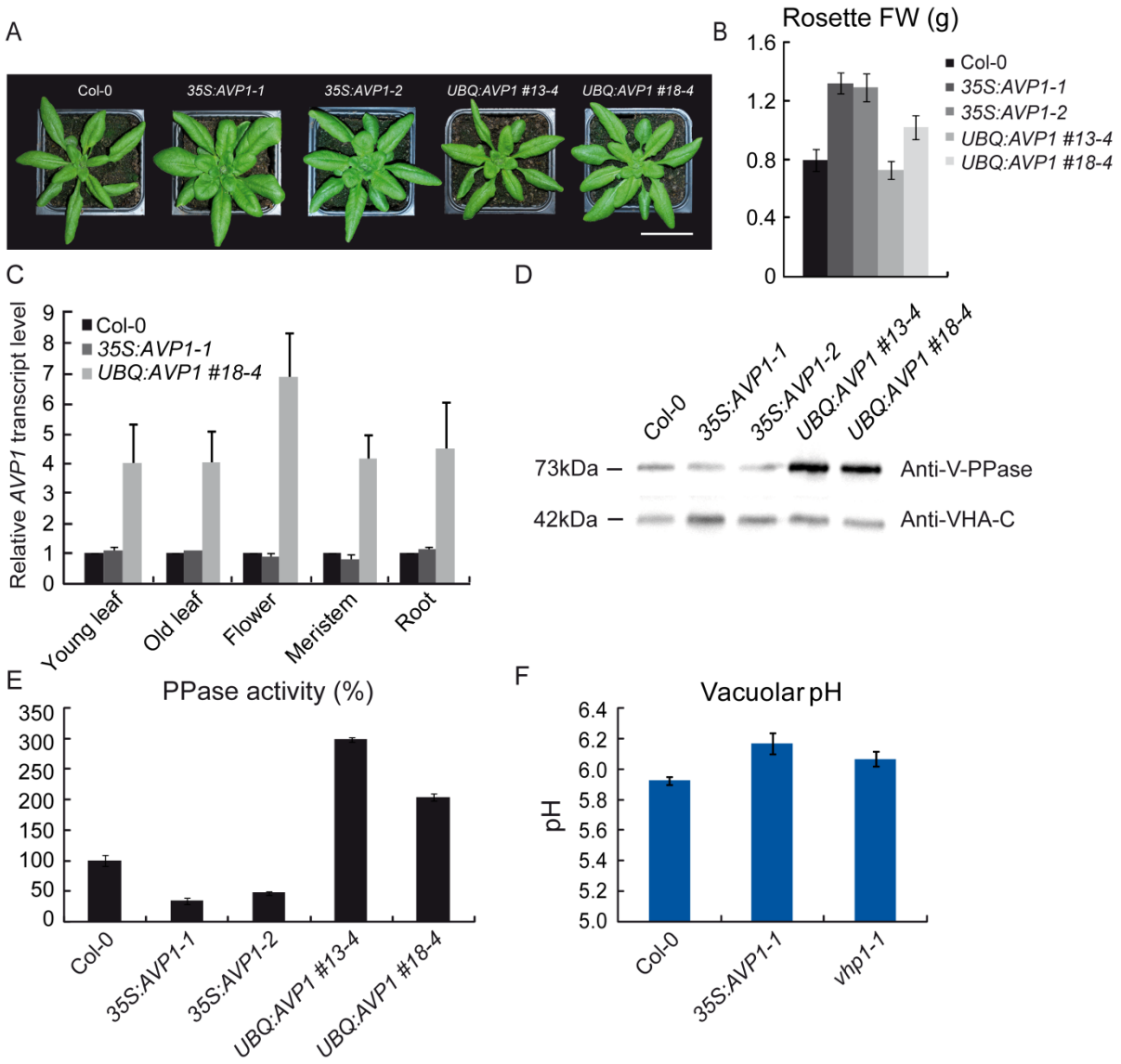

Figure 1. Misexpression of *AVP1* in *35S:AVP1* plants.

(A) Phenotypes and (B) rosette fresh weight of 4-week-old *35S:AVP1* plants compared to *UBQ:AVP1* lines grown under LD conditions. Error bars indicate SE of n = 8 to 11 plants. Bar = 3.5 cm.
(C) *UBQ:AVP1* but not *35S:AVP1* show higher *AVP1* transcript level. The *AVP1* mRNA level was measured by qRT-PCR in 5-week-old plants (young leaf, old leaf, flower and meristem) and 5-day-old seedlings (root) of wild type, *35S:AVP1-1 and UBQ:AVP1 #18-4* grown under LD conditions. Error bars indicate SD of n = 3 biological replicates.
(D) Increased AVP1 protein abundance in *UBQ:AVP1* lines. Microsomal membrane proteins of 4-week-old wild type, *35S:AVP1* and *UBQ:AVP1* plants were extracted, separated by SDS-PAGE and subsequently immunoblotted with anti-V-PPase antibody. Equal protein loading is indicated by anti-VHA-C detection.
(E) Elevated K^+-stimulated PPase activity in *UBQ:AVP1* but not in *35S:AVP1* lines. Plants were grown for 4 weeks under LD conditions. Wild type activity was set to 100%. Graph shows result of one representative experiment of 3 biological replicates. Error bars show SD of n = 3 technical replicates.
(F) Vacuoles of *35S:AVP1* and *vhp1-1* root epidermal cells are slightly alkalinized. Vacuolar pH was measured in roots of 6-day-old plants. Error bars represent SD of n = 2 biological replicates.

One explanation for the observed reduction of AVP1 protein and activity levels in *35S:AVP1* lines is transgene silencing in the third generation seeds. To test this hypothesis, we grew *35S*- and *UBQ*-driven *AVP1* lines on MS medium containing kanamycin. Indeed, T_3 *35S:AVP1-1* and *35S:AVP1-2* lines have lost kanamycin resistance conferred by the NPTII-gene on the T-DNA (Fig. 2). *35S:AVP1-2* seedlings showed complete silencing while *35S:AVP1-1* is partially silenced since cotyledons exhibited green spots. This indicates that reduced V-PPase activity is due to transgene silencing in *35S:AVP1* lines.

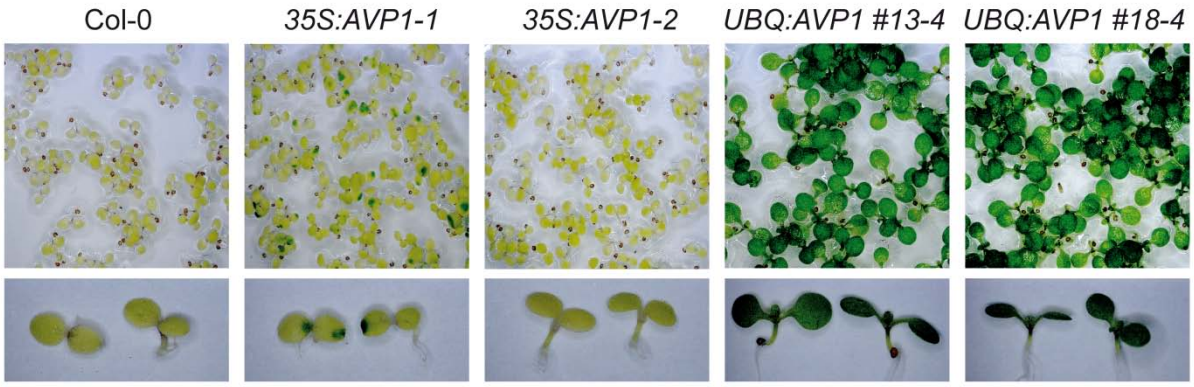

Figure 2. *AVP1* transgene is silenced in *35S:AVP1* lines.

35S-driven *AVP1* lines are sensitive to kanamycin. Seedlings of the indicated genotypes were grown for 6 days on 0.5 MS medium supplemented with kanamycin.

Increased light-induced stomatal opening in *35S:AVP1*

Since guard cells are symplastically isolated, mediated by a lack of functional plasmodesmata at their maturity, they are often spared from transgene silencing (Palevitz and Hepler, 1985; Erwee et al., 1985). We thus hypothesized that in *AVP1-1* and *AVP1-2* silencing might limit the *35S*-driven overexpression of *AVP1* to guard cells. Importantly, it has been previously suggested that AVP1 activity plays a role in stomatal movement (Bak et al., 2013). They showed that stomatal closure involves vacuolar acidification mediated by AVP1 since *vhp1-1* mutants were delayed in ABA-induced stomatal closure. Hence, elevated AVP1 levels in guard cells could have an effect on stomatal opening. We performed stomatal bioassays using epidermal peels from adult rosette leaves. Whereas in the dark stomata from all genotypes were closed to a similar extent, light-induced stomatal aperture was higher

for *AVP1-1, AVP1-2* (>20%) and to some extent *UBQ:AVP1 #13-4* (~15%; Fig. 3A), while the size of the guard cells was not affected (Fig. 3B). Increased stomatal aperture is known to facilitate CO_2 assimilation (Wang et al., 2014), which in turn could be causal for the enhanced biomass production observed in *AVP1-1* and *AVP1*-2 transgenic lines.

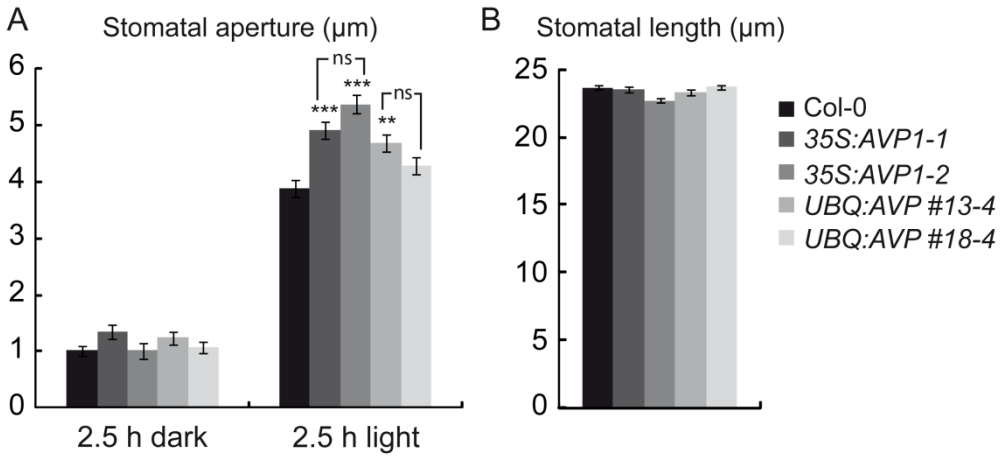

Figure 3. Increased light-induced stomatal opening in *35S:AVP1.*

(A) Stomatal apertures under 2.5 h of darkness or 2.5 h light (250 µmol $m^{-2} \cdot s^{-1}$). Data represent the mean and SE of the absolute values of aperture of at least 40 stomata per line and per treatment. Asterisks indicate statistically significant differences relative to the wild type for each treatment by the Students *t* test (*P < 0.05; **P < 0.005; ***P < 0.001).
(B) Stomatal size is not altered. Values represent the mean and SE (n=160) of the length of fully developed stomata.
Experiments presented in A and B were performed by Zaida Andrés.

35S:AVP1 plants are confirmed to be more drought resistant

Previously, it has been shown that expressing *35S:AVP1* confers enhanced salt and drought resistance (Gaxiola et al., 2001). To find out whether silenced *35S:AVP1* plants still show tolerance towards abiotic stress, we tested wild type and *AVP1* transgenic plants for their drought tolerance by subjecting them to water deprivation. Plants were grown for more than 4 weeks under fully watered conditions at 22°C before watering was stopped. After 9 days of water deprivation, plants were rewatered and analyzed for their recovery status (Fig. 4A). Interestingly, both *35S:AVP1* lines were more resistant to drought with *AVP1-2* showing a better recovery after rewatering than *AVP1-1*. In more detail, all leaves of *AVP1-2*, and to a

minor extent also of *AVP1-1*, were green and healthy while the older leaves of the remaining lines died and only the youngest part of the rosette survived.

Due to the previous observation that *35S:AVP1* lines showed increased light-induced stomatal opening, we further analyzed whether these lines are also affected in stomatal closure. However, when we measured ABA-induced closure of light-opened stomata no differences between transgenic lines and the wild type were observed (Fig. 4B). Taken together, *35S:AVP1* lines show proper stomatal closure and were confirmed to be more drought tolerant than wild type plants.

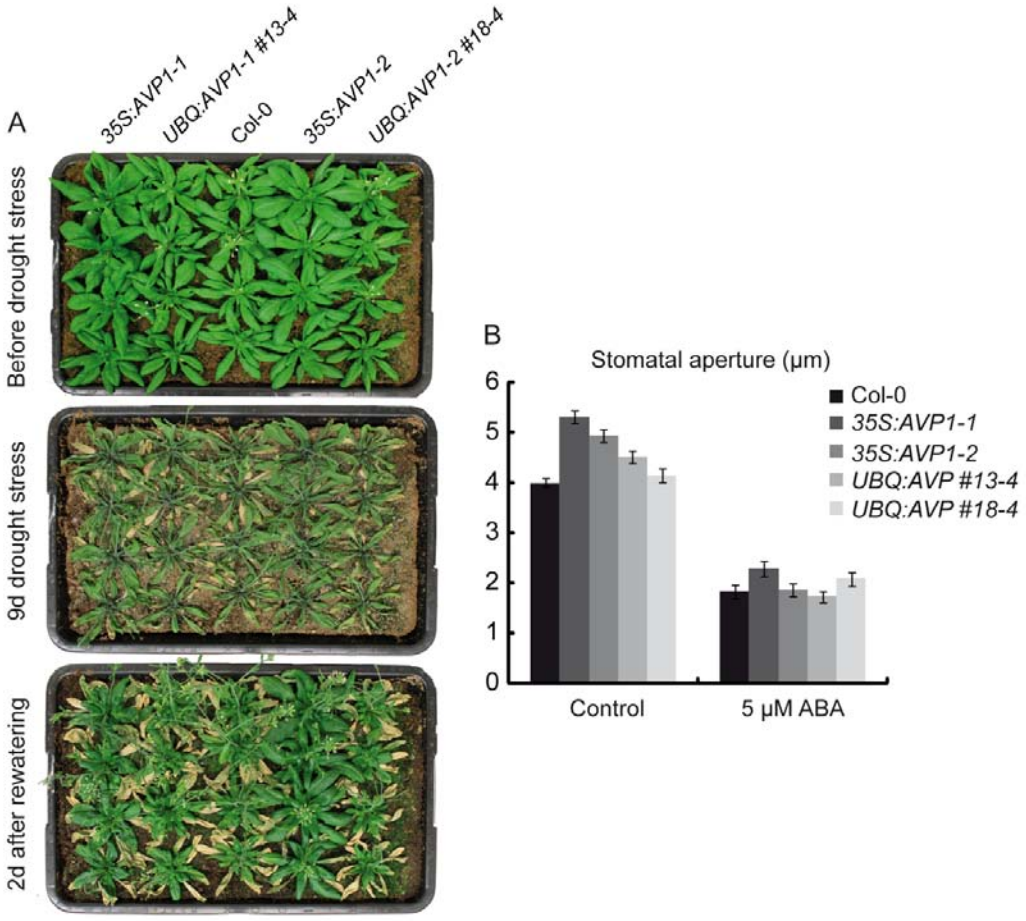

Figure 4. *35S:AVP1* plants are more drought tolerant.

(A) Drought tolerance test of wild type, *35S:AVP1-1*, *35S:AVP1-2*, *UBQ:AVP1 #13-4* and *UBQ:AVP1 #18-4* grown in one soil tray. Plants were grown for 33 days under LD conditions and then subjected to drought stress by ceasing watering for 9 days. After that plants were rewatered for 2 days and pictures were taken.
(B) Stomatal closure is not affected in *35S:AVP1*. Stomatal apertures were determined under 2.5 h of light (control) or after 1 h of treatment with 5 µM ABA. Data represent the mean and SE of the absolute values of aperture of at least 40 stomata per line and per treatment. Experiment presented in B was performed by Zaida Andrés.

avp1-1 carries T-DNA insertions in *AVP1* and *GNOM*

Our studies that involved the characterization of the V-PPase and its importance for vacuolar acidification, as addressed in chapter 1 of this thesis, included the analysis of V-PPase mutants besides the use of AVP1 overexpressing lines. However, over the past decade, a variety of V-PPase mutants that greatly differ in their phenotypes have been published (Li et al., 2005; Ferjani et al., 2011; Pizzio et al., 2015). Due to fact that *avp1-1* mutants show severely impaired shoot and root development that are in contrast to mild cellular phenotypes of *vhp1-1*/*fugu5*, we hypothesized that *avp1-1* phenotypes could be caused by a linked second-site mutation. Therefore, we performed whole genome sequencing of the *avp1-1* (GABI-Kat 005D04) line and found that in addition to the insertion in *AVP1*, GABI-Kat 005D04 contains a second T-DNA insertion in the 3' end of At1g13980, which encodes the ARF guanine nucleotide exchange factor (ARF-GEF) GNOM (Fig. 5A and 5B). GNOM activity is required for polar auxin transport (Geldner et al., 2003) and weak alleles cause fused cotyledon phenotypes that were also observed in *avp1-1* (Geldner et al., 2004). Genotyping of the *avp1-1* mutant using T-DNA specific and gene-specific primers confirmed the presence of T-DNAs in *AVP1* and *GNOM* (Fig. 5C) while a combination of two gene-specific primers for each gene did not result in an amplification product.

To test if the second insertion in *GNOM* is responsible for the *avp1-1* phenotype, we performed allelism tests among the *avp1/vhp1/fugu*-alleles and the *gnom*-allele *emb30-1* (Mayer et al., 1993). The *gnom* phenotype was observed in 25% of seedlings in the F1 progeny from a cross between the *avp1-1/*+ and *emb30/*+ lines, whereas crosses among *avp1-1/*+ and homozygous *vhp1-1* and *fugu5-1* plants resulted only in wild-type and *fugu5-1* seedling phenotypes (Fig. 6A and 6B).

As another independent verification, we tried to complement *avp1-1* by expressing VHP1-mGFP that has been previously shown to complement the rectangular cotyledon phenotype of *vhp1-1* mutant plants (Segami et al., 2014). The F2 progeny of the cross between *avp1-1/*+ and VHP1-mGFP was sown on MS medium containing hygromycin in order to select for seedlings that contain VHP1-mGFP. Seedlings positive for VHP1-mGFP were identified that also showed characteristic *gnom* mutant phenotypes (Fig. 6C left).

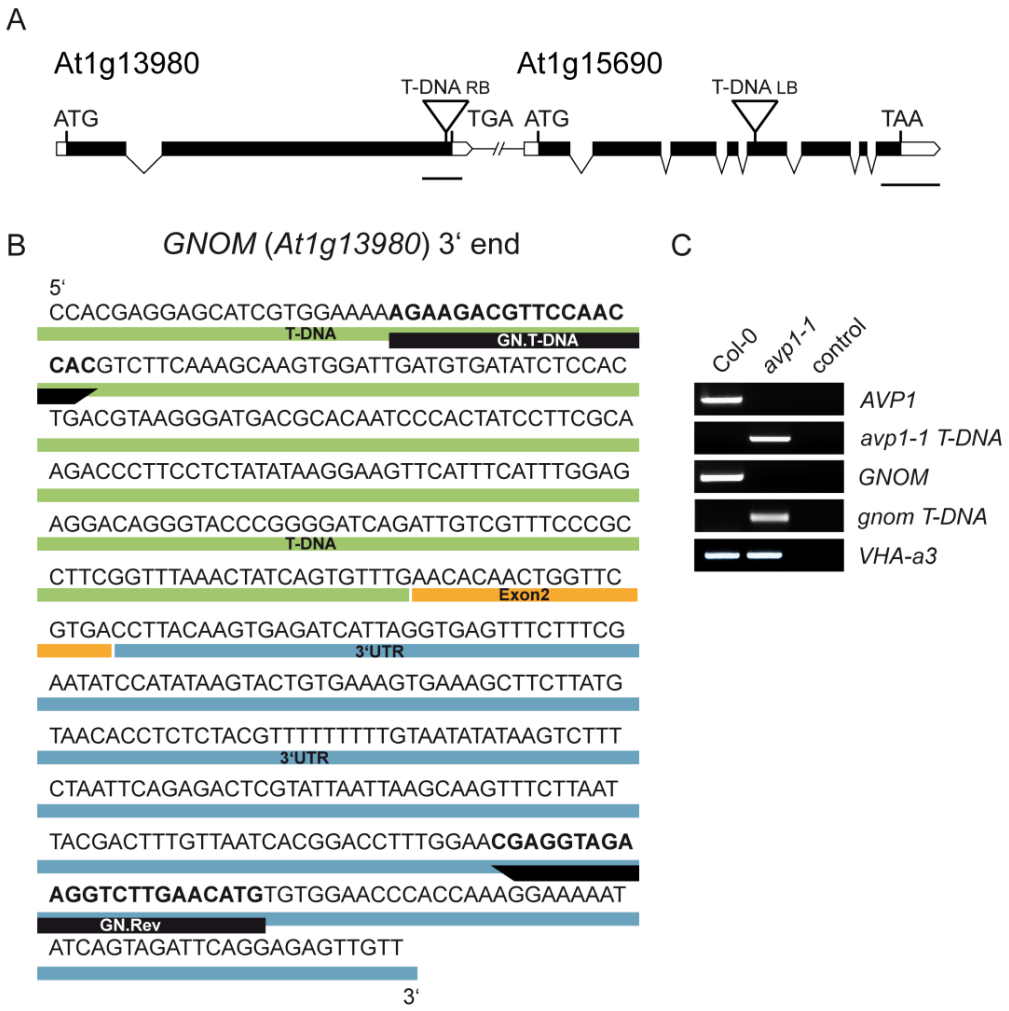

Figure 5. *avp1-1* carries T-DNA insertions in *AVP1* and *GNOM.*

(A) Position of the two T-DNA Insertions on Chr. 1 in the GABI-Kat 005D04 line. Bars = 500 bp.
(B) Position of the T-DNA insertion in *GNOM*. Shown is the 3' end of *GNOM* with the T-DNA (green bar), Exon 2 (orange bar), 3' UTR (blue bar) and the primer sequences (GN_T-DNA, GN_Rev; black bar) used for T-DNA identification.
(C) Genotyping of T-DNA insertions in *avp1-1*. PCR on genomic DNA of wild type and *avp1-1* using T-DNA-specific primer pairs for *AVP1* and *GNOM* shows the presence of the T-DNA in both genes. Gene-specific primer pairs were used to demonstrate the absence of the intact gene in *avp1-1*. Amplification of *VHA-a3* served as a control. Water served as a negative control for PCR reactions.

Since these seedlings with abnormal shoot and root development showed proper tonoplast localization of VHP1-mGFP as revealed by CLSM analysis in roots of 6-day-old seedlings (Fig. 6C middle and right), we can conclude that the phenotype of *avp1-1* mutants is not due to loss of *AVP1*. Together, these results showed that the *avp1-1* phenotype is caused by a linked second site mutation in *GNOM*, whereas the *fugu5/vhp1* phenotype reflects the lack of AVP1/VHP1 activity.

A

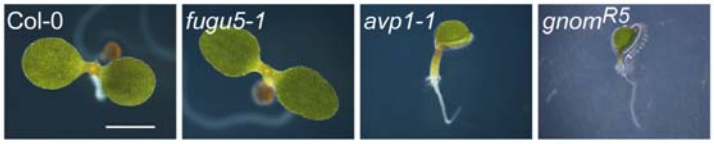

B

Crosses	Col-0	*fugu5-1*	*gnom*^{R5}
avp1-1/+ x vhp1-1	55.6	43.8	0.7
avp1-1/+ x fugu5-1	44.6	55.4	0.0
avp1-1/+ x emb30-1/+	74.3	0.7	25.0
fugu5-1 x emb30-1/+	100.0	0.0	0.0
fugu5-1 x vhp1-1	0.0	100.0	0.0
fugu5-1 x avp1-1/+	65.9	33.5	0.6

C

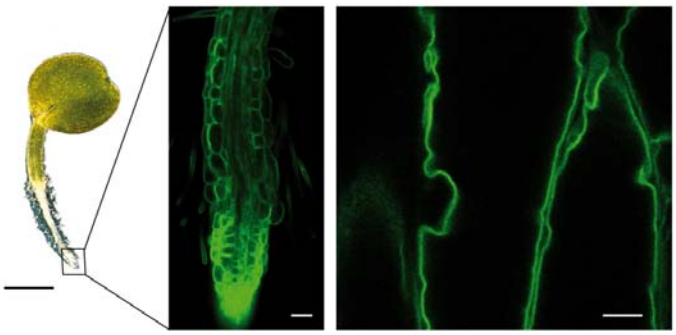

Figure 6. T-DNA insertion in *GNOM* causes phenotypic defects in *avp1-1*.

(A) Comparison of the phenotypes of 5-day-old wild type, *fugu5-1*, *avp1-1* and *gnom*^{R5} seedlings. Bar = 1 cm.
(B) Allelism test between V-PPase and *gnom* mutants. V-PPase mutants (*vhp1-1*, *fugu5-1*) were crossed with *avp1-1/+* or with *gnom/+* (*emb30-1*) mutants. Phenotypes of 6-day-old F1 seedlings (n = 80 to 190) were counted. Numbers given in the table are in percentage (%).
(C) Introduction of VHP1-mGFP failed to rescue *gnom* phenotypes of *avp1-1*. In the F2 generation of the cross between *avp1-1/+* and VHP1-mGFP seedlings with *gnom* phenotypes were selected and subsequently analyzed for their GFP fluorescence. Depicted is one 6-day-old seedling with *gnom* phenotype (left) showing GFP fluorescence in the root tip (middle). The picture on the right demonstrates tonoplast localization of VHP1-mGFP in *avp1-1*. From left to right: scale bars = 1 mm; 50 µm; 5 µm. CLSM images shown in C were taken by Falco Krüger.

II.4 Discussion

Increased biomass of *35S:AVP1* is not due to ubiquitous overexpression

It has been 14 years ago that Gaxiola and colleagues found that overexpression of *AVP1* in Arabidopsis resulted in increased salt tolerance and drought resistance (Gaxiola et al., 2001). The salt tolerance was explained by an increased accumulation of Na^+ and K^+ in the leaf tissue of transgenic plants likely due to the elevated activity of the vacuolar Na^+,K^+/H^+ antiporter, NHX1 and NHX2, while the drought resistance could be due to higher water retention as a consequence of elevated vacuolar solute content. In another study, four ecotypes of Arabidopsis were tested for their salinity tolerance by comparing expression profiles of Na^+ transport related genes (Jha et al., 2010). Although AVP1 is not directly involved in Na^+ transport, ecotypes with higher *AVP1* expression showed elevated salt tolerance which is due to its role in establishing and maintaining the electrochemical gradient across the tonoplast. Over the past years, *AVP1* overexpression became a universal strategy to generate a number of crop plants such as, for example, barley, cotton, rice, tomato and maize with enhanced salt- and drought tolerance (Schilling et al., 2014; Pasapula et al., 2011; Yang et al., 2007; Li et al., 2008). Moreover, elevated AVP1 levels led to improved nitrogen use efficiency in romaine lettuce and enhanced phosphorus nutrition in Arabidopsis, tomato and rice (Paez-Valencia et al., 2013; Yang et al., 2007). Arabidopsis plants expressing *35S:AVP1* were shown to have a higher number of rosette leaves and a significantly increased leaf area compared to wild type plants (Li et al., 2005; Gonzalez et al., 2010). This was entirely attributed to a higher cell number since cell area was shown to be unchanged. Here we show that the molecular basis for the biomass increase and abiotic stress tolerance in Arabidopsis *35S:AVP1* lines (*AVP1-1* and *AVP1-2*) needs to be re-evaluated. Although increased amounts of protein in leaves of *AVP1-1* and *AVP1-2* were initially reported (Gaxiola et al., 2001), we could not detect increased *AVP1* RNA or protein in leaves and other tissues in T_3 plants which is in contrast to our *UBQ:AVP1* lines. Instead, we detected a decrease in enzyme activity and a slight increase in vacuolar pH in *35S:AVP1* plants. This is presumably because overexpression was lost due to transgene silencing. Given that a fragment containing two copies of the *35S* promoter was used in the original construct and that multiple copies of the T-DNA have been

detected in the transgenic lines (data not shown), it is not unexpected that expression of the transgene was lost over time. Indeed, it was shown that exceeding a gene-specific threshold of a certain transgene copy number initiates silencing (Schubert, 2004). What is however surprising is that the two lines *AVP1-1* and *AVP1-2* still display the significant increase in rosette biomass and show drought resistance as it was originally reported. Although we showed here that constitutive overexpression of *AVP1* in Arabidopsis in the *35S*-lines was lost by transgene silencing, it remains possible that overexpression is maintained in particular cell types or tissues. It was shown recently that guard cell specific overexpression of the plasma membrane H^+-ATPase AHA2 (PMA2, AT4G30190) causes enhanced stomatal aperture and increased photosynthetic activity, ultimately resulting in larger leaves (Wang et al., 2014). We therefore measured light-induced stomatal opening and found that increased CO_2-assimilation due to increased stomatal aperture could be responsible for the increased biomass. It remains to be determined if this is indeed due to overexpression of AVP1 in guard cells. A role of AVP1 in guard cells has been suggested previously, since mutants lacking *AVP1* were delayed in ABA-induced stomatal closure (Bak et al., 2013). To support the role of AVP1 in stomatal opening it would be useful to specifically express *AVP1* in guard cells and analyze its effect on growth. However, independent of the underlying mechanism it is clear that the increased biomass of *AVP1-1* and *AVP1-2* is likely to be multifactorial and requires further attention. This is particularly important as expression of *AVP1* under the control of the *35S* promoter is a very successful strategy to improve crop performance. Our results in *Arabidopsis* thus suggest that constitutive overexpression is neither necessary nor sufficient for improved growth and stress tolerance.

A second T-DNA insertion in *GNOM* is responsible for the *avp1-1* phenotype

T-DNA insertion mutants are central to reverse genetics but, as our data reveal, careful validation of mutant lines obtained from T-DNA collections are necessary. In case of *AVP1*, the so far characterized mutant lines vary strongly in their phenotypes and thus opposing functions for AVP1 have been reported (Li et al., 2005; Ferjani et al., 2011). Since we aimed to investigate the role of AVP1 for vacuolar acidification (see chapter 1), the use of *avp1* mutants was of pivotal importance. Due to the fact

that the *avp1-1* mutant line showed severe shoot and root developmental defects in contrast to several additional *avp1* mutant alleles (*avp1-2*/*vhp1-1*/*fugu5*) that had only mild cotyledon phenotypes, we decided to analyze *avp1-1* in detail. Based on whole genome sequencing and allelism tests, we can conclude that the severe developmental phenotype of *avp1-1* is due to the presence of a second T-DNA insertion close to the 3' end of the gene encoding the ARF-GEF GNOM which is required for PIN cycling (Blakeslee et al., 2005; Geldner et al., 2003). Further, the phenotypes caused by *gnom*^{R5}, a weak allele of *GNOM*, are highly similar to *avp1-1* (Geldner et al., 2004), which is an *avp1-1*/*gnom* double mutant. How Li and colleagues were then able to complement the *avp1-1* mutant allele by using a dexamethasone-inducible AVP1 cassette remains unsolved. As expected, our attempt to rescue *avp1-1* phenotypes by introducing VHP1-mGFP failed. *avp1-1* has been demonstrated to exhibit reduced auxin transport, however based on *DR5:GUS* expression and its response to exogenous IAA, the *fugu5-1* mutant has been shown to have a normal auxin distribution and response (Ferjani et al., 2011). In fact, *vhp1-1/*fugu5 mutant alleles did not show any of the developmental defects observed for *avp1-1* which supports our findings. Interestingly, it has been previously suggested that *avp1-1* may have more than one T-DNA insertion site (Ferjani et al., 2012). Together, we can conclude that AVP1 does not play a role in auxin-mediated organ development, and phenotypic defects caused by the lack of the V-PPase comprise impaired cell proliferation due to cytosolic accumulation of PP_i (Ferjani et al., 2011, 2012).

Conclusion

Here, we demonstrate that the reason for the increased growth of *35S*-driven *AVP1* lines is not the ubiquitous overexpression of *AVP1*. Direct comparison of *35S:AVP1* and *UBQ:AVP1* lines concerning their RNA, protein and enzyme activity level revealed transgene silencing in *35S*-lines since all these examined parameters were either unchanged or even reduced when compared to the wild type. In contrast, *UBQ:AVP1* lines, that overexpress AVP1 do not show the strong biomass increase. Thus, our results in *Arabidopsis* suggest that constitutive overexpression is neither necessary nor sufficient for improved growth and stress tolerance. In addition, we show that the seedling lethal phenotype of *avp1-1* mutants is caused by a second T-DNA insertion in the ARF-GEF GNOM as revealed by whole genome sequencing. T-DNA insertions were confirmed by genotyping using T-DNA specific and gene-specific primers for *AVP1* and *GNOM*. Further, allelism tests between the different *AVP1* mutant alleles and the fact that the rescue of *avp1-1* using VHP1-mGFP failed, supports our data. This shows that careful validation and the use of independent mutant alleles is important in order to deduce gene functions.

II.5 Material and Methods

Plant material and growth conditions

Arabidopsis thaliana, Columbia 0 (Col-0) ecotype was used in all experiments. Transgenic *35S:AVP1* lines (*AVP1-1* and *AVP1-2)* were previously established (Gaxiola et al., 2001). The two V-PPase mutant lines *fugu5-1* and *vhp1-1* were previously described (Ferjani et al., 2011). The loss-of-function mutant, *avp1-1* (005D04), was obtained from the GABI-KAT collection (www.gabi-kat.de). The GNOM mutants *gnom*^{R5} and *emb30-1* were described previously (Mayer et al., 1993). VHP1-mGFP was provided by Shoji Segami (Segami et al., 2014). For growth on plates, seeds were surface sterilized by shaking them in a solution of 70% Ethanol mixed with 0.05% Triton-X-100 for 20 min followed by 10 min sterilization in 95% Ethanol. Thereafter seeds were dried on a sterile filter paper. For stratification, seeds were kept at 4°C for at least 24 h before transferring them to light. Plants were grown at 22°C under long day (LD) conditions with 16 h light and 8 h dark.

Plant material used for immunoblotting, qRT-PCR, V-PPase activity assay, fresh weight determination and stomatal aperture measurements was grown on soil for the indicated time periods at 22°C under LD conditions.

Seedlings for root vacuolar pH measurements and for allelism tests were grown for 6 days on sterile plates containing 1/2 MS, 0.5% sucrose, 0.5% phyto agar with the pH set to 5.8 using KOH.

Transgene silencing was monitored using seedlings grown for 6 days on 1/2 MS medium containing 0.5% sucrose, 0.5% phyto agar, 10 mM MES (pH 5.8 using KOH) and 50 µg/µl kanamycin.

Plants for drought stress experiment were grown for 33 days under LD conditions. To start drought, watering of plants was omitted for 9 days. To check for the rate of recovery, plants were rewatered for 2 days. Plants were photographed after every change of conditions.

Construct design

Generation of UBQ:AVP1

To generate transgenic plants expressing *AVP1* under the control of the *UBQ10* promoter the plant binary vector *UBQ:AVP1* was generated. First, a 2331 bp fragment of *AVP1* was amplified from cDNA using AVP1-*Xba*I-Fw and AVP1-*Sal*I-Rv. After subcloning into pJET1.2blunt (Thermo Scientific, www.thermoscientificbio.com) the fragment was released using the introduced *Xba*I and *Sal*I restriction sites and inserted into the backbone of the binary vector pTKan (Krebs et al., 2012) to receive pTKan-AVP1. In addition, a 661 bp fragment of the Arabidopsis *UBQ10* promoter was amplified using UBQ10-*Kpn*I-Fw and UBQ10-*Kpn*I-Rv. After subcloning of *UBQ10* into pJET1.2blunt, the fragment was released via the *Kpn*I site and inserted into pTKan-AVP1 to finally receive *UBQ:AVP1*. The *UBQ:AVP1* construct was cloned by Melanie Krebs.

Plant transformation

The *UBQ:AVP1* construct was introduced into the *Agrobacterium tumefaciens* strain GV3101:pMP90 and selected on 5 µg/ml rifampicin, 10 µg/ml gentamycin and 100 µg/ml spectinomycin. *Arabidopsis thaliana* ecotype Col-0 was used for transformation using standard procedures.

Genetic crosses

Flowers that were used as female parents were emasculated by removing the anthers with forceps. These flowers were then pollinated by touching the stigma with anthers from the male parent. For one crossing combination 5-6 flowers were used and their siliques were pooled. Seeds of the F1 generation were sown on 1/2 MS medium (see above) and grown for 6 days. Thereafter seedlings were counted (n = 80-190) and classified according to their phenotype.

Genome sequencing

For genome sequencing, *avp1-1* seedlings showing strong shoot and root abnormalities were collected and used for DNA preparation. DNA was isolated according to manufacturer's instructions using the DNeasy Plant Mini Kit (Qiagen).

The library was produced at the CellNetworks Deep Sequencing Core Facility (Heidelberg) and sequenced at the EMBL Genomics Core Facility (Heidelberg) as 50 bps single-end reads, multiplexed on a HiSeq2000 (Illumina).

Sequences were mapped to the TAIR10 genome using bowtie2 (version 2.0.5) (Langmead and Salzberg, 2012) with the fast-local option. 21.7 mio reads mapped for the *avp1* mutant line. The *avp1* mutant was additionally mapped against the GABI-KAT plasmid pAC106 (Kirik et al., 2006; Kleinboelting et al., 2012). The mappings were converted to bam format, sorted and indexed using samtools (version 0.1.16) (Li et al., 2009) and displayed on the Integrative Genomics Viewer (Robinson et al., 2011; Thorvaldsdóttir et al., 2013). Reads that showed partial mapping to the T-DNA borders were compared to gaps in the genomic alignment in order to identify the insertion sites.

RNA isolation and cDNA synthesis

For the analysis of *AVP1* transcript levels in different plant tissues, RNA was isolated according to manufacturer's instructions using the RNeasy Plant Mini Kit (Qiagen). cDNA was synthesized from 2 µg of total RNA using M-MuLV reverse transcriptase (Thermo) and an oligo dT primer.

Real-time RT PCR

For quantitative analysis of gene expression real-time RT PCR was applied. cDNA samples were diluted 1:50 in nuclease-free water. Real-time PCR reactions were performed using the DNA Engine Opticon System (DNA Engine cycler and Chromo4 detector, BioRad) and ABsolute qPCR SYBR Green Mix (Thermo Scientific). The real-time PCR reaction mixture with a final volume of 20 µl contained 0.5 µM of each forward and reverse primer, 10 µl SYBR Green Mix, 4 µl cDNA and 4 µl of RNase-free water. The thermal cycling conditions were composed of an initial denaturation step at 95°C for 15 min followed by 40 cycles at 95°C for 15 sec, 59°C for 30 sec and 72°C for 15 sec and ended with a melting curve. For the analysis of each sample three analytical replicas were used. Target genes were normalized to the expression of *Actin2*. Primer sequences for *AVP1* (AVP1qRT.For and AVP1qRT.Rev) and *Actin2* (ActinQRT_f and ActinQrt_r) are listed in the table below this section.

Genotyping

Genomic DNA was extracted as described previously (Edwards et al., 1991).

To check for the presence of the T-DNA in the *AVP1* gene, PCR was performed using a T-DNA left border specific primer (LB-JL202) and a *AVP1* specific reverse primer (AVP1.Rev). To identify the *AVP1* wild type allele, two gene specific primers were used (AVP1.For and AVP1.Rev).

In order to analyze whether *avp1-1* mutants also carry a T-DNA insertion in *GNOM*, a T-DNA right border primer (GN.T-DNA) and a *GNOM* specific reverse primer (GN.REV) was used. The *GNOM* wild type allele was identified using GNOM forward and reverse primer (GN.For and GN.Rev).

Amplification of *VHA-a3* using *VHA-a3* specific forward (S029786.for) and reverse (S029786.rev) primer served as a control.

Primer sequences are listed in the table below this section.

Preparation of microsomal membranes

Microsomal membrane proteins were extracted as described before (Schumacher et al., 1999) with minor modifications. Briefly, shoots from wild type and mutant plants were harvested and frozen in liquid nitrogen until further use. For protein extraction, rosette leaves were ground in liquid nitrogen, plant powder was filled into a falcon tube and homogenized in homogenization buffer (2 ml/g fresh weight) containing 350 mM sucrose, 70 mM Tris-HCl (pH 8), 10% (vol/vol) glycerol, 3 mM Na_2EDTA, 0.15% (wt/vol) BSA, 1.5% (vol/vol) PVP-40, 4 mM DTT and 1x complete protease inhibitor cocktail (Roche). The homogenate was filtered through two layers of Miracloth and centrifuged at 15,000 g for 15 min at 4°C. The supernatent was filtered through Miracloth again and then centrifuged at 100,000 g for 45 min at 4°C. The microsomal membrane pellet was resuspended in resuspension buffer containing 350 mM sucrose, 10 mM Tris-MES (pH 7), 2 mM EGTA, 2 mM DTT and 1x complete protease inhibitor cocktail. Protein concentrations were determined as reported previously (Bradford, 1976).

SDS-PAGE and immunoblotting analysis

To analyse the protein level in microsomal membranes extracted from wild type and mutant plants SDS-PAGE and immunoblotting was applied. After electrophoresis, proteins were transferred to a nitrocellulose membrane (Whatman). The following primary antibodies were used: the V-PPase antibody (Cosmo Bio; 1:5000; amino acid sequence of antigen, DLVGKIERNIPEDDPRN; (Kobae et al., 2006)) and an antibody against VHA-C (Schumacher et al., 1999). Antigen on the membrane was visualized with horseradish peroxidase-coupled anti-rabbit IgG (Promega) and chemiluminescent substrate (Peqlab). Immunostained bands were analyzed using a cooled CCD camera system (Intas).

V-PPase activity assay

V-PPase activity was measured colorimetrically as Pi release (Heinonen and Lahti, 1981).

The V-PPase assay medium contained 25 mM Tris-MES (pH 7.5), 2 mM $MgSO_4$ *7 H_2O, 0.1 mM Na_2MoO_4, 0.02% Brij 58, 0.2 mM PPi and 50 mM KCl. The reaction was started by adding 10 µg microsomal membrane proteins to the medium. After 20 min at 28°C the reaction was stopped by the addition of 12 µl of 1 M citric acid. Thereafter the amount of Pi released in the presence or absence of KCl was determined. For that a 30 µl aliquot of the reaction mixture was mixed with 240 µl of acetone-acid-molybdate solution (2.5 mM $(NH_4)_6Mo_7O_{24}$*4 H_2O, 1.25 N H_2SO_4, 50% acetone) and afterwards the Pi release was colorimetrically determined by measuring absorbance at 355 nm in a microplate reader (Tecan Infinite M1000). BSA (10 µg) was used as a control in order to calculate a blank value.

Measurement of Stomatal Aperture and Size

Stomatal apertures were measured as described previously in Andres et al. (Andrés et al., 2014) with some modifications. Leaves from overnight dark-adapted 3- to 4-week-old plants were incubated for 1 h in darkness in stomatal incubation buffer containing 10 mM MES·KOH (pH 6.5), 30 mM KCl and 50 µM $CaCl_2$, and then for 2.5 h under dark or light (250 µmol $m^{-2}·s^{-1}$) at 22 °C. For ABA-induced stomatal closure experiments, leaves were preincubated for 2.5 h under light to induce stomatal

opening. Then 5 µM of ABA was added, and stomatal aperture was measured 1 h after treatment. Strips of leaf abaxial epidermis were imaged under the Leica SP5II confocal laser scanning microscope using the bright field. Values represent the mean ± SEM of 40 stomata per line and treatment. Stomatal bioassays were performed three times and measured as blind experiments. The length of 160 stomata (length between the junctions of the guard cells at each end of the stomata) was measured in the pictures taken to measure stomatal aperture.

pH measurements

To measure vacuolar pH, seedlings were incubated in liquid medium containing 1/2 MS and 0.5% sucrose (pH 5.8) supplemented with 10 µM of the membrane-permeant pH sensitive dye BCECF-AM (Molecular Probes, Invitrogen) and 0.02% Pluronic F-127 (Molecular Probes, Invitrogen). After 1 h of staining in darkness at 22°C with gentle agitation, seedlings were washed twice in liquid MS medium for 5 min. BCECF fluorescence was detected using a Leica SP5II confocal laser scanning microscope equipped with a HCX PL APO CS 20.0 x 0.70 IMM UV water immersion objective (Leica). BCECF was excited at 458 nm and 488 nm with a VIS-Argon laser and the emission was detected between 510 nm and 550 nm. Images have been taken in fully elongated cells of the root hair zone. Average fluorescence intensity values of captured images of both excitation wavelengths were obtained using the software ImageJ 1.49 (NIH, USA). Ratios were calculated by dividing values received for 488 nm by values obtained for 458 nm. Ratios were then used to calculate the vacuolar pH on the basis of a calibration curve. To perform in vivo calibration of BCECF, seedlings were incubated in liquid medium containing the dye as described before. Prior to the measurement seedlings were incubated for 20 min in pH equilibration buffers containing 50 mM MES-BTP (pH 5.2 to 6.4) or 50 mM Hepes-BTP (pH 6.8 to 8.0) and 50 mM ammonium acetate. The calibration curve was obtained by plotting ratio values against the pH. To generate calibration curves sigmoidal Boltzman fit was used.

Confocal microscopy

Confocal laser scanning microscopy was performed using a Leica TCS SP5II microscope equipped with a Leica HCX PL APO lambda blue 63.0x1.20 UV water

immersion objective. GFP was excited at 488 nm with a VIS-argon laser and fluorescence emission was detected between 500 and 555 nm. For image acquisition Leica Application Suite Advanced Fluorescence software was used. Processing of images was performed using Fiji (based on ImageJ 1.47t).

Imaging

Pictures of rosettes from adult plants and from drought stressed plants were taken using a Nikon D60 digital camera. Images of wild type, *fugu5-1*, *avp1-1* and *gnom*^{R5} seedlings were observed at the Zeiss stereomicroscope Stemi 2000-CS equipped with an Axio cam HRc using the AxioVision Rel. 4.7 software. Images were processed using Adobe Photoshop CS4.

Appendix

Primer sequences

Primer name	Sequence 5'-3'
AVP1-XbaI-Fw	TCCTCTAGAATGGTGGCGCCTGCTTTGTTAACC
AVP1-SalI-Rv	CAGGTCGACTTAGAAGTACTTGAAAAGGATACCACCG
UBQ10-KpnI-Fw	AAGGTACCCGACGAGTCAGTAATAAACGGCG
UBQ10-KpnI-Rv	GATGGTACCCGCACTCGAGCTGTTAATCAG
S029786.for (VHA-a3)	CTGATGTTACTATTGTACCGAAC
S029786.rev (VHA-a3)	TCGCGATATTCAAATAACAGCT
AVP1.For	CCAGCATTGAAGAACCAGCTC
AVP1.Rev	CCAATGATAACTTTAGGGGTCAAA
LB-JL202	CATTTTATAATAACGCTGCGGACATCTAC
GN.For	GCAACTCCAAGAGCTATCTCAG
GN.Rev	CATGTTCAAGACCTTCTACCTCG
GN.T-DNA	AGAAGACGTTCCAACCAC
AVP1qRT.For	GGAGACACAATTGGAGACCC
AVP1qRT.Rev	GTGAGTGGCGAAGAAGGGAG
ActinQRT_f	TCTTCCGCTCTTTCTTTCCA
ActinQrt_r	TCACCATACCGGTACCATTG

Abbreviations

°C	Degree Celsius
%	Percent
µg	Microgram
µm	Micrometer
µM	Micromolar
ABA	Abscisic acid
ADP	Adenosine diphosphate
amiRNA	Artificial microRNA
Arabidopsis	*Arabidopsis thaliana*
ARF-GEF	ADP-ribosylation factor - guanine nucleotide exchange factor
ATP	Adenosine triphosphate
BafA	Bafilomycin A
BCECF	2′,7′-bis-(2-carboxyethyl)-5-(and-6)-carboxyfluorescein
bp	Base pair
cDNA	Complementary DNA
Chr.	Chromosom
CL	Constant light
CLSM	Confocal laser scanning microscopy
cm	Centimetre
DNA	Desoxyribonucleic acid
Col-0	Columbia-0
ConcA	Concanamycin A
DAG	Days after germination
DEX	Dexamethasone
DMSO	Dimethyl sulfoxide
E. coli	*Escherichia coli*
EZ	Elongation zone
F	Filial generation
F-ATPase	F-type ATP synthase
Fig.	Figure

g	Gram
GA	Gibberellic acid
GFP	Green fluorescent protein
h	Hour(s)
HPLC	High pressure liquid chromatography
kDa	Kilodalton
LD	Long day
LV	Lytic vacuole
mGFP	Nondimerizing GFP
MZ	Meristematic zone
mm	Millimeter
mM	Millimolar
min	Minute
MS	Murashige and Skoog
PA	Proanthocyanidin
P-ATPase	P-type H^+- adenosintriphosphatase
PC	Phosphatidylcholine
PEP	Phosphoenolpyruvate
P_i	Inorganic phosphate
PP_i	Pyrophosphate
PSV	Protein storage vacuole
qRT PCR	Quantitative real time polymerase chain reaction
RNA	Ribonucleic acid
RNAi	RNA interference
SD	Standard deviation
SDS-PAGE	Sodium dodecylsulfate polyacrylamide gel electrophoresis
SE	Standard Error
T-DNA	Transfer DNA
TGN/EE	Trans-Golgi network/early endosome
UBQ	*Ubiquitin-10* promoter
V-ATPase, VHA	V-type H^+- adenosintriphosphatase
V-PPase	H^+-pyrophosphatase

References

Andrés, Z., Pérez-Hormaeche, J., Leidi, E.O., Schlücking, K., Steinhorst, L., McLachlan, D.H., Schumacher, K., Hetherington, A.M., Kudla, J., Cubero, B., and Pardo, J.M. (2014). Control of vacuolar dynamics and regulation of stomatal aperture by tonoplast potassium uptake. Proc. Natl. Acad. Sci. U. S. A. **111**: E1806–14.

Arif, A., Zafar, Y., Arif, M., and Blumwald, E. (2013). Improved Growth, Drought Tolerance, and Ultrastructural Evidence of Increased Turgidity in Tobacco Plants Overexpressing Arabidopsis Vacuolar Pyrophosphatase (AVP1). Mol. Biotechnol. **54**: 379–392.

Bak, G., Lee, E.-J., Lee, Y., Kato, M., Segami, S., Sze, H., Maeshima, M., Hwang, J.-U., and Lee, Y. (2013). Rapid structural changes and acidification of guard cell vacuoles during stomatal closure require phosphatidylinositol 3,5-bisphosphate. Plant Cell **25**: 2202–16.

Bao, A.K., Wang, S.M., Wu, G.Q., Xi, J.J., Zhang, J.L., and Wang, C.M. (2009). Overexpression of the Arabidopsis H+-PPase enhanced resistance to salt and drought stress in transgenic alfalfa (Medicago sativa L.). Plant Sci. **176**: 232–240.

Bassil, E., Tajima, H., Liang, Y.-C., Ohto, M.-A., Ushijima, K., Nakano, R., Esumi, T., Coku, A., Belmonte, M., and Blumwald, E. (2011). The Arabidopsis Na+/H+ antiporters NHX1 and NHX2 control vacuolar pH and K+ homeostasis to regulate growth, flower development, and reproduction. Plant Cell **23**: 3482–97.

Batelli, G., Verslues, P.E., Fern, Agius, F., Agius, a, Qiu, Q., Fujii, H., Pan, S., Schumaker, K.S., Grillo, S., and Zhu, J.-K. (2007). SOS2 promotes salt tolerance in part by interacting with the vacuolar H+-ATPase and upregulating its transport activity. Mol. Cell. Biol. **27**: 7781–7790.

Baxter, I., Tchieu, J., Sussman, M.R., Boutry, M., Palmgren, M.G., Gribskov, M., Harper, J.F., and Axelsen, K.B. (2003). Genomic Comparison of P-Type ATPase Ion Pumps in Arabidopsis and Rice. Plant Physiol. **132**: 618–628.

Baxter, I., Young, J., Armstrong, G., Foster, N., Bogenschutz, N., Cordova, T., Peer, W., Hazen, S., Murphy, A., and Harper, J. (2005). A plasma membrane H+-ATPase is required for the formation of proanthocyanidins in the seed coat endothelium of Arabidopsis thaliana. Proc. Natl. Acad. Sci. U. S. A. **102**: 2649–2654.

Becker, B. (2007). Function and evolution of the vacuolar compartment in green algae and land plants (Viridiplantae). Int. Rev. Cytol.

Blakeslee, J.J., Peer, W.A., and Murphy, A.S. (2005). Auxin transport. Curr. Opin. Plant Biol. **8**: 494–500.

Bolte, S., Talbot, C., Boutte, Y., Catrice, O., Read, N.D., and Satiat-Jeunemaitre, B. (2004). FM-dyes as experimental probes for dissecting vesicle trafficking in living plant cells. J. Microsc. **214**: 159–173.

Bowman, E., Graham, L., Stevens, T., and Bowman, B. (2004). The Bafilomycin/Concanamycin Binding Site in Subunit c of the V-ATPases from Neurospora crassa and Saccharomyces cerevisiae. J. Biol. Chem. **279**: 33131–33138.

Bradford, M. (1976). A rapid and sensitive method for the quantitation of microgram quantities of protein utilizing the principle of protein-dye binding. Anal. Biochem. **72**: 248–254.

Brüx, A., Liu, T.-Y., Krebs, M., Stierhof, Y.-D., Lohmann, J.U., Miersch, O., Wasternack, C., and Schumacher, K. (2008). Reduced V-ATPase activity in the trans-Golgi network causes oxylipin-dependent hypocotyl growth Inhibition in Arabidopsis. Plant Cell **20**: 1088–1100.

Carystinos, G.D., MacDonald, H.R., Monroy, a F., Dhindsa, R.S., and Poole, R.J. (1995). Vacuolar H(+)-translocating pyrophosphatase is induced by anoxia or chilling in seedlings of rice. Plant Physiol. **108**: 641–649.

Cellier, F., Conéjéro, G., Ricaud, L., Luu, D.T., Lepetit, M., Gosti, F., and Casse, F. (2004). Characterization of AtCHX17, a member of the cation/H+ exchangers, CHX family, from Arabidopsis thaliana suggests a role in K+ homeostasis. Plant J. **39**: 834–46.

Cheng, N.-H., Pittman, J.K., Barkla, B.J., Shigaki, T., and Hirschi, K.D. (2003). The Arabidopsis cax1 Mutant Exhibits Impaired Ion Homeostasis, Development, and Hormonal Responses and Reveals Interplay among Vacuolar Transporters. Plant Cell **15**: 347–364.

Cheng, N.-H., Pittman, J.K., Shigaki, T., Lachmansingh, J., LeClere, S., Lahner, B., Salt, D.E., and Hirschi, K.D. (2005). Functional association of Arabidopsis CAX1 and CAX3 is required for normal growth and ion homeostasis. Plant Physiol. **138**: 2048–60.

Craft, J., Samalova, M., Baroux, C., Townley, H., Martinez, A., Jepson, I., Tsiantis, M., and Moore, I. (2005). New pOp/LhG4 vectors for stringent glucocorticoid-dependent transgene expression in Arabidopsis. Plant J. **41**: 899–918.

Darley, C.P., Davies, J.M., and Sanders, D. (1995). Chill-Induced Changes in the Activity and Abundance of the Vacuolar Proton-Pumping Pyrophosphatase from Mung Bean Hypocotyls. Plant Physiol. **109**: 659–665.

Davies, O.D. (1986). What ' s New in Plant Physiology The fine control of cytosolic pH. East: 702–706.

Dettmer, J., Hong-Hermesdorf, A., Stierhof, Y.-D., and Schumacher, K. (2006). Vacuolar H+-ATPase Activity Is Required for Endocytic and Secretory Trafficking in Arabidopsis. Plant Cell **18**: 715–730.

Dettmer, J., Schubert, D., Calvo-Weimar, O., Stierhof, Y.-D., Schmidt, R., and Schumacher, K. (2005). Essential role of the V-ATPase in male gametophyte development. Plant J. **41**: 117–124.

Dietz, K. (1998). Modulation of the vacuolar H+ -ATPase by adenylates as basis for the transient CO2 -dependent acidification of the leaf vacuole upon illumination. Biochim. Biophys. Acta (BBA)- **1373**: 87–92.

Drozdowicz, Y. and Rea, P.A. (2001). Vacuolar H(+) pyrophosphatases: from the evolutionary backwaters into the mainstream. Trends Plant Sci. **6**: 206–211.

Dschida, W. and Bowman, B. (1995). The vacuolar ATPase: sulfite stabilization and the mechanism of nitrate inactivation. J. Biol. Chem. **270**: 1557–1563.

Edwards, K., Johnstone, C., and Thompson, C. (1991). A simple and rapid method for the preparation of plant genomic DNA for PCR analysis. Nucleic Acids Res. **19**: 1349.

Eisenach, C., Baetz, U., and Martinoia, E. (2014). Vacuolar proton pumping: More than the sum of its parts? Trends Plant Sci. **19**: 344–346.

Endler, A., Reiland, S., Gerrits, B., Schmidt, U.G., Baginsky, S., and Martinoia, E. (2009). In vivo phosphorylation sites of barley tonoplast proteins identified by a phosphoproteomic approach. Proteomics **9**: 310–321.

Erwee, M.G., Goodwin, P.B., and Van Bel, A.J.E. (1985). Cell-cell communication in the leaves of Commelina cyanea and other plants. Plant, Cell Environ. **8**: 173–178.

Faraco, M., Spelt, C., Bliek, M., Verweij, W., Hoshino, A., Espen, L., Prinsi, B., Jaarsma, R., Tarhan, E., de Boer, A.H., Di Sansebatiano, G.-P., Koes, R., and Quattrocchio, F.M. (2014). Hyperacidification of vacuoles by the combined action of two different P-ATPases in the tonoplast determines flower color. Cell Rep. **6**: 32–43.

Von der Fecht-Bartenbach, J., Bogner, M., Krebs, M., Stierhof, Y.-D., Schumacher, K., and Ludewig, U. (2007). Function of the anion transporter AtCLC-d in the trans-Golgi network. Plant J. **50**: 466–74.

Felle, H.H. (2001). pH: signal and messenger in plant cells. Plant Biol.: 1–15.

Ferjani, A., Segami, S., Horiguchi, G., Muto, Y., Maeshima, M., and Tsukaya, H. (2011). Keep an eye on PPi: the vacuolar-type H+-pyrophosphatase regulates postgerminative development in Arabidopsis. **23**: 2895–2908.

Ferjani, A., Segami, S., Horiguchi, G., Sakata, A., Maeshima, M., and Tsukaya, H. (2012). Regulation of pyrophosphate levels by H+-PPase is central for proper resumption of early plant development. Plant Signal. Behav. **7**: 38–42.

Garg, A.K., Kim, J.-K., Owens, T.G., Ranwala, A.P., Choi, Y. Do, Kochian, L. V, and Wu, R.J. (2002). Trehalose accumulation in rice plants confers high tolerance levels to different abiotic stresses. Proc. Natl. Acad. Sci. U. S. A. **99**: 15898–15903.

Gaxiola, R., Li, J., Undurraga, S., Dang, L., Allen, G., Alper, S., and Fink, G. (2001). Drought- and salt-tolerant plants result from overexpression of the AVP1 H+-pump. Proc. Natl. Acad. Sci. U. S. A. **98**: 11444–11449.

Gaxiola, R., Palmgren, M., and Schumacher, K. (2007). Plant proton pumps. FEBS Lett. **581**: 2204–2214.

Geitmann, A. and Ortega, J.K.E. (2009). Mechanics and modeling of plant cell growth. Trends Plant Sci. **14**: 467–478.

Geldner, N., Anders, N., Wolters, H., Keicher, J., Kornberger, W., Muller, P., Delbarre, A., Ueda, T., Nakano, A., and Jürgens, G. (2003). The Arabidopsis GNOM ARF-GEF mediates endosomal recycling, auxin transport, and auxin-dependent plant growth. Cell **112**: 219–230.

Geldner, N., Richter, S., Vieten, A., Marquardt, S., Torres-Ruiz, R., Mayer, U., and Jürgens, G. (2004). Partial loss-of-function alleles reveal a role for GNOM in auxin transport-related, post-embryonic development of Arabidopsis. Development **131**: 389–400.

Gendreau, E., Traas, J., Desnos, T., Grandjean, O., Caboche, M., and Höfte, H. (1997). Cellular basis of hypocotyl growth in Arabidopsis thaliana. Plant Physiol. **114**: 295–305.

Gonzalez, N., De Bodt, S., Sulpice, R., Jikumaru, Y., Chae, E., Dhondt, S., Van Daele, T., De Milde, L., Weigel, D., Kamiya, Y., Stitt, M., Beemster, G.T.S., and Inzé, D. (2010). Increased leaf size: different means to an end. Plant Physiol. **153**: 1261–1279.

Grefen, C., Donald, N., Hashimoto, K., Kudla, J., Schumacher, K., and Blatt, M.R. (2010). A ubiquitin-10 promoter-based vector set for fluorescent protein tagging facilitates temporal stability and native protein distribution in transient and stable expression studies. Plant J. **64**: 355–65.

Haruta, M., Burch, H., Nelson, R., Barrett-Wilt, G., Kline, K., Mohsin, S., Young, J., Otegui, M., and Sussman, M. (2010). Molecular Characterization of Mutant Arabidopsis Plants with Reduced Plasma Membrane Proton Pump Activity. J. Biol. Chem. **285**: 17918–17929.

Heinonen, J.K. and Lahti, R.J. (1981). A new and convenient colorimetric determination of inorganic orthophosphate and its application to the assay of inorganic pyrophosphatase. Anal. Biochem. **113**: 313–317.

Hong-Hermesdorf, A., Brüx, A., Grüber, A., Grüber, G., and Schumacher, K. (2006). A WNK kinase binds and phosphorylates V-ATPase subunit C. FEBS Lett. **580**: 932–939.

Huang, S., Colmer, T.D., and Millar, a. H. (2008). Does anoxia tolerance involve altering the energy currency towards PPi? Trends Plant Sci. **13**: 221–227.

Hurth, M.A., Suh, S.J., Kretzschmar, T., Geis, T., Bregante, M., Gambale, F., Martinoia, E., and Neuhaus, H.E. (2005). Impaired pH Homeostasis in Arabidopsis Lacking the Vacuolar Dicarboxylate Transporter and Analysis of Carboxylic Acid Transport across the Tonoplast. Plant Physiol. **137**: 901–910.

Huss, M., Ingenhort, G., König, S., Gaßel, M., Dröse, S., Zeeck, A., Altendorf, K., and Wieczorek, H. (2002). Concanamycin A, the Specific Inhibitor of V-ATPases, Binds to the Vo Subunit c. J. Biol. Chem. **277**: 40544–40548.

Jauh, G., Fischer, A., Grimes, H., Ryan, C., and Rogers, J. (1998). delta-Tonoplast intrinsic protein defines unique plant vacuole functions. Proc. Natl. Acad. Sci. U. S. A. **95**: 12995–12999.

Jha, D., Shirley, N., Tester, M., and Roy, S.J. (2010). Variation in salinity tolerance and shoot sodium accumulation in Arabidopsis ecotypes linked to differences in the natural expression levels of transporters involved in sodium transport. Plant, Cell Environ. **33**: 793–804.

Kane, P. (1995). Disassembly and reassembly of the yeast vacuolar H(+)-ATPase in vivo. J. Biol. Chem. **270**: 17025–17032.

Kempa, S., Krasensky, J., Dal Santo, S., Kopka, J., and Jonak, C. (2008). A central role of abscisic acid in stress-regulated carbohydrate metabolism. PLoS One **3**: e3935.

Kirik, A., Pecinka, A., Wendeler, E., and Reiss, B. (2006). The chromatin assembly factor subunit FASCIATA1 is involved in homologous recombination in plants. Plant Cell **18**: 2431–2442.

Kishor, P., Hong, Z., Miao, G.H., Hu, C., and Verma, D. (1995). Overexpression of [delta]-Pyrroline-5-Carboxylate Synthetase Increases Proline Production and Confers Osmotolerance in Transgenic Plants. Plant Physiol. **108**: 1387–1394.

Kleinboelting, N., Huep, G., Kloetgen, A., Viehoever, P., and Weisshaar, B. (2012). GABI-Kat SimpleSearch: New features of the Arabidopsis thaliana T-DNA mutant database. Nucleic Acids Res. **40**: D1211–5.

Klychnikov, O.I., Li, K.W., Lill, H., and De Boer, a. H. (2007). The V-ATPase from etiolated barley (Hordeum vulgare L.) shoots is activated by blue light and interacts with 14-3-3 proteins. J. Exp. Bot. **58**: 1013–1023.

Kobae, Y., Mizutani, M., Segami, S., and Maeshima, M. (2006). Immunochemical analysis of aquaporin isoforms in Arabidopsis suspension-cultured cells. Biosci. Biotechnol. Biochem. **70**: 980–987.

Krasensky, J. and Jonak, C. (2012). Drought, salt, and temperature stress-induced metabolic rearrangements and regulatory networks. J. Exp. Bot. **63**: 1593–1608.

Krebs, M., Beyhl, D., Görlich, E., Al-Rasheid, K. a S., Marten, I., Stierhof, Y.-D., Hedrich, R., and Schumacher, K. (2010). Arabidopsis V-ATPase activity at the tonoplast is required for efficient nutrient storage but not for sodium accumulation. Proc. Natl. Acad. Sci. U. S. A. **107**: 3251–3256.

Krebs, M., Held, K., Binder, A., Hashimoto, K., Den Herder, G., Parniske, M., Kudla, J., Schumacher, K., Herder, G., Parniske, M., Kudla, J., and Schumacher, K. (2012). FRET-based genetically encoded sensors allow high-resolution live cell imaging of Ca2+ dynamics. Plant J. **69**: 181–192.

Krussel, L., Junemann, J., Wirtz, M., Birke, H., Thornton, J., Browning, L., Poschet, G., Hell, R., Balk, J., Braun, H., and Hildebrandt, T. (2014). The Mitochondrial Sulfur Dioxygenase ETHYLMALONIC ENCEPHALOPATHY PROTEIN1 Is Required for Amino Acid Catabolism during Carbohydrate Starvation and Embryo Development in Arabidopsis. PLANT Physiol. **165**: 92–104.

Lampropoulos, A., Sutikovic, Z., Wenzl, C., Maegele, I., Lohmann, J., and Forner, J. (2013). GreenGate - A Novel, Versatile, and Efficient Cloning System for Plant Transgenesis. PLoS One **8**: e83043.

Langmead, B. and Salzberg, S.L. (2012). Fast gapped-read alignment with Bowtie 2. Nat. Methods **9**: 357–359.

Li, B., Wei, A., Song, C., Li, N., and Zhang, J. (2008). Heterologous expression of the TsVP gene improves the drought resistance of maize. Plant Biotechnol. J. **6**: 146–159.

Li, H., Handsaker, B., Wysoker, A., Fennell, T., Ruan, J., Homer, N., Marth, G., Abecasis, G., and Durbin, R. (2009). The Sequence Alignment/Map format and SAMtools. Bioinformatics **25**: 2078–2079.

Li, J., Yang, H., Peer, W.A., Richter, G., Blakeslee, J., Bandyopadhyay, A., Titapiwantakun, B., Undurraga, S., Khodakovskaya, M., Richards, E.L., Krizek, B., Murphey, A.S., Gilroy, S., and Gaxiola, R. (2005). Arabidopsis H+-PPase AVP1 regulates auxin-mediated organ development. Science **310**: 121–125.

Li, S., Liu, L., Zhuang, X., Yu, Y., Liu, X., Cui, X., Ji, L., Pan, Z., Cao, X., Mo, B., Zhang, F., Raikhel, N., Jiang, L., and Chen, X. (2013). MicroRNAs inhibit the translation of target mRNAs on the endoplasmic reticulum in arabidopsis. Cell **153**: 562–574.

Liu, Q., Zhang, Q., Burton, R., Shirley, N., and Atwell, B. (2010). Expression of vacuolar H+-pyrophosphatase (OVP3) is under control of an anoxia-inducible promoter in rice. Plant Mol. Biol. **72**: 47–60.

Maeshima, M. (2001). Tonoplast transporters: organization and function. Annu. Rev. Plant Biol. **52**: 1–32.

Maeshima, M. (2000). Vacuolar H+-pyrophosphatase. Biochim. Biophys. Acta - Biomembr. **1465**: 37–51.

Mann, M. and Jensen, O.N. (2003). Proteomic analysis of post-translational modifications. Nat. Biotechnol. **21**: 255–261.

Martinoia, E., Meyer, S., De Angeli, A., and Nagy, R. (2012). Vacuolar Transporters in Their Physiological Context. Annu. Rev. Plant Biol. **63**: 183–213.

Martinoia, E., Maeshima, M., and Neuhaus, H.E. (2006). Vacuolar transporters and their essential role in plant metabolism. J. Exp. Bot. **58**: 83–102.

Marty, F. (2001). Plant Cell Vacuoles: An Introduction (Csiro Publishing).

Marty, F. (1999). Plant vacuoles. Plant Cell **11**: 587–600.

Mathieu, Y., Guern, J., Kurkdjian, a., Manigault, P., Manigault, J., Zielinska, T., Gillet, B., Beloeil, J.-C., and Lallemand, J.-Y. (1989). Regulation of Vacuolar pH of Plant Cells: I. Isolation and Properties of Vacuoles Suitable for 31P NMR Studies. Plant Physiol. **89**: 19–26.

Mayer, U., Büttner, G., and Jürgens, G. (1993). Apical-basal pattern formation in the Arabidopsis embryo: studies on the role of the gnom gene. Dev. Suppl. **1**: 149–162.

Morsomme, P. and Boutry, M. (2000). The plant plasma membrane H(+)-ATPase: structure, function and regulation. Biochim. Biophys. Acta **1465**: 1–16.

Müntz, K. (2007). Protein dynamics and proteolysis in plant vacuoles. J. Exp. Bot. **58**: 2391–2407.

Mustroph, A., Albrecht, G., Hajirezaei, M., Grimm, B., and Biemelt, S. (2005). Low levels of pyrophosphate in transgenic potato plants expressing E. coli pyrophosphatase lead to decreased vitality under oxygen deficiency. Ann. Bot. **96**: 717–726.

Neuhaus, J.-M. and Martinoia, E. (2001). Plant Cell Vacuoles. Plant Sci. **160**: 757–758.

Neuhaus, H.E. and Trentmann, O. (2014). Regulation of transport processes across the tonoplast. Front. Plant Sci. **5**: 1-8.

Niñoles, R., Rubio, L., García-Sánchez, M.J., Fernández, J. a., Bueso, E., Alejandro, S., and Serrano, R.R. (2013). A dominant-negative form of Arabidopsis AP-3 β-adaptin improves intracellular pH homeostasis. Plant J. **74**: 557–568.

Nishi, T. and Forgac, M. (2002). THE VACUOLAR (H+)-ATPASES — NATURE'S MOST VERSATILE PROTON PUMPS. Nat. Rev. Mol. Cell Biol. **3**: 94–103.

Nishizawa, A., Yabuta, Y., and Shigeoka, S. (2008). Galactinol and raffinose constitute a novel function to protect plants from oxidative damage. Plant Physiol. **147**: 1251–1263.

Norris, S.R., Meyer, S.E., and Callis, J. (1993). The intron of Arabidopsis thaliana polyubiquitin genes is conserved in location and is a quantitative determinant of chimeric gene expression. Plant Mol. Biol. **21**: 895–906.

Oh, D., Lee, S.Y., Bressan, R.A., Yun, D., and Bohnert, H.J. (2010). Intracellular consequences of SOS1 deficiency during salt stress. Plant Sign. Behav. **5**: 766-768.

Oh, D.-H., Leidi, E., Zhang, Q., Hwang, S.-M., Li, Y., Quintero, F.J., Jiang, X., D'Urzo, M.P., Lee, S.Y., Zhao, Y., Bahk, J.D., Bressan, R.A., Yun, D.-J., Pardo, J.M., and Bohnert, H.J. (2009). Loss of halophytism by interference with SOS1 expression. Plant Physiol. **151**: 210–222.

ÖZTÜRK, Z.N., GREINER, S., and RAUSCH, T. (2014). Subcellular localization and developmental regulation of cytosolic, soluble pyrophosphatase isoforms in *Arabidopsis thaliana*. Turk. J. Botany **38**: 1036–1049.

Padmanaban, S., Chanroj, S., Kwak, J.M., Li, X., Ward, J.M., and Sze, H. (2007). Participation of endomembrane cation/H+ exchanger AtCHX20 in osmoregulation of guard cells. Plant Physiol. **144**: 82–93.

Paez-Valencia, J., Sanchez-Lares, J., Marsh, E., Dorneles, L.T., Santos, M.P., Sanchez, D., Winter, A., Murphy, S., Cox, J., Trzaska, M., Metler, J., Kozic, A., Facanha, A.R., Schachtman, D., Sanchez, C.A., and Gaxiola, R.A. (2013). Enhanced Proton Translocating Pyrophosphatase Activity Improves Nitrogen Use Efficiency in Romaine Lettuce. Plant Physiol. **161**: 1557–1569.

Palevitz, B. a. and Hepler, P.K. (1985). Changes in dye coupling of stomatal cells of Allium and Commelina demonstrated by microinjection of Lucifer yellow. Planta **164**: 473–479.

Paris, N., Stanley, C.M., Jones, R.L., and Rogers, J.C. (1996). Plant cells contain two functionally distinct vacuolar compartments. Cell **85**: 563–572.

Park, S., Li, J., Pittman, J., Berkowitz, G., Yang, H., Undurraga, S., Morris, J., Hirschi, K., and Gaxiola, R. (2005). Up-regulation of a H+-pyrophosphatase (H+-PPase) as a strategy to engineer drought-resistant crop plants. Proc. Natl. Acad. Sci. U. S. A. **102**: 18830–18835.

Pasapula, V., Shen, G., Kuppu, S., Paez-Valencia, J., Mendoza, M., Hou, P., Chen, J., Qiu, X., Zhu, L., Zhang, X., Auld, D., Blumwald, E., Zhang, H., Gaxiola, R., and Payton, P. (2011). Expression of an Arabidopsis vacuolar H+-pyrophosphatase gene (AVP1) in cotton improves drought- and salt tolerance and increases fibre yield in the field conditions. Plant Biotechnol. J. **9**: 88–99.

Pei, L., Wang, J., Li, K., Li, Y., Li, B., Gao, F., and Yang, A. (2012). Overexpression of Thellungiella halophila H+-pyrophosphatase Gene Improves Low Phosphate Tolerance in Maize. PLoS One **7**: e43501.

Peleg, Z., Apse, M.P., and Blumwald, E. (2011). Engineering Salinity and Water-Stress Tolerance in Crop Plants. Getting Closer to the Field. Adv. in Bot. Research **57**: 405-443.

Pérez-Castiñeira, J.R., Hernández, A., Drake, R., and Serrano, A. (2011). A plant proton-pumping inorganic pyrophosphatase functionally complements the vacuolar ATPase transport activity and confers bafilomycin resistance in yeast. Biochem. J. **437**: 269–78.

Pittman, J.K. (2012). Multiple Transport Pathways for Mediating Intracellular pH Homeostasis: The Contribution of H+/ion Exchangers. Front. Plant Sci. **3**:1-8.

Pittman, J.K., Shigaki, T., Marshall, J.L., Morris, J.L., Cheng, N.-H., and Hirschi, K.D. (2004). Functional and regulatory analysis of the Arabidopsis thaliana CAX2 cation transporter. Plant Mol. Biol. **56**: 959–71.

Pizzio, G.A., Paez-Valencia, J., Khadilkar, A.S., Regmi, K., Patron-Soberano, A., Zhang, S., Sanchez-Lares, J., Furstenau, T., Li, J., Sanchez-Gomez, C., Valencia-Mayoral, P., Yadav, U.P., Ayre, B.G., and Gaxiola, R.A. (2015). Arabidopsis proton-pumping pyrophosphatase AVP1 expresses strongly in phloem where it is required for PPi metabolism and photosynthate partitioning. Plant Physiol.: pp.114.254342.

Qi, J., Wang, Y., and Forgac, M. (2007). The vacuolar (H+)-ATPase: Subunit arrangement and in vivo regulation. J. Bioenerg. Biomembr. **39**: 423–426.

Ratajczak, R. (2000). Structure, function and regulation of the plant vacuolar H(+)-translocating ATPase. Biochim. Biophys. Acta **1465**: 17–36.

Rienmüller, F., Dreyer, I., Schönknecht, G., Schulz, A., Schumacher, K., Nagy, R., Martinoia, E., Marten, I., and Hedrich, R. (2012). Luminal and cytosolic pH feedback on proton pump activity and ATP affinity of V-type ATPase from Arabidopsis. J. Biol. Chem. **287**: 8986–8993.

Robinson, J.T., Thorvaldsdóttir, H., Winckler, W., Guttman, M., Lander, E.S., Getz, G., and Mesirov, J.P. (2011). Integrative genomics viewer. Nat. Biotechnol. **29**: 24–26.

Rojo, E., Gillmor, C.S., Kovaleva, V., and Somerville, C.R. (2001). VACUOLELESS1 Is an Essential Gene Required for Vacuole Formation and Morphogenesis in Arabidopsis. Dev. Cell **1**: 303–310.

Schilling, R.K., Marschner, P., Shavrukov, Y., Berger, B., Tester, M., Roy, S.J., and Plett, D.C. (2014). Expression of the Arabidopsis vacuolar H+-pyrophosphatase gene (AVP1) improves the shoot biomass of transgenic barley and increases grain yield in a saline field. Plant Biotechnol. J. **12**: 378–386.

Schubert, D. (2004). Silencing in Arabidopsis T-DNA Transformants: The Predominant Role of a Gene-Specific RNA Sensing Mechanism versus Position Effects. Plant Cell **16**: 2561–2572.

Schulze, W.X., Schneider, T., Starck, S., Martinoia, E., and Trentmann, O. (2012). Cold acclimation induces changes in Arabidopsis tonoplast protein abundance and activity and alters phosphorylation of tonoplast monosaccharide transporters. Plant J. **69**: 529–541.

Schumacher, K. (2014). pH in the plant endomembrane system—an import and export business. Curr. Opin. Plant Biol. **22**: 71–76.

Schumacher, K. and Krebs, M. (2010). The V-ATPase: small cargo, large effects. Curr. Opin. Plant Biol. **13**: 724–730.

Schumacher, K., Vafeados, D., McCarthy, M., Sze, H., Wilkins, T., and Chory, J. (1999). The Arabidopsis det3 mutant reveals a central role for the vacuolar H+-ATPase in plant growth and development. Genes Dev. **13**: 3259–3270.

Segami, S., Makino, S., Miyake, A., Asaoka, M., and Maeshima, M. (2014). Dynamics of Vacuoles and H + -Pyrophosphatase Visualized by Monomeric Green Fluorescent Protein in Arabidopsis: Artifactual Bulbs and Native Intravacuolar Spherical Structures. Plant Cell: 1–20.

Segami, S., Nakanishi, Y., Sato, M.H., and Maeshima, M. (2010). Quantification, organ-specific accumulation and intracellular localization of type II H-pyrophosphatase in Arabidopsis thaliana. Plant Cell Physiol. **51**: 1350–1360.

Sondergaard, T., Schulz, A., and Palmgren, M. (2004). Energization of Transport Processes in Plants. Roles of the Plasma Membrane H+-ATPase. PLANT Physiol. **136**: 2475–2482.

Strizhov, N., Abrahám, E., Okrész, L., Blickling, S., Zilberstein, a, Schell, J., Koncz, C., and Szabados, L. (1997). Differential expression of two P5CS genes controlling proline accumulation during salt-stress requires ABA and is regulated by ABA1, ABI1 and AXR2 in Arabidopsis. Plant J. **12**: 557–569.

Strompen, G., Dettmer, J., Stierhof, Y.-D., Schumacher, K., Jürgens, G., and Mayer, U. (2005). Arabidopsis vacuolar H+-ATPase subunit E isoform 1 is required for Golgi organization and vacuole function in embryogenesis. Plant J. **41**: 125–132.

Swanson, S. and Jones, R. (1996). Gibberellic Acid Induces Vacuolar Acidification in Barley Aleurone. Plant Cell **8**: 2211–2221.

Sze, H., Schumacher, K., Müller, M., Padmanaban, S., and Taiz, L. (2002). A simple nomenclature for a complex proton pump: VHA genes encode the vacuolar H(+)-ATPase. Trends Plant Sci. **7**: 157–161.

Székely, G., Ábrahám, E., Cséplo, Á., Rigó, G., Zsigmond, L., Csiszár, J., Ayaydin, F., Strizhov, N., Jásik, J., Schmelzer, E., Koncz, C., and Szabados, L. (2008). Duplicated P5CS genes of Arabidopsis play distinct roles in stress regulation and developmental control of proline biosynthesis. Plant J. **53**: 11–28.

Taji, T., Ohsumi, C., Iuchi, S., Seki, M., Kasuga, M., Kobayashi, M., Yamaguchi-Shinozaki, K., and Shinozaki, K. (2002). Important roles of drought- and cold-inducible genes for galactinol synthase in stress tolerance in Arabidopsis thaliana. Plant J. **29**: 417–426.

Thorvaldsdóttir, H., Robinson, J.T., and Mesirov, J.P. (2013). Integrative Genomics Viewer (IGV): High-performance genomics data visualization and exploration. Brief. Bioinform. **14**: 178–192.

Urano, K., Maruyama, K., Ogata, Y., Morishita, Y., Takeda, M., Sakurai, N., Suzuki, H., Saito, K., Shibata, D., Kobayashi, M., Yamaguchi-Shinozaki, K., and Shinozaki, K. (2009). Characterization of the ABA-regulated global responses to dehydration in Arabidopsis by metabolomics. Plant J. **57**: 1065–1078.

Verweij, W., Spelt, C., Di Sansebastiano, G.-P., Vermeer, J., Reale, L., Ferranti, F., Koes, R., and Quattrocchio, F. (2008). An H+ P-ATPase on the tonoplast determines vacuolar pH and flower colour. Nat. Cell Biol. **10**: 1456–1462.

Viotti, C., Bubeck, J., Stierhof, Y.-D., Krebs, M., Langhans, M., van den Berg, W., van Dongen, W., Richter, S., Geldner, N., Takano, J., Jürgens, G., de Vries, S.C., Robinson, D.G., and Schumacher, K. (2010). Endocytic and Secretory Traffic in Arabidopsis Merge in the Trans-Golgi Network/Early Endosome, an Independent and Highly Dynamic Organelle. Plant Cell **22**: 1344–1357.

Viotti, C. (2014). ER and vacuoles: never been closer. Front. Plant Sci. **5**: 1–7.

Viotti, C., Krüger, F., Krebs, M., Neubert, C., Fink, F., Lupanga, U., Scheuring, D., Boutté, Y., Frescatada-Rosa, M., Wolfenstetter, S., Sauer, N., Hillmer, S., Grebe, M., and Schumacher, K. (2013). The endoplasmic reticulum is the main membrane source for biogenesis of the lytic vacuole in Arabidopsis. Plant Cell **25**: 3434–49.

Wang, Y., Inoue, T., and Forgac, M. (2005). Subunit a of the Yeast V-ATPase Participates in Binding of Bafilomycin. J. Biol. Chem. **280**: 40481–40488.

Wang, Y., Noguchi, K., Ono, N., Inoue, S.-I., Terashima, I., and Kinoshita, T. (2014). Overexpression of plasma membrane H+-ATPase in guard cells promotes light-induced stomatal opening and enhances plant growth. Proc. Natl. Acad. Sci. **111**: 533–538.

Ward, J. and Sze, H. (1992). Proton Transport Activity of the Purified Vacuolar H-ATPase from Oats : Direct Stimulation by Cl. Plant Physiol. **99**: 925–931.

Wink, M. (1993). The plant vacuole: a multifunctional compartment. J. Exp. Bot. **44**: 231–246.

Wirtz, M., Droux, M., and Hell, R. (2004). O-acetylserine (thiol) lyase: an enigmatic enzyme of plant cysteine biosynthesis revisited in Arabidopsis thaliana. J. Exp. Bot. **55**: 1785–1798.

Xiang, L., Etxeberria, E., and Ende, W. (2013). Vacuolar protein sorting mechanisms in plants. FEBS J. **280**: 979–993.

Xu, P., Zhang, Y., Kang, L., Roossinck, M.J., and Mysore, K.S. (2006). Computational estimation and experimental verification of off-target silencing during posttranscriptional gene silencing in plants. Plant Physiol. **142**: 429–440.

Yamada, M., Morishita, H., Urano, K., Shiozaki, N., Yamaguchi-Shinozaki, K., Shinozaki, K., and Yoshiba, Y. (2005). Effects of free proline accumulation in petunias under drought stress. J. Exp. Bot. **56**: 1975–1981.

Yamaguchi, T., Fukada-tanaka, S., Inagaki, Y., Saito, N., Yonekura-, K., Tanaka, Y., Kusumi, T., and Iida, S. (2001). Genes Encoding the Vacuolar Na+/H+ Exchanger and Flower Coloration tion: an increase in the vacuolar pH causes blueing of. Plant Cell Physiol. **42**: 451–461.

Yamanishi, H. and Kasamo, K. (1993). Modulation of the activity of purified tonoplast H+-ATPase from mung bean (Vigna radiata L.) hypocotyls by various lipids. Plant Cell Physiol. **34**: 411–419.

Yang, H., Knapp, J., Koirala, P., Rajagopal, D., Peer, W., Silbart, L., Murphy, A., and Gaxiola, R. (2007). Enhanced phosphorus nutrition in monocots and dicots over-expressing a phosphorus-responsive type I H+-pyrophosphatase. Plant Biotechnol. J. **5**: 735–745.

Zhang, C., Hicks, G., and Raikhel, N. (2014). Plant vacuole morphology and vacuolar trafficking. Front. Plant Sci. **5**: 1-9.

Zhang, J., Li, J., Wang, X., and Chen, J. (2011). OVP1, a Vacuolar H+-translocating inorganic pyrophosphatase (V-PPase), overexpression improved rice cold tolerance. Plant Physiol. Biochem. **49**: 33–38.

Danksagung

Zuallererst bedanke ich mich sehr herzlich bei Prof. Dr. Karin Schumacher für die intensive Betreuung meiner Doktorarbeit. Vielen Dank für die vielen Ideen zu meinem Projekt, für motivierende Worte, für das Lehren wie eine mitreißende und gut aufgebaute Präsentation auszusehen hat, für ihre stets offene Tür und für aufregende Reisen zu Konferenzen.

Weiterhin bedanke ich mich bei Prof. Dr. Jan Lohmann, Dr. Alexis Maizel und Dr. Steffen Lemke für ihre Bereitschaft Mitglieder meines TACs und meiner Prüfungskommission zu sein.

Einen großen Dank an Sebastian Wolf, Melanie Krebs und Zaida Andrés für die Korrektur von Teilen meiner Doktorarbeit.

Ganz herzlich möchte ich mich bei der gesamten AG Schumacher für die tolle Arbeitsatmosphäre, die Hilfsbereitschaft und die vielen witzigen Momente bedanken. Ich bin sehr glücklich, Teil dieser Arbeitsgruppe gewesen zu sein!

Ein besonderer Dank gilt

Melanie Krebs für das Anleiten zu Beginn meiner Doktorarbeit, für viele Tipps zur Durchführung von Experimenten und auch für das Einfordern unseres wöchentlichen Mädels-Lauftrainings zum fit bleiben.

Falco Krüger für die unzähligen Male, die du für viel Spaß im Labor/Mensa gesorgt hast, für deine Unterstützung mit wunderschönen CLSM-Bildern, für unsere kleinen Pausen um nach den Pflanzen im Keller zu schauen und für die musikalische Untermalung des Laboralltags.

Görkem Patir Nebioglu for being a wonderful Master student, for your help with experiments, for your kind words and your delicious sweets during our coffee breaks.

Zaida Andrés for scientific discussions, for your great support in the AVP1 project, for your friendship and many wonderful evenings in restaurants with delicious food, wine and cocktails.

Stefan Scholl für die Unterstützung in unserem gemeinsamen Projekt und für seine unendliche Ausdauer was die Wiederholung von Experimenten betrifft.

Fabian Fink für die Hilfe im Labor und seine herzliche Art, die mich immer besonders erfreut.

Besonders bedanke ich mich bei Ines Steins für das Managen verschiedenster bürokratischer Angelegenheiten, bei Beate Schöfer und Barbara Jesenofsky für Hilfe mit Pflanzen- und Laborarbeiten und bei Katja Piiper für ihre unermüdliche Hilfe was die Convirons, Schädlingsbekämpfung und die generelle Organisation angeht.

Auch bei den ehemaligen Mitgliedern der AG Schumacher Esther Jawurek, Christoph Neubert und Corrado Viotti möchte ich mich für die herzliche Aufnahme in die Arbeitsgruppe und für ihre Hilfe zu Beginn meiner Doktorarbeit bedanken.

Danke dem gesamten COS für die hilfsbereite Atmosphäre.

Thanks to Anna Medzihradszky for her contribution to the AVP1 project.

Ein großer Dank gilt auch meinen ehemaligen und aktuellen WG Mädels Lena W., Constanza, Sarah, Lili, Lena G. und Vicky. Eure Geschichten und Späße haben mich immer sehr gut von meiner Arbeit abgelenkt. Vielen Dank natürlich auch für eure Fürsorge und fürs Zuhören wenn ich mal Dampf ablassen musste.

Vielen Dank meinen lieben brasilianischen Mädels Roberta, Marina, Mariana und Luana für unzählige schöne Tage mit eurer fröhlichen Mentalität und eurer Verrücktheit die immer für viel Freude gesorgt hat. Muito obrigada por tudo!

Zu guter Letzt möchte ich mich von ganzem Herzen bei meinen Eltern bedanken. Danke, dass ihr immer für mich da seid und mich unterstützt. Danke meiner liebsten Schwester für ihr offenes Ohr zu jeder Zeit. Vielen Dank an Jo für seine Geduld, aufmunternden Worte und für die unzähligen schönen Momente.